ADVANCING DISTRIBUTION AUTOMATION THROUGH MODEL-BASED AND MACHINE LEARNING APPROACHES

A Dissertation
Presented to
The Academic Faculty

by

Zhengrong Chen

In Partial Fulfillment
of the Requirements for the Degree
Doctor of Philosophy in the
School of Electrical and Computer Engineering

Georgia Institute of Technology
December 2024

ADVANCING DISTRIBUTION AUTOMATION THROUGH MODEL-BASED AND MACHINE LEARNING APPROACHES

Approved by:

Dr. A.P. Meliopoulos, Advisor
School of Electrical and Computer Engineering
Georgia Institute of Technology

Dr. Ying Zhang
School of Electrical and Computer Engineering
Georgia Institute of Technology

Dr. Santiago Grijalva
School of Electrical and Computer Engineering
Georgia Institute of Technology

Dr. Constance Crozier
School of Industrial and Systems Engineering
Georgia Institute of Technology

Dr. Daniel Molzahn
School of Electrical and Computer Engineering
Georgia Institute of Technology

Date Approved: December 3, 2024

ACKNOWLEDGEMENTS

Pursuing a Ph.D. is not easy, but I'm glad I chose the right four years ago. I had a rough beginning due to the unexpected COVID-19. I remembered spending a year in China for remote studies while anxiously awaiting my visa. Eventually, I had the opportunity to continue my studies at the Atlanta campus. This three and a half years' journey has been a wonderful treasure for me, filled with unforgettable memories. Despite being beaten by difficulties, I have grown up in academic skills and being a better person with a strong mindset. A single man cannot accomplish this alone, so I want to thank everyone who supports and cares for me.

First and foremost, I would like to express my deepest gratitude to my advisor, Dr. A. P. Sakis Meliopoulos. I could not have completed my Ph.D. studies without his patience, motivation, and support. I am grateful for the countless hours he dedicated to helping me with problem formulation and encouraging me to strive for excellence in my work. He is a kind, gentle, and talented person who supports me in exploring new methods like AI to solve problems. Additionally, he offered me valuable opportunities to apply the knowledge I acquired in solving real-world problems, particularly in power systems, enhancing my practical experience and bridging the gap between theory and application. I hope to continue contributing to the power and energy society as he does.

Next, I want to thank the members of my committee, Dr. Santiago Grijalva, Dr. Daniel Molzahn, Dr. Ying Zhang, and Dr. Constance Crozier. Their thoughtful advice and constructive critiques have greatly enriched this thesis, and I am thankful for the time and effort they invested in helping me achieve my goals.

My sincere appreciation goes to my lab mates in the Power Systems Control and Automation Laboratory (PSCAL), including Dr. Yu Liu, Dr. Jiahao Xie, Dr. Gad Monga Ilunga, Dr. Kiayu Liu, Dr. Dayou Lu, Siyao Cai, Fahad Alsaeed, Dr. Abdulaziz Qwbaiban, Zan Yang, Yuan Nie**.** Moreover, I especially want to thank Dr. George Cokkinides for his support in software development and hardware implementation. I would also like to thank my friends from the College of Engineering, Yiming Chen, Zhisheng Zhao, Yuchen Zhang, Zexian Zeng, Justin Zhang, Ruomu Hao, Jorge Fernandez, Samuel Talkington, for their support and accompaniment during this journey.

I would be grateful for the internship at Eaton Corporation. This experience has been enriching, and I am deeply grateful for the opportunity to grow professionally and personally. I want to thank my manager, Dr. Dongbo Zhao, for this opportunity. I sincerely appreciate Dr. Liuxi (Calvin) Zhang, our director, for his support, encouragement, and feedback. I want to extend my heartfelt gratitude to my mentors, Dr. Chirath Pathiravasam and Dr. Kaiyu Liu, whose guidance and support have been invaluable. I'd also like to thank my colleagues: Dr. Dmitry Ishchenko, Dr. Qi Li, Asmaa Romia, Dr. Jinan Zhang, and Dr. Soumyabrata Talukder. Your insights and encouragement have inspired me to aim higher and challenge myself in new ways.

Finally, I would like to express my heartfelt gratitude to my family for their unwavering love and encouragement. I am especially thankful to my parents, Xiongwei Chen and Xiaoyi Chen, for leading me to a world of possibilities and for their unconditional support throughout the years. This dissertation is dedicated to my beloved family, particularly the younger generations, including my brother, Ruiqiang Chen, my sister, Wenqi Chen, and my son, Jiaheng Chen.

TABLE OF CONTENTS

LIST OF TABLES

LIST OF FIGURES

LIST OF ACRONYMS

1D-CNN	One-dimensional convolutional neural network
2D-CNN	Two-dimensional convolutional neural network
ADN	Active distribution network
AI	Artificial intelligence
AMI	Advanced Meter Infrastructure
ANNs	Artificial neural networks
ASMDP	Adversarial State Markov Decision Process
CDF	Cumulative Distribution Function
CEO	Constant Elasticity of Own-price Model
CP	Conformal Prediction
DA	Distribution Automation
DAS	Distribution Automation System
DDPG	Deep deterministic policy gradient
DER	Distributed energy resources
DL	Deep learning
DQN	Deep Q Network
DRL	Deep reinforcement learning
DRNN	Deep recurrent neural network
DSE	Dynamic state estimation
DSO	Distribution System Operators
EBFL	Estimation-based fault locating
EBP	Estimation-based protection
EnbPI	Ensemble Batch Prediction Intervals
EV	Electric Vehicle
FDI	False data injection
FLISR	Fault Localization, Isolation, and Service Restoration

IBRs	Inverter-based resources
IEDs	Intelligent Electronic Devices
ISO	Independent System Operators
LSTM	Long short-term memory
LTCs	Load Tap Changers
MDP	Markov Decision Process
MICP	Mixed-Integer Conic Programming
MLP	Multilayer perceptron
MU	Merging unit
PI	Prediction Interval
PV	Photovoltaic
QDM	Quadratized device model
RDRL	Robust deep reinforcement learning
RL	Reinforcement learning
SAC	Soft Actor-Critic
SCADA	Supervisory Control and Data Acquisition
SCAQCF	State and control algebraic quadratic companion form
SCs	Switched Capacitors
SVM	Support vector machine
TEM	Transactive Energy Market
VVO	Voltage-VAR Optimization
VVR	Voltage Violation Ratio

SUMMARY

With the rise in distributed energy resources (DERs) and electric vehicles (EVs), electric power systems, especially distribution systems, are transforming into active systems with renewable and low-carbon energy resources. Shifting from passive to active is one of the most significant characteristics of distribution systems, allowing bidirectional power flow from DERs. Such change brings challenges to distribution systems, including growing complexity, heightened uncertainty, frequent voltage violations, dynamic load demand, and cybersecurity issues. With the development of advanced metering infrastructures (AMI), leveraging extensive sampled and historical data enables real-time monitoring and control to enhance the resilience of Active Distribution Networks (ADNs) under uncertainties and cyberattacks. This dissertation aims to advance distribution automation (DA) in terms of protection, control, and optimization to ensure secure, reliable, and resilient distribution system operation. Specifically, this dissertation explores advanced model-based and data-driven methodologies in this framework, including state estimation, fault diagnosis, voltage control, and load management.

First, we propose a Dynamic State Estimation-Based Protection (EBP) scheme for addressing protection challenges posed by Inverter-Based Resources (IBRs). Unlike the legacy state estimation method, Dynamic State Estimation (DSE) uses two consecutive sample values to compute the estimation instead of steady-state current and voltage phasors. The object-oriented DSE algorithm requires high-fidelity device models, measurement models, and a DSE process. The main idea of EBP is to detect faults by checking the consistency between the measurements and the mathematical system model.

The fault is identified by a low confidence level, suggesting an inconsistency between the measurements and the model. Simulation results demonstrate the benefits of the proposed EBP method, including simple settings, high accuracy, and fast response time.

Once the fault is detected, a real-time fault diagnosis framework is proposed for fault classification and fault locating. We utilize a supervised Deep Learning (DL) model for real-time fault classification. Compared with other Machine Learning (ML) methods, this model has lower computational complexity and is more efficient for processing long sequences of real-time data. This advantage makes it more efficient for processing long sequences of real-time data. Moreover, it can automatically learn relevant features from sequential data, reducing the need for manual feature engineering. The main idea of the Dynamic State Estimation-Based Fault Locating (EBFL) algorithm is to treat the fault location as a state to obtain its best estimation. A non-linear weighted least square (WLS) estimator is applied for the state estimation process. Note that the DSE applications, including EBP and EBFL, use the dynamic device model of distribution systems, expressed in a standard syntax referred to as State Control and Parameter Algebraic Quadratic Companion Form (SCPAQCF).

A model-free Vol-VAR Optimization (VVO) method via Robust Deep Reinforcement Learning (RDRL) algorithm is developed to enhance the voltage profile of distribution systems. Unlike a standard DRL, RDRL offers improved performance in unpredictable conditions and the ability to handle power injection uncertainties, where the uncertainties are considered adversarial attacks, making it highly effective in finding an optimal or suboptimal solution without solving complex min-max optimization problems. Moreover, we design the uncertainty sets acquired by conformal prediction as the inputs of actor-critic networks. This information provides robustness during training. Numerical results illustrate the effectiveness of the proposed RDRL methodology for the online application of the VVO problems with enhanced safety regions.

Finally, we focus on the load management system, which is a critical part of the DA. In the dynamic energy market, active consumers can adjust their energy usage based on real-time pricing. We model this price-responsive demand to understand consumer behavior better. However, with the increasing reliance on cyber assets and communications, power systems are becoming more vulnerable to cyberattacks. Specifically, the attackers can alter electricity price signals from the aggregator to the consumer or change the load signals from the customer to the aggregator. In this dissertation, we only consider the real-time pricing attacks and propose a robust optimization method to address them. By setting the level of robustness, customers can obtain an optimal and secure energy consumption plan based on their preferences.

To sum up, the main contributions of this dissertation include: (1) the design of the DA platform, which utilizes smart meter data for distribution system applications to enhance resilience; (2) the development of the real-time fault diagnosis framework with high accuracy and robustness; (3) the innovation of the RDRL method to solve optimization problem under uncertainties; (4) the formulation and mitigation methodology for pricing integrity attacks on the energy market.

CHAPTER 1. INTRODUCTION

1.1 Problem Statement

The integration of distributed energy resources (DERs) in the power system is an emerging tendency to promote the carbon reduction policy. DERs are small-scale power generation sources connected directly to distribution systems [1]. DERs include renewable generation units like photovoltaics (PVs) and wind turbines, and energy storage such as batteries and electric vehicles (EVs). It has been projected by the U.S. Energy Information Administration (EIA) that the U.S. power grid will see an addition of 42.6 gigawatts (GW) of new utility-scale electric-generating capacity in the second half of 2024. Most of this capacity, over half (60%), will be from solar power (25GW), followed by battery storage (10.8GW) [2].

Most of the transformation is taking place at the distribution grid level. The increased integration of renewable energy poses operational challenges for Distribution System Operators (DSO), including growing complexity, heightened uncertainty, and increased volatility. Consequently, the concept of active distribution network (ADN) has been proposed to improve the power system's stability, reliability, and resilience [3]. Unlike the traditional "passive" distribution system, ADN allows for bidirectional power flow and various operation modes by employing intelligent control and operation strategies.

Several practical problems need to be tackled in ADN. Firstly, the proliferation of DERs can cause voltage fluctuations, which degrade the quality of the grid's voltage profile. Simultaneously, distribution systems are continuously exposed to fault occurrences due to extreme weather events and human errors, which may lead to bulk power outages.

The low-amplitude fault current and the low inertia of power electronic inverters [4] present challenges to legacy protection schemes, leading to potential mis-operation as these schemes cannot accurately interpret and respond to such atypical fault dynamics. A typical case happened in the 2016 Southern Australia blackout [5]. This risk to the operation of protective devices is especially of concern when the system faces low levels of strength that may be experienced due to system splitting.

On the other hand, with the overwhelming adoption of smart meters and communication infrastructures, cybersecurity issues against power grid operation and energy market have become a significant concern. For instance, in 2020, the UK grid was attacked by cybercriminals who deployed ransomware on the business systems to steal and post sensitive internal data, causing a considerable loss [6]. Power distribution systems are also vulnerable to cyber-attacks due to the increasing number of active consumers and the integration of DERs. For example, the attacks may implement false data injection (FDI) attacks to manipulate the electricity prices or compromise the measurements from meters, leading to unobservable economic loss for customers and grid operators.

The uncertainties introduced by DERs and more frequent failures call for developing resilient ADNs. Resilience signifies the capacity to resist, absorb, recover from, and adapt to disturbances or disruptions. According to Electric Power Research Institute (EPRI), distribution system resilience contains three elements: prevention, recovery, and survivability [7]. It involves secure and intelligent protection, control, and optimization strategies to reliably deliver electrical energy to customers, even in the face of challenges such as natural disasters, cyberattacks, equipment failures, or other unexpected events. Distribution automation (DA), deploying sensors, control devices, and communication technologies across the power distribution network, is recognized as the most effective method for DSO to increase operation efficiency and reliability. As a typical component for DA, state estimation monitors the system's operating status and is vital to ADN operation with DER penetration. Various new applications, such as fault locating, isolation, and service restoration (FLISR), feeder reconfiguration, fault diagnosis, load management, voltage control, and cyberattack mitigation, are employed to improve DA. However, towards developing resilient ADNs, DSOs must consider the following issues distinct from transmission systems:

- **Partial observability**: Distribution systems always have a limited number of metering instruments as full coverage of sensors is cost-prohibitive. In contrast, transmission systems hold a high level of data redundancy.
- **Power electronic interface**: DERs are connected to the grid through power electronic inverters. The low fault current and low inertia features of inverter-based resources (IBRs) can adversely impact the performance of legacy protection schemes.
- **Unbalanced operation**: Most distribution systems are highly unbalanced, leading to higher complexity in formulating distribution system state estimation. Also, considering the invisibility of network parameters and the phase angle information, this unbalanced property poses challenges to data-driven models.
- **Active consumer behavior:** Many consumers may feed excess energy back into the grid, complicating load management due to bidirectional power flow. Moreover, they often involve frequent sell/buying actions in response to grid signals. Load management systems must account for demand response program variability.

These distribution system characteristics increase the challenges of operation and control, so it is crucial to advance DA for resilient ADN development.

1.2 Research Objectives and Accomplishments

The proposed research aims to advance DA on the scope of protection, control, and optimization via dynamic state estimation (DSE) and machine learning (ML) approaches. With abundant real-time and historical data from advanced metering infrastructures, such methods can ensure the safe, reliable, and efficient operation of ADNs, even under uncertainties and cyberattacks. Figure 1.1 shows the general schematic of a model-based and ML-based DA platform. In the platform, the uncertainties from DER and load are captured by statistical methods based on database and deemed as the inputs of the ML models while DSE is implemented to get the best estimation of key states. Then, we can extend the measurements from smart meters and those estimated states to DA applications like protection, voltage control, fault diagnosis and demand management.

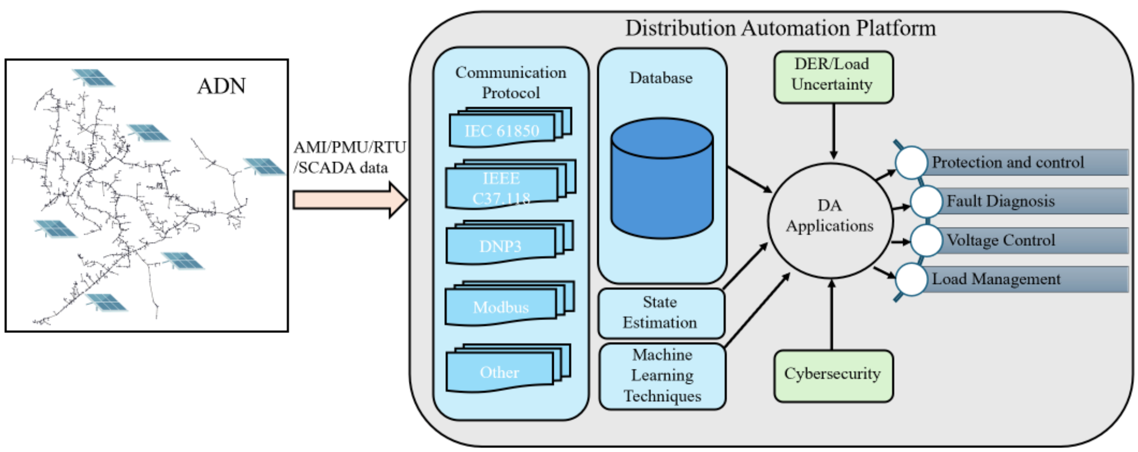

Figure 1.1 Research scheme of this thesis for distribution automation

Specifically, the main accomplishments of this dissertation are provided as:

- **DSE & Protection.** A Dynamic State Estimation-Based Protection (EBP) scheme is developed to ensure accurate and secure fault detection and isolation against the impact of IBRs. The object-oriented DSE algorithm requires high-fidelity device models, measurement models, and a DSE process. The EBP detects faults by checking the consistency between the measurements and the protection zone model. When an internal fault occurs, even high impedance faults or faults on inverters, the DSE reliably detects the abnormality, and a trip signal can be issued. This setting-less EBP can ensure high fault detection accuracy.
- **Real-time fault diagnosis**. Fast and accurate fault location is crucial for isolating faults and accelerating restoration. A real-time fault diagnosis framework based on DSE and AI methods is proposed. The framework comprises two tasks: (a) supervised deep-learning (DL) for fault classification; and (b) Dynamic state estimation-based fault locating (EBFL). With the fault type information, DSE is implemented to estimate the fault location based on the physically informed three-phase dynamic models. Its high accuracy and low computation cost show potential in real-world applications.
- **AI for control/optimization**. Using machine learning and artificial intelligence for solving control/optimization problem. Considering the increasing uncertainties like load fluctuation and renewable generation, an online Volt-VAR Optimization (VVO) method is proposed for effective voltage control via robust deep reinforcement learning (RDRL). The objective of VVO is to maintain voltage levels within specified limits while minimizing the losses. Unlike a standard RL, RDRL offers improved performance in unpredictable conditions, enhanced handling of noisy data,

and resilience to adversarial attacks, making it highly effective for solving VVO problem.

- **Optimization & Cyberattack Mitigation.** Active consumers can adapt their load demand in response to real-time pricing and optimize their energy use. However, the increased reliance on cyber assets and communications makes these systems prone to cyberattacks. The impact of real-time pricing integrity attacks on price-responsive demand is investigated and quantified. Then, a robust optimization method is proposed to handle the real-time pricing attack as uncertainty to obtain the optimal energy consumption plan based on consumers' preferences. This method can save more than 2% economic loss compared with the traditional deterministic method.

1.3 Thesis Outline

The dissertation is outlined as follows.

Chapter 2 provides background and literature review of DA, focusing on the impacts of IBRs on protection schemes, fault management, VVO, and cybersecurity in load management. The state-of-the-art techniques, their disadvantages, and the additional challenges posed by power electronics interfaces, uncertainty from DERs and load, as well as cybersecurity, are all included.

Chapter 3 presents the proposed EBP scheme for distribution system protection. The DSE algorithm encompasses dynamic models of distribution systems using a general syntax called state and control algebraic quadratic companion form (SCAQCF). A DSE process is executed using the derived measurement SCAQCF object to identify internal and external faults within the protection zone. The simulation results demonstrate that the proposed EBP scheme for ADNs is resistant to the fault characteristics of inverters.

Chapter 4 extends the work proposed in Chapter 3 and proposes a real-time fault diagnosis framework based on DSE and ML methods. The fault diagnosis procedure includes fault detection, classification, and locating. It starts when the proposed EBP detects the fault and generates a trip command. Then, a supervised DL model is used for fault classification, and the EBFL algorithm is implemented with the fault type to estimate the fault location. Extensive simulations validate the accuracy, efficiency, and robustness of this framework under various fault scenarios, including measurement noise, which shows promise for real-time applications.

Chapter 5 proposes an RDRL framework for VVO via a robust deep deterministic policy gradient (DDPG) algorithm. This algorithm can effectively manage hybrid action spaces, considering control devices like capacitors, voltage regulators, and smart inverters. Additionally, it is designed to handle uncertainties by quantifying uncertainty sets with conformal prediction and modeling uncertainties as adversarial attacks to guarantee safe exploration across action spaces.

Chapter 6 develops a robust optimization-based load management system under cyberattacks. The false data injection (FDI) attack, a real-time pricing integrity attack, manipulates electricity prices to study the impact on price-responsive demand. To address this issue, a robust optimization method is used to determine an optimal energy consumption plan for active consumers.

Finally, Chapter 7 concludes the research work and discusses future work.

CHAPTER 2. DISTRIBUTION AUTOMATION

2.1 Introduction

This chapter provides the background of distribution automation (DA) and an overview of technologies related to the proposed topics. Section 2.1 presents the definition and structure of Distribution Automation System (DAS). Section 2.2 illustrates the impact of IBRs on legacy protection schemes. Section 2.3 reviews fault diagnosis in previous research, especially for the state-of-art and research gap of fault classification and fault locating. Section 2.4 summarizes the VVO methods used in distribution systems and their limitations. Section 2.5 describes the cybersecurity issue on load management systems with active consumers. Finally, a summary of this chapter is given in Section 2.6.

2.2 Distribution Automation System

DA involves implementing advanced control, monitoring, and data acquisition systems in the electrical power distribution network, and it plays a crucial role in smart grid. [8]. Advances in the development of intelligent electronic devices (IEDs) and communication have given rise to the DAS concept [9]. DAS are technologies applied to the electric power distribution network that allows for the automatic control, monitoring, and operation of electrical distribution systems without human intervention. The primary objective of DAS is to enhance the reliability, efficiency, and quality of power distribution by facilitating real-time management and control of the distribution network, especially with the growing penetration of distributed generations (DGs) and electric vehicles (EVs) [10-12]. The following sections present the key components and applications of DAS.

2.2.1 Sensors and Monitoring Devices

The widespread implementation of Advanced Meter Infrastructure (AMI), also known as smart meters, is vital to the DAS concept, especially in improving power quality in distribution systems. AMI can improve outage response time, predict harmonic scenarios, implement load shedding to prevent power disturbances and outages, monitor waveforms, support demand-side management initiatives, and provide consumers with energy consumption information for potential cost savings [13]. Smart meters are equipped with two-way communication, offering numerous benefits to customers and utilities and improving operational efficiencies. Figure 1 shows the commonly used sensors in smart grid. Based on the measurement type, these sensors can be classified into three categories: (i) electrical sensors, (ii) environment sensors, and (iii) working condition sensors. As distribution systems continue to evolve, the role of these devices will become increasingly important, supporting the transition to smarter, more resilient power grids.

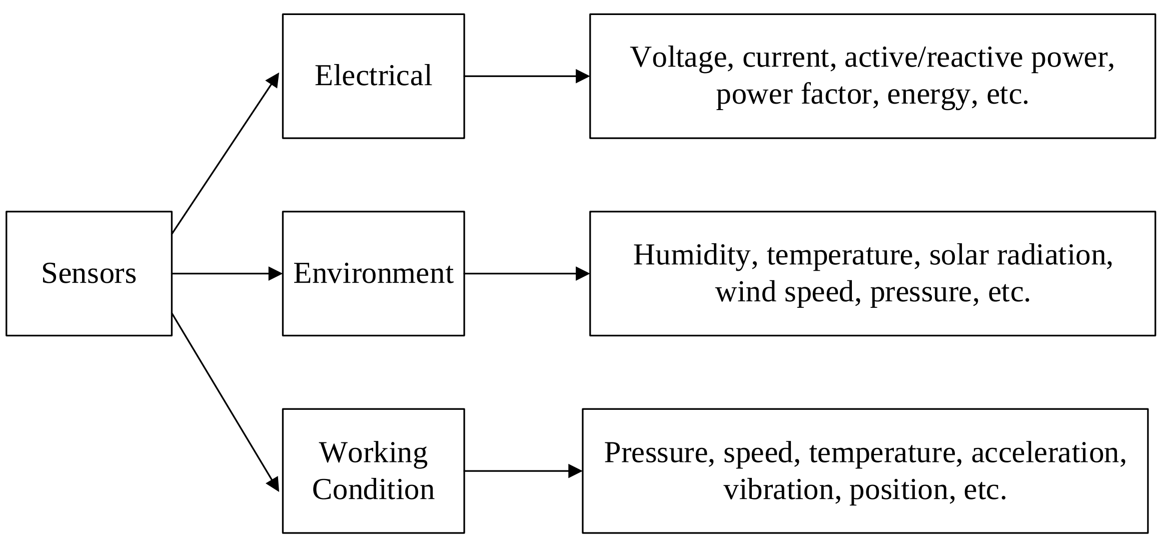

Figure 2.1 Sensors in smart grid

2.2.2 Control Systems

Utilities worldwide use Supervisory Control And Data Acquisition (SCADA) to monitor, control, and manage equipment and processes in real time. SCADA is a centralized controlling system that involves a system operator to use available data in decisions relating to the distribution network control [14]. By analyzing data on voltage, current, load, and faults, control systems can automatically reroute power, isolate faulty sections, restore service, and optimize the distribution network's performance. This automation reduces the need for manual intervention, minimizes downtime, and enhances the overall efficiency and reliability of the power grid. Due to the challenges posed by the interconnection of DERs and EVs, the control issues of DAS can be summarized as follows [15]:

- Local control: This level focuses on the real-time, decentralized management of individual components within the distribution network, such as transformers, circuit breakers, switches, voltage regulators, and capacitor banks. It involves autonomous decision-making by Intelligent Electronic Devices (IEDs) or local controllers based on data from nearby sensors.
- Global control: It operates at a centralized level, overseeing the entire distribution network to ensure coordinated operation across multiple local controllers. This level of control typically involves a central control system that collects data from all parts of the network, processes it, and sends coordinated control commands back to local devices. An exemplary application of this is observed in demand-side management (DSM), which leverages real-time data within SCADA systems to achieve optimal control of DERs input.

- Market-level control: Market-level control involves broader decision-making that goes beyond technical operations to include economic, regulatory, and market-driven factors. It encompasses the interaction between the distribution network and the electricity market, including demand response, dynamic pricing, and integration of distributed energy resources (DERs). For example, we must consider market implications, such as whether specific loads can be curtailed through demand response programs to maintain grid stability or how the fault impacts energy pricing and market participation.

Addressing these control issues required robust communication systems, advanced data analytics and intelligent control algorithms. Moreover, effective coordination across all three control levels is necessary to minimize disruption, maintain reliability, and balance economic considerations.

2.2.3 Communication Standards and Protocols

As mentioned in section 2.2, robust and reliable communication systems are required to enable real-time monitoring, control and automation of distribution networks. Several working groups established an international standard for DA, involving organizations such as the Institute of Electrical and Electronics Engineers (IEEE), the American National Standards Institute (ANSI), the International Electrotechnical Committee (IEC), and several other committees. Table 2.1 presents the commonly used standards with their applications as well as advantages and disadvantages. Note that the IEC 61850 standard specifies new communication protocols, including Generic Oriented Object Substation Event (GOOSE), Sampled Analog Values (SV), and Manufacturing Messages Specific (MMS) protocols for substation automation, which can also be used for DA. To facilitate

Table 2.1 Communication standards used in distribution systems

Standard	Application	Advantages	Disadvantages
IEEE 61850	Substation automation and control. Integration of IEDs.	High interoperability. high-speed. Object-oriented data modeling.	Complex configuration and implementation. High initial cost.
IEC 60870-5	Telecontrol between control centers and substations. Real-time data acquisition.	Reliable for wide-area network communication. Well-suited for large-scale distribution networks.	Older standard with lower data rates. Requires robust infrastructure.
IEEE 802.15.4	Wireless sensor networks Connectivity in hard-to-reach or expansive areas.	Low power consumption. Good for low-data-rate applications.	Limited range and data throughput.
IEC 62351 (Cybersecurity)	Securing communication in power system automation. Protecting DAS from cyber threats.	Provides comprehensive security measures. Ensures data integrity and confidentiality.	Adds complexity to system design. Can impact performance due to encryption overhead.
ANSI C12.22	AMI communication. Facilitates data exchange over wide-area networks.	Enables secure, flexible data communication over various networks. Supports real-time data exchange.	Higher complexity and cost compared to simpler protocols. Requires robust network infrastructure.

Table 2.2 Communication protocols used in distribution systems

Protocol	Description	Application	Advantages	Challenges
DNP3	Widely used in SCADA systems.	SCADA	Reliable, low bandwidth, remote.	Limited bandwidth
Modbus	Used in industrial automation systems.	Communication between devices in automation systems.	Simple, widely adopted, easy to implement.	Limited security, low speed, security concerns.
Zigbee	Used for low-power, low-data-rate wireless networks.	Home automation, smart meters, sensor.	Low power, mesh networking, scalable.	Limited data rate, shorter range.
Wi-Fi	Wireless networking technology for local area networks.	Internet of Things (IoT) devices, smart grid communication.	High data rate, wide availability.	High consumption, security concerns.
Cellular (4G/5G)	High-speed wireless communication.	SCADA, AMI.	High speed, wide coverage, reliable.	High consumption, costly fees.
PLC	Communication over existing power lines.	AMI, load control, demand response.	Low cost, reliable in short range.	Limited bandwidth, noise interference.

the adoption of smart grid technology, various power system operators and research institutes have advocated for the utilization of existing communication protocols, as detailed in Table 2.2. Similarly, Table 2.2 illustrates their description, application, advantages and challenges.

Besides the above communication standards, the IEEE 1547 standard [16], published in 2003, is also pertinent to FA, which describes interconnection criteria for DERs with the electric grid. It provides guidelines for safe and reliable DER integration, enhancing grid stability and supporting renewable energy adoption. However, updates to the standard may require upgrades to existing systems.

2.2.4 Distribution Automation Applications

Implementing automation applications has been pivotal in transitioning from traditional power distribution systems to active distribution systems to ensure reliability, resilience, and security. The key applications of DA are represented as follows:

- Protection scheme automation: The protection scheme is at the core of any distribution system. Its primary function is to prevent damage to the connected equipment during adverse operating conditions. This includes fault detection and fault isolation. Fast and accurate protection can reduce restoration time, as well as customer and utility losses.
- FLISR: Fault Location, Isolation, and Service Restoration (FLISR) is another significant application of DA. Once a fault is detected, the fault location algorithm identifies the exact location of the fault (faulted line section and fault locating information). After locating the fault, the FLISR system isolates the affected section of the network by automatically opening and closing circuit breakers, switches, or reclosers. Service restoration is the final step to restore service to the unaffected areas by closing switches and reconfiguring the network to bypass the faulted section. The

FLISR can be completed within seconds or minutes to reduce the duration and frequency of outages and to improve grid efficiency and safety.

- Volt-VAR control: The main goals of Volt-VAR control, also known as VVO, are to maintain optimal voltage profiles while minimizing power losses of distribution systems. The conventional VVO approaches use switched capacitors (SCs), load tap changers (LTCs) and voltage regulators. However, the integration of DERs and EVs poses challenges to this task: a) uncertainties from DER and load, b) traditional downstream control cannot work for fast-time scale at sub-minute level, c) coordination issues among different type regulation devices. Thus, more advanced VVO in DA is highly required by using smart inverters, static VAR compensators (SVCs) as well as IEDs and Remote Terminal Units (RTUs) to realize voltage control.
- Load management: Load management is crucial for balancing power flow in electrical grids. It involves monitoring and controlling loads to optimize distribution, reduce peak loads, and enhance grid stability. This function helps utilities adapt to demand fluctuations, integrate renewable energy, and provide reliable power cost-effectively.
- DER control: DER provides benefits to the distribution industry by supplying energy to connected customers, such as balancing load and power supply during peak times, improving power quality, and strengthening grid stability. DER control in DA involves voltage regulation, demand-side management, reactive power control, and microgrid operation, enhancing resilience, efficiency, and sustainability in the transition to a more decentralized energy system.

2.3 Impact of IBRs on Protection Schemes

Legacy protection functions in distribution systems are classified into three categories: current-based protection schemes, impedance-based protection schemes, and voltage-frequency (V-f) based protection schemes. Current-based protection schemes mainly include overcurrent protection and earth fault protection; impedance-based protection schemes mainly include distance protection and differential protection; V-f-based schemes mainly include over/under voltage and frequency protection.

Different from the traditional synchronous generators (SG), IBRs have significantly different characteristics under fault conditions [17-18]: (a) low-amplitude current: a steady-state fault current that is typically around 1.1–1.5 pu of the inverter's current rating, (b) low inertia: deviation of system frequency leading to significant system disturbances, and (c) dynamic changing phase angle depending on IBR control scheme (e.g., grid-following [19] and grid-forming [20]). As a result, large-scale integration of IBRs would introduce new challenges to the legacy protection functions.

Many researchers have studied the impact of IBRs on legacy protection functions. Overcurrent protection ensures system safety by disconnecting circuits when the current exceeds a threshold. However, traditional relays may fail to detect the faults as the fault current is below their current pickup settings under a single fault on the IBRs side [21]. For directional protection, the unpredictable negative-sequence currents (almost zero) can compromise the performance of legacy protection schemes [22]. In [23], the authors noted that the voltage and current signals were significantly affected by fault current limiters (FCL) during the first quarter cycle after a fault. Distance protection, while effective in transmission systems without communication requirements [24], faces challenges in distribution networks as IBRs could amplify the influence of fault resistance [25]. For differential protection, Han et al. [26] conducted a thorough investigation of the reliability and sensitivity of conventional two-terminal differential protection. For line current differential protection [27], the relay may mistakenly classify an internal fault as external due to an incorrect characteristic region of the fault current.

The EBP known as "setting-less protection," is an effective protection scheme to identify the faults and issue the trip command correspondingly [28]. The EBP has been developed and implemented in protection zones of transformers [29] and a three-feeder distribution system [30]. Further, we implemented the EBP in a real-world distribution system with PVs [31], which shows that the EBP is immune to the impact of IBRs.

2.4 Fault Diagnosis

Various subtasks are involved in protecting active distribution systems: fault detection, fault classification, and fault location. The fault detection function monitors the system continuously to identify abnormal conditions, such as short circuits, overloads, or other disturbances. Once a fault is detected, it is classified to determine the type of fault. Accurate fault location is the next crucial step as it enables a quick response and minimizes downtime.

This section presents the literature review on fault diagnosis methods in distribution systems. Specifically, section 2.4.1 illustrates the state-of-art and research gap of fault classification, and section 2.4.2 focuses on fault locating methods.

2.4.1 Fault Classification Methods

Fault-type classification is an essential part of protecting transmission lines and power distribution systems. Most classification methods adopt classifier models based on statistical learning theory [32], while others use logic flows [33-34] based on experience and observation of collected data. This field has been developed rapidly due to advances in pattern recognition and machine learning, particularly supervised learning algorithms for classification, such as artificial neural networks (ANNs) [35], support vector machine (SVM) [36], fuzzy logic methods [37-38], etc.

Recently, DL has become a vital part of state-of-the-art methods. Reference [39] shows an outstanding performance in applying a novel DL classification model based on Deep Recurrent Neural Networks (DRNN) and Long Short-Term Memory (LSTM). Authors in [40] proposed a novel fault classification model based on spatiotemporal graph learning, with more robust feature extraction and anti-interference abilities. In [41], the authors proposed a CNN-based image similarity recognition method to solve fault classification problems via a Hilbert–Huang transform band-pass filter. A DL framework is presented in [42] for identifying system operation states and fault types using a combination of deep auto-encoder and CNN. Reference [43] illustrates the robustness and explainability of the proposed CNN model on field data with high classification accuracy.

The studies above, however, have limitations in their application due to high computational costs and overreliance on feature selection. Moreover, increasing the complexity of the model to achieve better accuracy leads to overfitting and difficulty in training the model.

2.4.2 Fault Locating Methods

Fault locating methods can be divided into three categories: traveling wave methods [44], impedance-based methods [45-46], and machine learning methods [47-48]. Traveling wave methods rely on precise fault transient measurements with high sampling rates, which is not economical for distribution systems. Impedance-based methods derive fault location by calculating equivalent impedance from current and voltage phase information. However, they are sensitive to network parameter variations and inaccurate with fluctuating fault resistance and load conditions. In [48], a general regression neural network is utilized for locating the fault. While machine learning is a powerful tool for classification and regression, its training process is time-consuming, and scalability remains a concern.

Based on the measurement type, these approaches can be classified into phasor domain methods and time domain methods. Phasor domain methods harness synchronized phasor measurements to gain insights into the electrical network's behavior from a frequency-domain perspective. Synchronized phasor measurement units (PMUs) play a crucial role in phasor-based techniques [49], allowing for the real-time analysis of voltage and current phase angles and magnitudes during fault events. Regardless of fundamental harmonic measurements, time-domain methods are less vulnerable to fault transients. The circuit is represented with its time-domain model using differential equations. With the dynamic transmission line model, the fault is located using the recorded current and voltage measurements before and after the fault [50]. Lu et al proposed a time-domain fault location method for transmission lines with a novel prepositive to solve the partial differential equations (PDEs) [51].

However, there is still a gap in the time domain fault locating method for distribution systems due to the complexity of topology and the integration of IBRs. With accurate and reliable fault locating algorithms, utility operators can deploy a specialized crew for restoration purposes to minimize repair time, consequently reducing losses for both utility and customers.

2.5 Volt-VAR Optimization

The VVO aims to optimize voltage files and minimize network losses. This is achieved by employing regulation equipment such as voltage regulators, capacitor banks, the DGs, and static var compensators. However, the rapid fluctuations and significant uncertainties arising from varying and often unpredictable load demands, renewable generations, and measurement errors pose new challenges for voltage control.

The literature on VVC problems can be categorized into model-based and model-free methods. Model-based control methods rely on detailed network simulations, incorporating factors such as line impedances, load profiles, and control device characteristics to create sophisticated models of the power distribution network. These methods include mixed-integer linear programming (MILP) [52], dynamic programming [53], mixed-integer quadratically constrained programming (MIQCP) [54], and Meta-heuristic algorithms [55-56]. Significant efforts have been put into the design of real-time VVC. [57] integrates local and remote-control mechanisms to maintain voltage stability and efficiency in the power distribution network. A reactive power control algorithm that rapidly responds to voltage fluctuations is proposed in [58]. The VVC problem is addressed by real-time reactive power control with photovoltaic inverters [59]. However, these methods come with certain limitations: 1) dependence on accurate network models, where any inaccuracies in these models can lead to suboptimal or even counterproductive control actions; 2) significant cost due to the coordination of various control devices and communication systems; 3) intensive computational complexity in large-scale ADNs.

To this end, several studies propose model-free methods for VVC, such as the alternating direction multiplier method (ADMM) [60], k-nearest neighbor (kNN) regression [61], and RL [62-63]. In particular, DRL has become increasingly popular due to its success in addressing challenging sequential decision-making problems with stable convergence results [64]. A model-free multi-agent DRL based on the forward-backward sweep method is developed in unbalanced distribution systems [65]. Considering the fast timescale continuous control devices, a Bi-level off-policy DRL [66] and a two-stage optimization framework with multi-agent DRL [67] are proposed. However, they rely on a simulated environment to train the agent, which does not guarantee the safety of the learning process. Wang et al. in [68] formulate the VVC problem as a constrained Markov decision process (CMDP) to satisfy voltage constraints in exploration. A novel approach to real-time voltage control is utilizing the Lyapunov function to ensure formal voltage stability [69]. To guarantee the final learned control policy is safe, a safety layer is added to the actor network [70]. However, they tend to overlook the issue of robustness. This is mainly due to approximation errors between the linear approximator and the actual ADN model.

Additionally, uncertainties originating from DERs, loads, and measurements contribute to the VVO problem [64]. As DER penetration increases in distribution systems, the training of DRL algorithms for VVO problems should consider the uncertainties of DERs. The modeling approaches of DER uncertainties can be classified into two categories, probabilistic approaches and nonparametric approaches. Probabilistic approaches model uncertainty as a distribution function with known mean and variance. These methods have less computational time and provide accurate empirical estimation. However, these methods require prerequisites of distribution information, and one distribution may not work for all cases [71]. The nonparametric approaches usually model DERs as inequality constraints with upper and lower limits. However, the nonparametric approaches require longer computational time. Real-world VVO uses forecasted PV generation and load for the next step's optimization. Thus, it is crucial to design an intelligent VVC algorithm that can handle uncertainties effectively.

2.6 Cybersecurity towards Load Management

The energy market for future grids with DGs will face new challenges due to the rising number of active consumers engaging in frequent buying and selling activities. The active consumers aim to optimize their energy consumption profile based on the price of electricity, consumption limits, and ramp-up/ramp-down limits. In the past, residential consumers have paid for their energy consumption at a fixed rate, while some utilities have implemented critical peak pricing. However, implementing time-varying electricity price policies will lead to a price-responsive demand [72], which requires communication infrastructures to deliver real-time price signals to consumers. Unfortunately, these communication infrastructures are vulnerable to cyberattacks that can affect the energy market or degrade the physical distribution system.

If cyber attackers have gained access to the transactive energy market, there are two methods they can use to carry out their malicious attack: 1) manipulating the electricity prices through the communication infrastructure; 2) compromising the smart meters to alter their measurements. Recently, there has been a notable increase in studies on FDI attacks, also known as data integrity attacks, in the energy market. In [73], an FDI attack against the state estimation to derive profitable financial misconduct in the energy market is presented. [74] illustrates the scheme of real-time pricing attacks as well as their impact on the demand dynamics. Authors in [75] find that an FDI attack on electricity price can have a much more severe effect on the power distribution system than an FDI attack on demand. Therefore, it's crucial to detect and mitigate such attacks and protect consumers from economic loss.

Several literatures have studied how to identify attacks and mitigate their impacts. Authors in [76] propose a defense scheme to mitigate the attack's impact by moving the equilibria quantity close to the optimal equilibrium. A game theory-based approach is presented with the costs of attacks and defenders to eliminate FDI attack threats [77]. In [78], an online anomaly detection algorithm that utilizes system information such as load forecasts and measurement data has successfully detected measurement anomalies. However, it's still impossible to know when the attackers would implement the attack and how much they would change the real-time electricity price, where consumers are still at risk of losing money.

2.7 Summary

This section introduces definitions, components, and applications of DA. Moreover, we present the overall literature review on various DA applications, illustrating the challenges arising from the growing prevalence of DERs and EVs, as well as uncertainties from load demand and cybersecurity issues. Consequently, developing advanced, reliable, robust, and intelligent algorithms and methods for distribution system protection, control and optimization within the DA framework is essential. The subsequent sections will delve into detailed model-based and machine learning-based techniques to address the above tasks.

CHAPTER 3. DYNAMIC ESTIMATION-BASED PROTECTION FOR ACTIVE DISTRIBUTION SYSTEMS

3.1 Introduction

This chapter represents a dynamic estimation-based protection (EBP) scheme for ADNs considering the power electronic interface. Section 3.2 illustrates the dynamic modeling method. Section 3.3 introduces the proposed EBP scheme. Section 3.4 displays the simulations results of the proposed EBP. Finally, section 3.5 concludes the performance and application of the proposed EBP scheme.

3.2 Dynamic Model of Distribution Systems

A distribution system consists of various devices, like transformers, distribution line sections, three-phase loads, capacitors, and inverters. A high-fidelity modeling method is proposed to represent the physical and mathematical properties of the devices [28]. In general, it starts with the physically based model referred to as the compact device model, which is a set of equations based on physical laws (e.g. KCL, KVL). After quadratization, the quadratized device model (QDM) can be described in a standard form:

$$\begin{aligned} i(t) &= Y_{eqx1}x(t) + Y_{equ1}u(t) + D_{eqxd1}\frac{dx(t)}{dt} + C_{eqc1} \\ 0 &= Y_{eqx2}x(t) + Y_{equ2}u(t) + D_{eqxd2}\frac{dx(t)}{dt} + C_{eqc2} \\ 0 &= Y_{eqx3}x(t) + Y_{equ3}u(t) + \begin{Bmatrix} \vdots \\ x(t)^T \left\langle F_{eqxx3}^{i} \right\rangle x(t) \\ \vdots \end{Bmatrix} + \begin{Bmatrix} \vdots \\ u(t)^T \left\langle F_{equu3}^{i} \right\rangle u(t) \\ \vdots \end{Bmatrix} + C_{eqc3} \end{aligned} \tag{3.1}$$

The above equations are in terms of the state vector $x(t)$, control vector $u(t)$ and through variable vector $i(t)$. All variables are in metric system (MKSA).

Using quadratic integration over two time steps to eliminate the differential terms and retains the quadratic form [79], a general syntax called state and control algebraic quadratic companion form (SCAQCF) as equation (3.2) is adopted to model all these devices in the zone.

$$\begin{gathered}
\begin{Bmatrix} i(t) \\ 0 \\ 0 \\ i(t_m) \\ 0 \\ 0 \end{Bmatrix} = Y_{eqx}\mathbf{x}\left(t,t_m\right) + \begin{Bmatrix} \vdots \\ \mathbf{x}\left(t,t_m\right)^T \left\langle F_{eqxx}^i \right\rangle \mathbf{x}\left(t,t_m\right) \\ \vdots \end{Bmatrix} - B_{eq} \\
B_{eq} = -Y_{equ}\mathbf{u}\left(t,t_m\right) - \begin{Bmatrix} \vdots \\ \mathbf{u}\left(t,t_m\right)^T \left\langle F_{equu}^i \right\rangle \mathbf{u}\left(t,t_m\right) \\ \vdots \end{Bmatrix} \\
- N_{eqx}\mathbf{x}(t-t_h) - N_{equ}\mathbf{u}(t-t_h) - M_{eq}i(t-t_h) - K_{eq}
\end{gathered} \tag{3.2}$$

where $t_m = t-h,\ t_h = t-2h.\ h$ is the time step.

A distribution system consists of various devices, like transformers, distribution line sections, three-phase loads, capacitors, and inverters. The detailed device QDMs of distribution line sections, three-phase loads, and inverters are provided in Appendix A.

3.3 Dynamic State Estimation based Protection

This section presents the procedure for creating the measurement model which is consistent to SCAQCF model in the protection zone in Figure 3.1. Note that each protection zone is designed based on the components of distribution systems. Then, DSE is proposed to compute the system's states to determine the trip decision without any other interference.

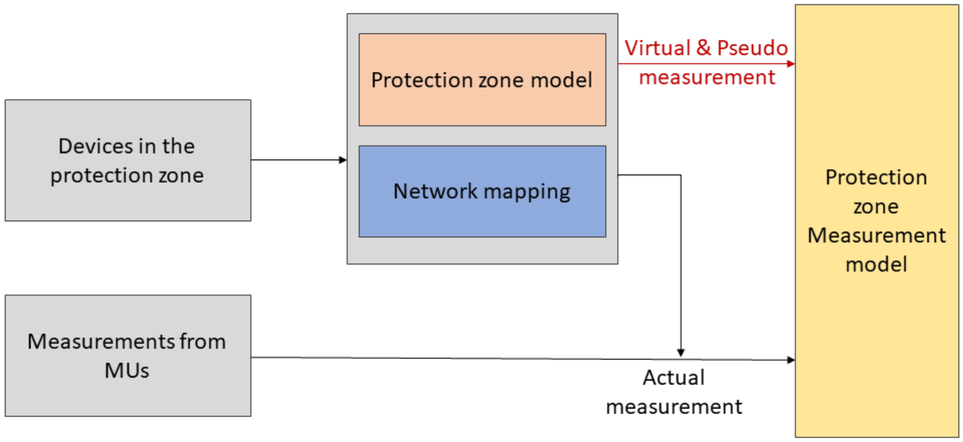

Figure 3.1 Procedure of constructing the zone measurement model

3.3.1 Measurement Model in Protection zone

As shown in Figure 3.1, the measurements are classified into three groups: a) actual measurements, collected by MUs from the field, b) virtual measurements, which represent the zero value on the left-hand side of the equations, c) pseudo measurements, which denote quantities that are typically not measured, such as current/voltage in the neutral.

A *protection zone* is a selected section of the distribution system. The protection zone may include a single device, or several components and/or breakers. An example to illustrate a distribution system with an electrical fault is shown in Figure 3.2. The illustrated section has two protection zones. Each protection zone has several power devices and several measurement sets (voltage and current) obtained from MUs.

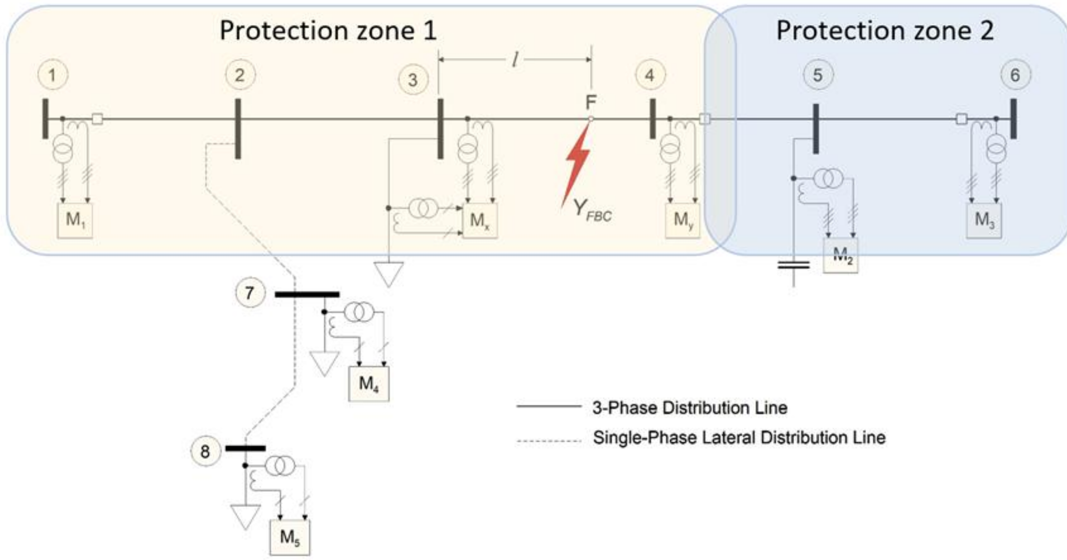

Figure 3.2 Illustration of a distribution section with a fault model

Given the actual measurements and the device SCAQCF model, the protection zone measurement model incorporating virtual and pseudo measurements can be derived as:

$$
\begin{aligned}
&z = h(x) + \eta = Y_{zx}x + \begin{Bmatrix} \vdots \\ x^T F_{zx}^i x \\ \vdots \end{Bmatrix} + B_z + \eta \\
&B_z = N_z x(t-2h) + M_z i(t-2h) + C_z
\end{aligned}
\tag{3.3}
$$

where z is the measurement vector, x is the device state vector, η represents the noise of the measurements, Y_{zx} and F_{zx}^i are the linear and nonlinear coefficient matrix, N_z and M_z are the linear coefficient matrices of past-history terms, and C_z is the constant vector.

3.3.2 Dynamic State Estimation Algorithm

Dynamic State Estimation (DSE) is a crucial process that involves real-time monitoring and estimation of the system's state variables, such as voltages, currents, and frequency, to enhance stability and reliability in smart grid. Unlike static state estimation, DSE accounts

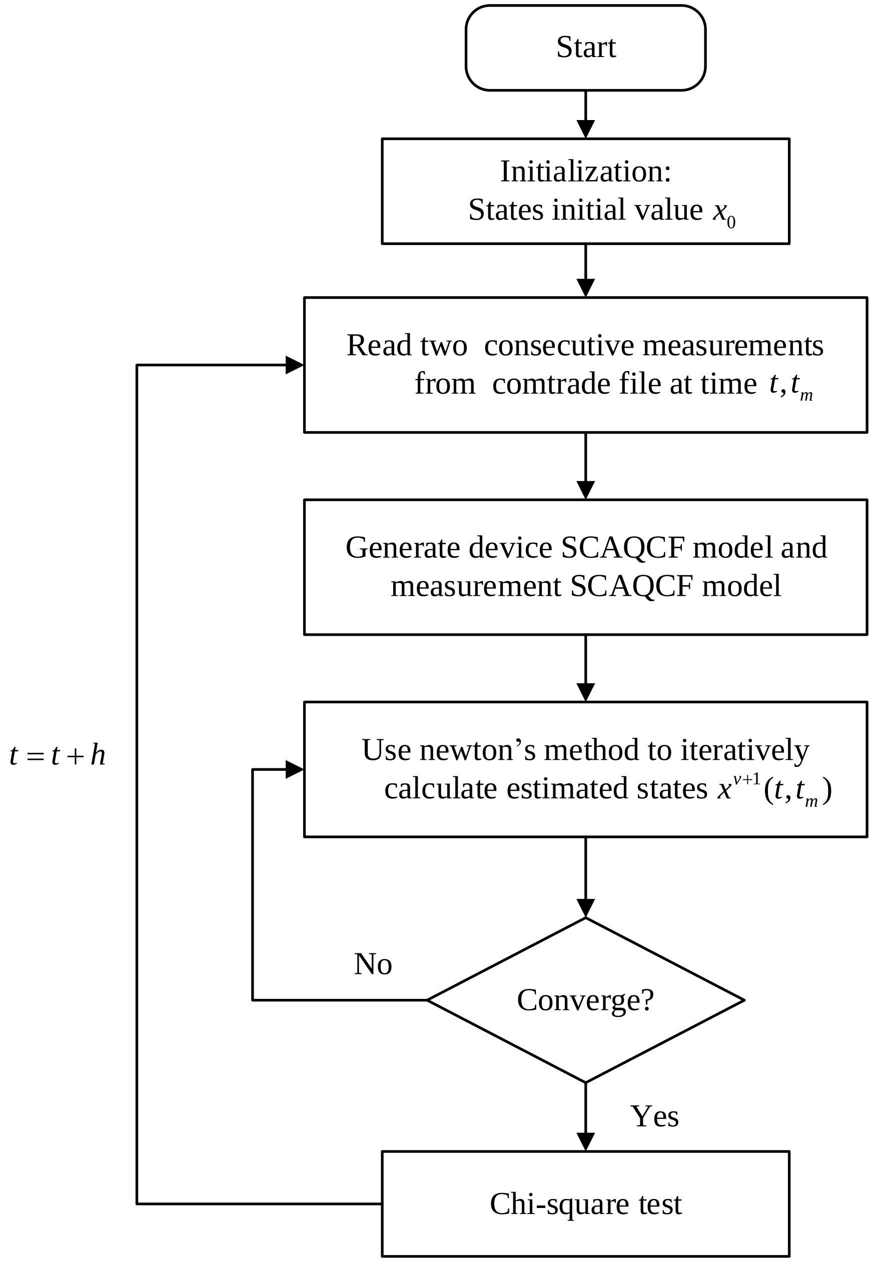

Figure 3.3 Flow chart of dynamic state estimation algorithm

for the system's dynamic behavior, capturing the rapid changes and transient events that occur due to disturbances, faults, or switching operations. The flow chart of the DSE is presented in Figure 3.3.

The weighted least squares (WLS) method is used for the state estimator, then, the objective function is defined as follows:

$$Minimize \quad J = (h(x) - z)^T W (h(x) - z) \tag{3.4}$$

where $W = diag\left\{1/\sigma_1^2, 1/\sigma_2^2, \cdots, 1/\sigma_m^2\right\}$ is the weight matrix defined as the inverse of the squared standard deviations for each measurement.

The solution is given with Newton's iterative algorithm:

$$x^{v+1} = x^v - (H^T W H)^{-1} H^T W (h(x^v) - z) \tag{3.5}$$

where $H = \dfrac{\partial h(x)}{\partial x}$ is the Jacobean matrix. At each time step of the estimation algorithm, the contributions of each measurement to the information matrix $H^T W H$ and the vector $H^T W (h(x^v) - z)$ must be computed. By updating the state x, the residuals between the measurements and the linearized measurement model are computed.

After the iteration of Newton's algorithm, the chi-square test is performed to check whether the measurements fit the system model. The goodness of fit between the model and the measurements is expressed by:

$$\xi = \sum_{i=1}^{m} s_i^2(\hat{x}) = \sum_{i=1}^{m} ((h_i(\hat{x}) - z_i)/\sigma_i)^2 \tag{3.6}$$

where ξ is the chi-square value, $\hat{x}$ is the solution of estimated state, s_i is the normalized residuals computed at the solution $\hat{x}$. Next, the confidence level is computed as:

$$\Pr[\chi^2 \geq \xi] = 1 - \Pr[\chi^2 \leq \xi] = 1 - \Pr(\xi, v) \tag{3.7}$$

where v is the degrees of the freedom, $\Pr(\xi, v)$ is the probability function.

3.3.3 Protection Logic

Trip command decision is determined based on the confidence level in the chi-square test. Two user-defined settings are defined: (a) reset time (T_r), and (b) delay time (T_d). Over a user selected interval, the trip command is obtained:

$$Trip(t) = \begin{cases} 1, & \text{if } \int_{t-T_r}^{t} \Pr(\xi, v, \tau) d\tau \geq T_d \\ 0, & \text{Otherwise} \end{cases} \tag{3.8}$$

Once the user sets up the selected parameters, this algorithm performs in real time to inspect the consistency of the measurements and the physical models.

3.4 Simulation Results of EBP

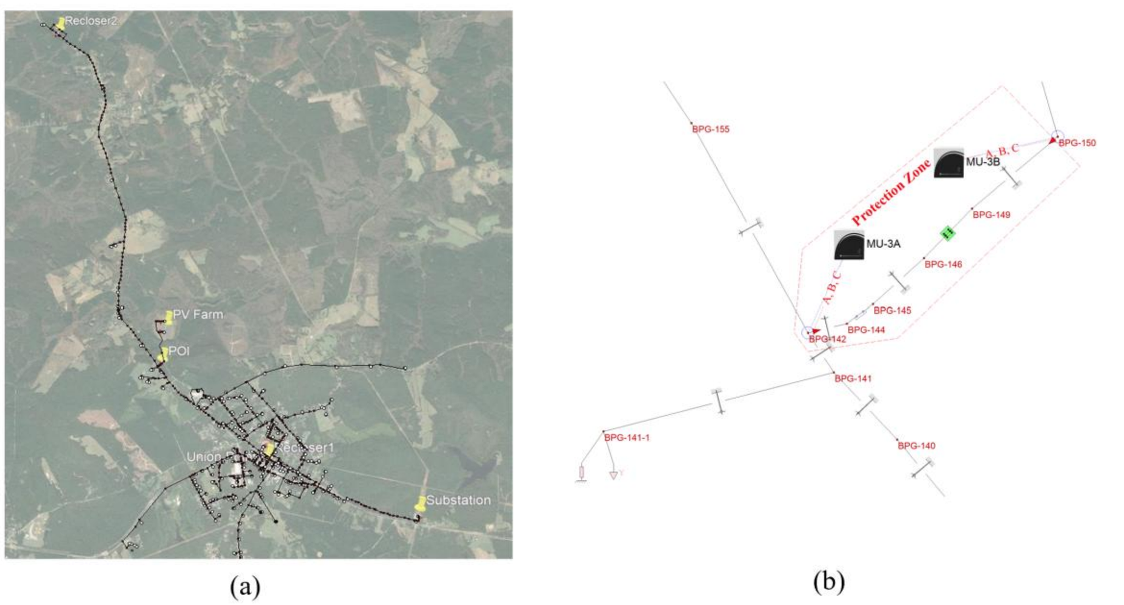

Figure 3.4 Diagram of a real-world distribution system with a solar farm, (a) overall configuration, (b) protection zone of interest at POI

Figure 3.4 (a) illustrates a real-world distribution system used to validate EBP. This system includes a 115kV/25kV substation, two reclosers, a 3MG solar farm, and a Point of

Interaction (POI). We have selected a protection zone of interest in Figure 3.4 (b) to demonstrate the simulation results. The events were simulated in WinIGS, and the EBP was implemented in WinXFM. Note that the merging unit collects 80 samples per cycle, as per standard IEC61850. The base frequency of this system is 60 Hz, which means the sampling rate is 4800 per second.

In the protection zone, MU-3A and MU-3B are installed to collect the voltage and current measurements of Bus BPG-142 and BPG-150, which means there are 12 actual measurements from MUs. As mentioned in the protection zone measurement model, the virtual and pseudo measurements are automatically formulated: 1) 131 virtual measurements (internal equations of switch, breaker, and distribution lines), and 2) 6 pseudo measurements (neutral voltage being close to zero at BPG-142, BPG-144, BPG-145, BPG-146, BPG-149, and BPG-150). In summary, there are 149 measurements and 128 states. Thus, the redundancy of the measurement model is 149/128 = 116.4%.

A). Event 1: Internal fault

A single-phase to neutral fault with 0.1 Ohms impedance is simulated at bus BPG-149. The electric fault starts at 0.5s and is cleared at 0.6s from the start of the data recording. The measurements obtained from the MUs and the results (including residuals, estimated states, confidence level, and trip command) of EBP are shown in Figure 3.5 and Figure 3.6, respectively. From Figure 3.6, we can see that the estimated states are consistent with measurements when there is no fault. However, the residuals and Chi-Square increase when the fault occurs and the confidence level drops immediately to zero at 0.5s. Thus, the proposed EBP method can detect the internal fault once it happens and create a trip command after 10ms to open the breaker.

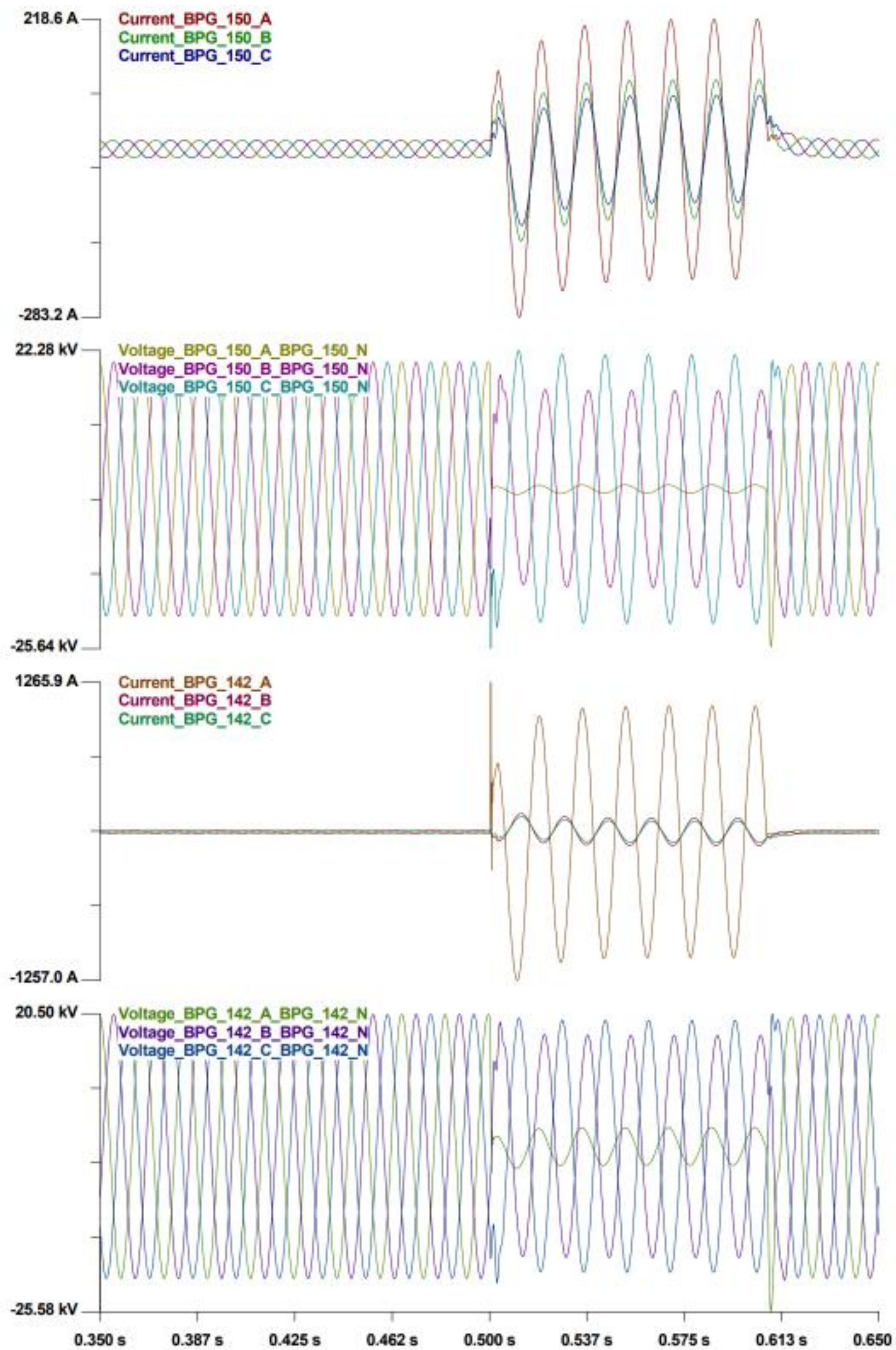

Figure 3.5 Voltage and current measurements of event 1

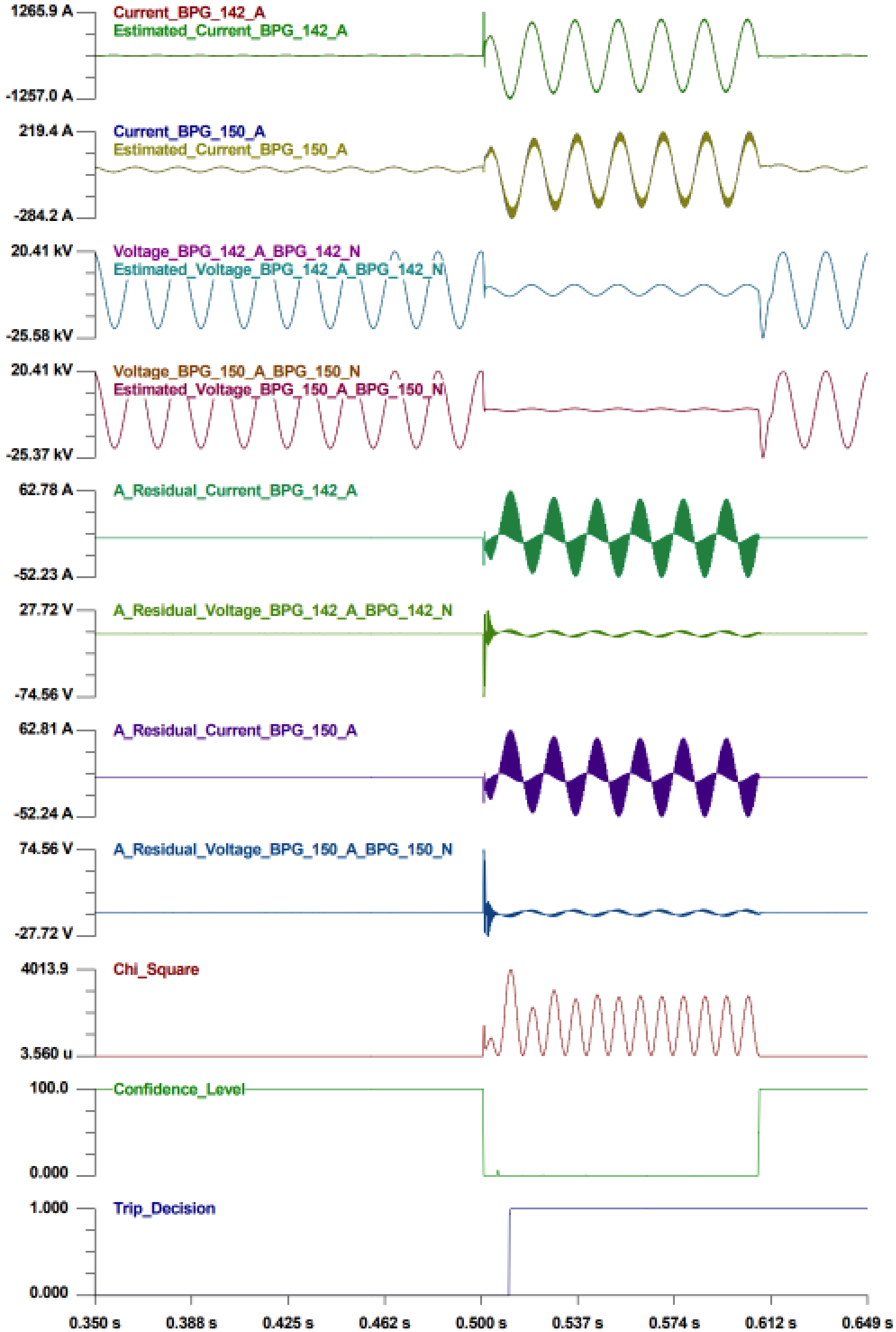

Figure 3.6 EBP results of event 1

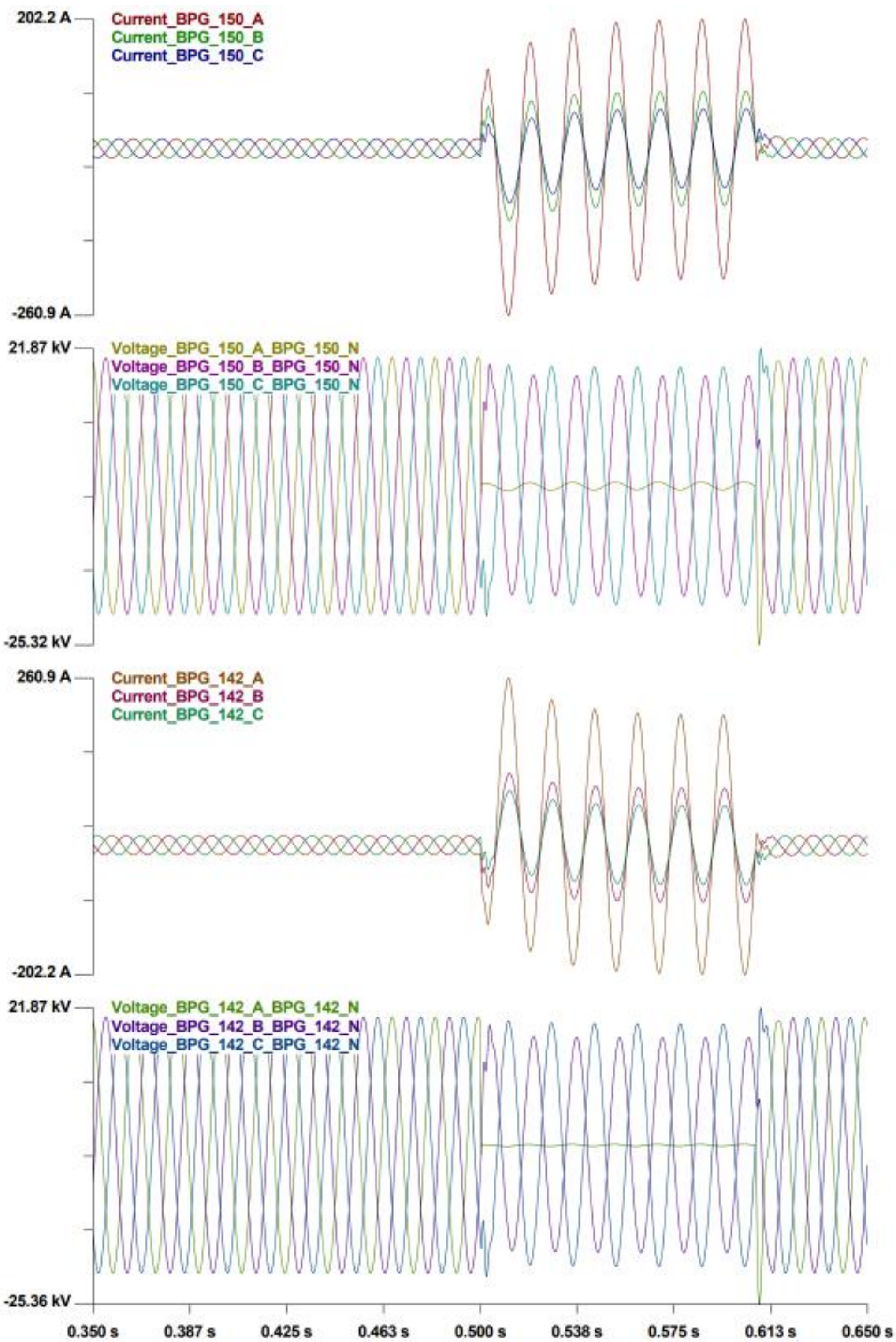

Figure 3.7 Voltage current measurements of event 2

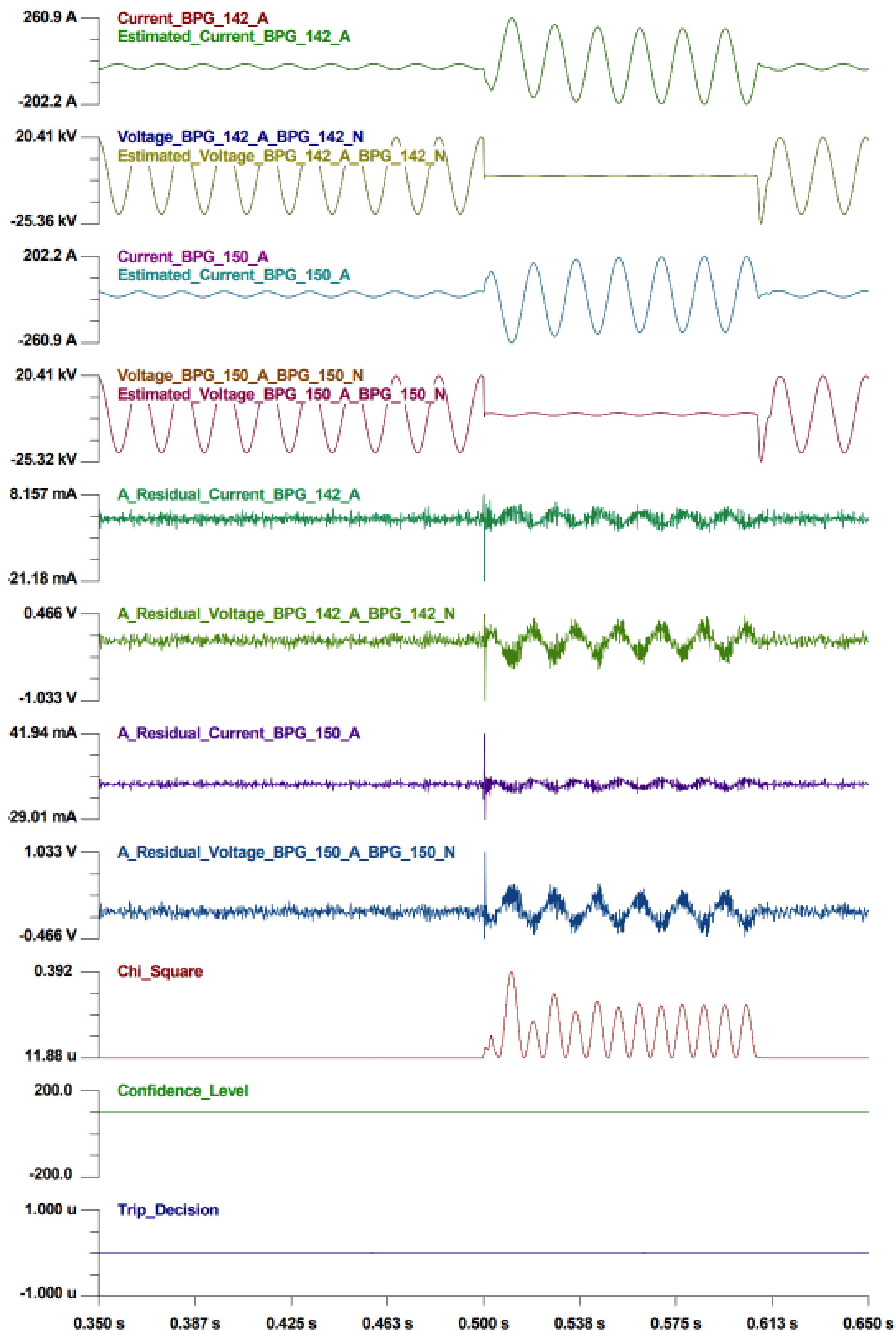

Figure 3.8 EBP results of event 2

B). Event 2: External fault

We implement a single-phase A to ground fault out of the protection zone in this event. Similarly, this fault starts from 0.5s with a duration of 0.1s. Figure 3.7 shows the collected measurements from MUs and Figure 3.8 illustrates the results of the EBP. As shown in Figure 3.8, the confidence level remains 100 % with a low residual of each state. Unlike Event 1, the residuals of voltage and current states at two sides of the protection zone are lower, and there is no trip command during this event. Thus, the external fault is successfully ignored without any misoperation.

3.5 Summary

This chapter proposes a dynamic estimation-based protection (EBP) scheme. The proposed scheme involves the modeling of distribution systems and a DSE algorithm to detect faults in the pre-determined protection zones. Extensive simulations show that this algorithm can detect the internal fault immediately with a trip command to open the breaker and identify the external fault to avoid the misoperation of the relay. In case of insufficient MUs installed in ADNs, the proposed method can still provide accurate trip command. The proposed EBP scheme is a promising solution that enables more accurate protection to handle the challenge introduced by the emerging IBRs, thus enhancing the resilience of ADNs.

CHAPTER 4. REAL-TIME FAULT DIAGNOSIS FRAMEWORK VIA DSE AND ML METHODS

4.1 Introduction

This chapter presents a real-time fault diagnosis framework, which provides accurate fault type and fault locating. Section 4.2 describes the procedure and data flow of the proposed framework. Section 4.3 introduces the DL-based fault classification model. Section 4.4 proposes the time-domain DSE-based fault locating (EBFL) algorithm. Section 4.5 shows the event studies to illustrate the effectiveness of the proposed framework. The summary of this chapter is provided in section 4.6.

4.2 Real-time Fault Diagnosis Framework

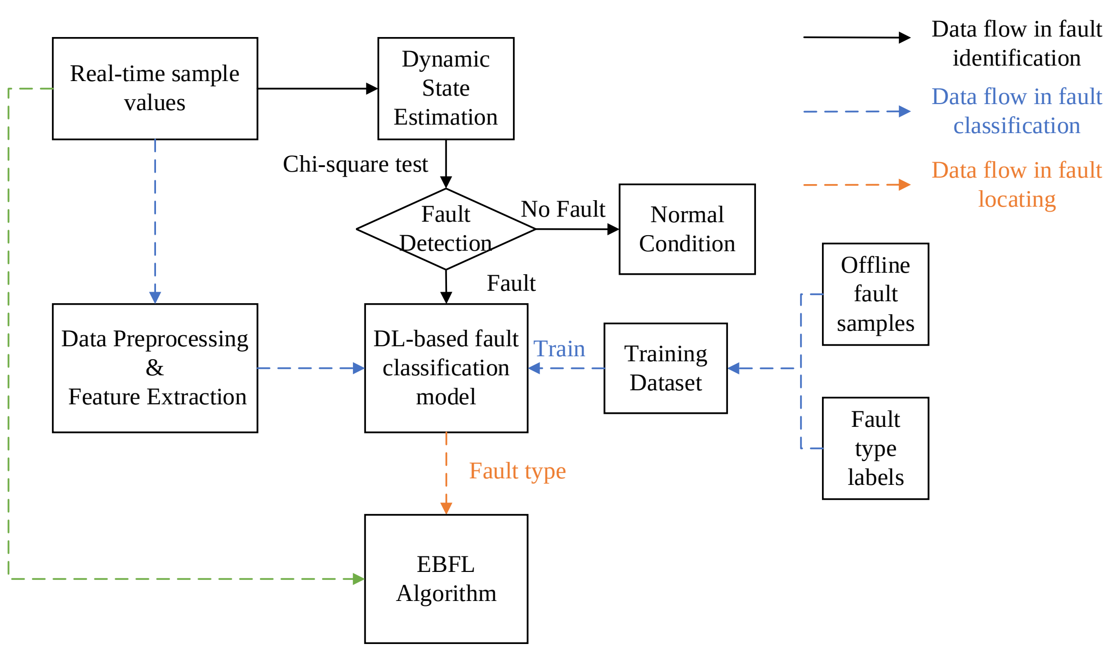

Figure 4.1 Proposed real-time fault diagnosis framework

The fault diagnosis procedure includes fault detection, classification, and locating. The DSE algorithm is used in the proposed EBP to enable proper decision-making for relays, which is equivalent to a fault detection process. Thus, the proposed real-time fault diagnosis framework focuses on fault classification via DL methods and EBFL algorithm. The structure of the proposed approach is depicted in Figure 4.1.

In Figure 4.1, the data flow is represented by three different processes: fault detection (black arrow), fault classification (blue dotted arrow), and fault locating (orange dotted arrow). We use a supervised DL model to classify faults, containing offline training and online analysis processes. Finally, the EBFL algorithm is implemented with the fault type to estimate the fault location.

4.3 DL-based Fault Classification Model

Once a fault is detected, the method proceeds to the fault classification. A 1D-CNN model is proposed to achieve the classification goal in real-time. Compared with 2D-CNN and other DL methods, this model has lower computational complexity and is more efficient for processing long sequences of real-time data. This advantage makes it more efficient for processing long sequences of real-time data. Moreover, it can automatically learn relevant features from sequential data, reducing the need for manual feature engineering.

4.3.1 CNN Model

The proposed 1D-CNN architecture for fault classification is illustrated in Figure 4.2. This model has seven hidden layers: two 1D convolution layers, two following 1D maxpooling layers, and one fully connected layer. A maxpooling layer is used after each convolution layer. After the flatten layer, a dropout layer is added to prevent overfitting by randomly dropping out a certain percentage of the neurons in a layer during training. The detailed parameters of this model are shown in Table 4.1.

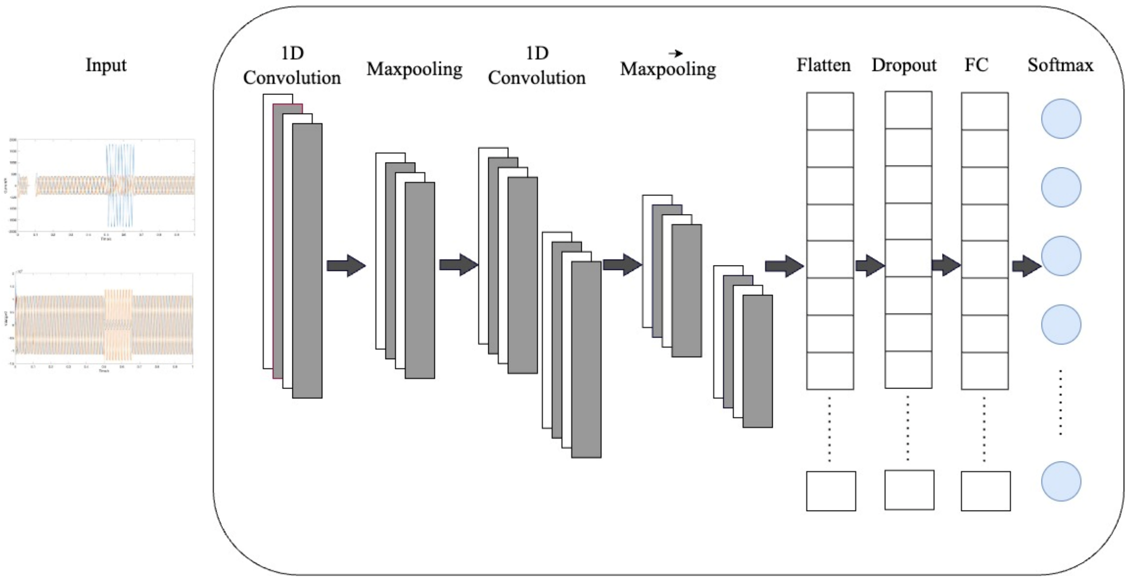

Figure 4.2 Structure of the proposed 1D-CNN model

Table 4.1 Parameters of each layer in the 1D-CNN model

Layer	Layer Type	Kernel Size	Filters	Output Size
1	1D Convolution + ReLU	3	32	10 × 32
2	Maxpooling1D	2	-	5 × 32
3	1D Convolution + ReLU	2	64	4 × 64
4	Maxpooling1D	2	-	2× 64
5	Flatten	-	-	128
6	Dropout	-	-	128
7	Fully connected	-	-	64
8	Softmax	-	-	12

4.3.2 Feature Selection and Offline Training

Feature selection: The three-phase voltage and current during the fault have contribution to the fault type classification based on the admittance differences. Consequently, the feature vector of the fault type classification is defined in (4.1).

$$\varphi = [V_{AN}^{m_i} \quad V_{BN}^{m_i} \quad V_{CN}^{m_i} \quad I_A^{m_i} \quad I_B^{m_i} \quad I_C^{m_i} \quad \ldots] \tag{4.1}$$

where $V_{AN}^{m_i}$, $V_{BN}^{m_i}$, $V_{CN}^{m_i}$ are RMS values of voltage measurements obtained from *i*-th merging unit in phase AN, BN, and CN, respectively. $I_A^{m_i}$, $I_B^{m_i}$, $I_C^{m_i}$ are RMS values of current measurements obtained from *i*-th merging unit in phase A, B, and C, respectively. The RMS values of the measurements were obtained with the following equation (phase AN is presented as an example).

$$\begin{aligned}
&v_{AN}^{m_i}(t_i); i = 1, 2, 3, \ldots, k \\
&\sum_{i=1}^{N} v_{AN}^{m_i}(t_i)\cos\omega t_i = \sqrt{2}a_1 \sum_{i=1}^{N}\cos^2\omega t_i + \sqrt{2}a_2 \sum_{i=1}^{N}\cos\omega t_i \sin\omega t_i \\
&\sum_{i=1}^{N} v_{AN}^{m_i}(t_i)\sin\omega t_i = \sqrt{2}a_1 \sum_{i=1}^{N}\sin\omega t_i \cos\omega t_i + \sqrt{2}a_2 \sum_{i=1}^{N}\sin^2\omega t_i \\
&V_{AN}^{m_i} = \sqrt{a_1^2 + a_2^2}
\end{aligned} \tag{4.2}$$

The training data is fed into the 1D-CNN model, and backpropagation is used to adjust the model's weights iteratively. To prevent overfitting, validation data is employed to monitor the model's performance during training. Early stopping may be implemented to halt the training process when validation performance no longer improves, thus avoiding excessive model complexity.

4.3.3 Classification Output

Note that at each 1D convolution layer, the ReLU activation function is utilized [80].

$$f(z^l) = \begin{cases} z^l, & \text{if } z^l \geq 0 \\ 0, & \text{otherwise} \end{cases} \tag{4.3}$$

where z^l is element of the output in the *l*-th convolutional layer.

After the softmax layer, the output for K classes is calculated as

$$z = [z_1, \ldots, z_K]^T = \sigma(\text{h}) \tag{4.4}$$

where z_K is the predicted fault type in the *k*-th category; $\sigma(\text{h})$ is the softmax function. The loss function is expressed as

$$\ell(\theta) = \frac{1}{|V|} \sum_{i \in V} \sum_{k=1}^{K} -\Gamma_k^i \log(z_k^i) \tag{4.5}$$

where $\Gamma_k^i = 1$ when *k* is the correct index of the *i*-th training sample, otherwise $\Gamma_k^i = 0$; θ is the parameters that can be learned to minimize the loss function through training set *V*.

The distribution line faults normally include single-phase, two-phase, three-phase short-circuit or grounding faults, and downed conductor fault. The fault types (totally 12 types) and corresponding class index used for fault classification is presented in Table 4.2. For example, if single phase A to ground fault is identified, the output is $z = 1$.

Table 4.2 Types of power system faults and corresponding class index

Type of Faults	Short Form (class index)
Single line to ground fault	SLG-A (1)
	SLG-B (2)
	SLG-C (3)
Double line to ground fault	DLG-AB (4)
	DLG-BC (5)
	DLG-CA (6)
Double line to line fault	DLL-AB (7)
	DLL-BC (8)
	DLL-CA (9)
Three phase line to line fault	TLL-ABC (10)
Three phase line to ground fault	TLG-ABC (11)
Single-phase downed conductor fault	SDC (12)

4.4 EBFL algorithm

The time domain EBFL algorithm is initiated upon detection of a fault power device and when the device is a transmission or distribution circuit. In general, the faulted device may be a set of distribution circuits representing a protection zone. Specifically, Appendix B represents the dynamic model of faulted lines. Note that our previous work has identified the fault type and the section of the distribution circuit where the fault is located. Subsequently the problem of fault locating is formulated as an optimization problem with an unknown that determines the location of the fault. The solution to this problem provides the location of the fault. Figure 4.3 illustrates the process.

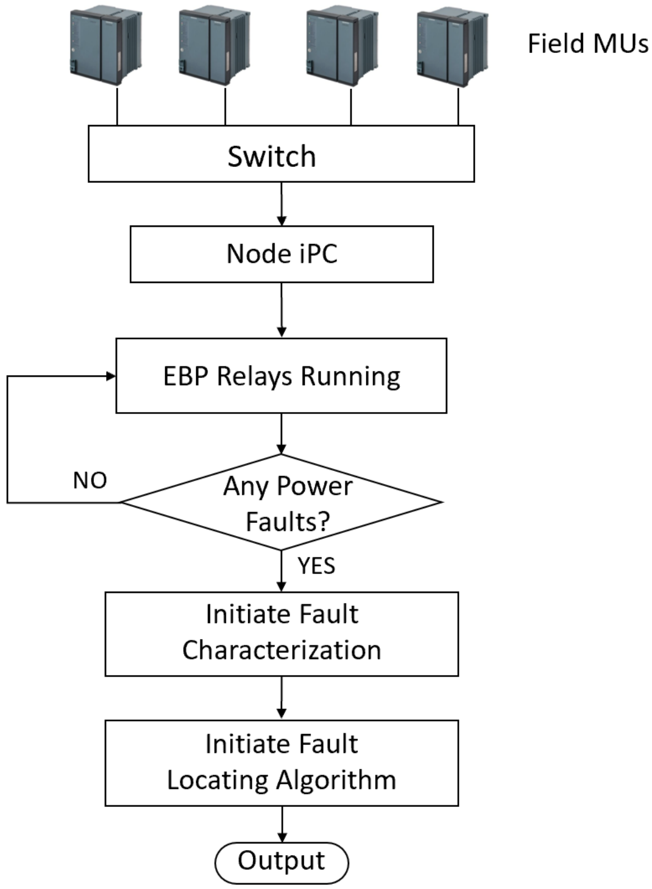

Figure 4.3 Fault locating logic

Sample value-based fault locating in the distribution system must consider the typical conditions in a distribution system. In general, the distribution system is connected to multiple loads, and devices along its length. Measurements can be distributed along with the distribution feeder. In addition, measurements can be of different technologies with widely varying accuracy.

We designate the location of the fault with the variable ℓ. The idea is to formulate the problem of fault locating as a state estimation problem, which will determine the best estimate of the fault location ℓ. Considering the system of Figure 3.2, the state of this system is defined as the voltages at each node of the system, line inductance current and the state variables that define the fault location, which is given with:

$$x = [v_{1A}(t) \quad v_{1B}(t) \quad v_{1C}(t) \quad i_{l12}^{A}(t) \quad i_{l12}^{B}(t) \quad i_{l12}^{B}(t) \quad \dots \quad \ell] \tag{4.6}$$

Let m_i denote the metering device. The set of network buses equipped with MUs is $\mathcal{D}$. The measurements set $z \in \mathbb{R}^{D}$ are represented symbolically as follows:

$$z = [V_{1AN}^{m_1}(t),\ V_{1BN}^{m_1}(t),\ V_{1CN}^{m_1}(t),\ I_{12A}^{m_1}(t), I_{12B}^{m_1}(t), I_{12C}^{m_1}(t), ...] \tag{4.7}$$

Given the actual measurements and the device SCAQCF model, the protection zone measurement model incorporating virtual and pseudo measurements can be derived as:

$$\begin{gathered} z(t,t_m) = h(x(t,t_m)) + \eta = Y_{zx}x(t,t_m) + \begin{Bmatrix} \vdots \\ x(t,t_m)^T F_{zx}^{i} x(t,t_m) \\ \vdots \end{Bmatrix} - B_z + \eta \\ B_z = N_z x(t-h) + M_z i(t-h) + C_z \end{gathered} \tag{4.8}$$

where $z(t,t_m)$ is the measurement vector, $x(t,t_m)$ is the state vector including the fault location ℓ, η represents the noise of the measurements, Y_{zx} is the linear coefficient matrix, F_{zx} is the nonlinear coefficient matrix, N_z and M_z are the linear coefficient matrices of past-history terms, and C_z is the constant vector.

A nonlinear weighted least squares state estimator (NWLS-SE) is used to obtain the best estimates of the fault location. Similarly, the objective function of this problem is:

$$Minimize \quad J = \sum_{j=1}^{k} \left(\frac{h_j(x) - z_j}{\sigma_j} \right)^2 \tag{4.9}$$

where $h_j(\cdot)$ is the dynamic model of the distribution section, k is the total number of measurements, n is the length of the state vector, σ_j is the standard deviations of j-th measurement, $\hat{l}$ is the estimate of the fault location.

The pseudo code of DSE is:

Algorithm 3.1: DSE for Fault Location

Input: SCAQCF object, W, T, z

for t=1:T **do**

  Initialize $x^0, r, it_{\max}$

  $z \leftarrow z(t, t_m)$

  while $it \le it_{\max}$ **do**

    $x^{it+1} = x^{it} - (H^T W H)^{-1} H^T W (h(x^{it}) - z)$

    $r \leftarrow W(h(x^{it+1}) - z)$

    if $r < \varepsilon$

      break

    end

    $it \leftarrow it + 1$

  end

  Output $\ell(t, t_m)$

end

4.5 Event Studies

This section presents case studies to evaluate the effectiveness of the proposed framework. We use the real-world distribution system in Figure 3.3 as the test case system. The events were simulated in WinIGS. The fault classification is implemented in TensorFlow. The EBFL algorithm was executed in MATLAB.

4.5.1 Results of Fault Classification

The number of fault samples is 16100. The dataset is split into the training set and the validation set with a 70:30 split ratio. Note that the sample rate is 4800 samples per second which is commonly used in real-time operation. Classification performance is evaluated after training the prepared dataset with the 1D-CNN model. The training and validation accuracy is measured by:

$$\text{Accuracy}=\frac{\text{Number of correct samples}}{\text{Total number of samples}} \tag{4.10}$$

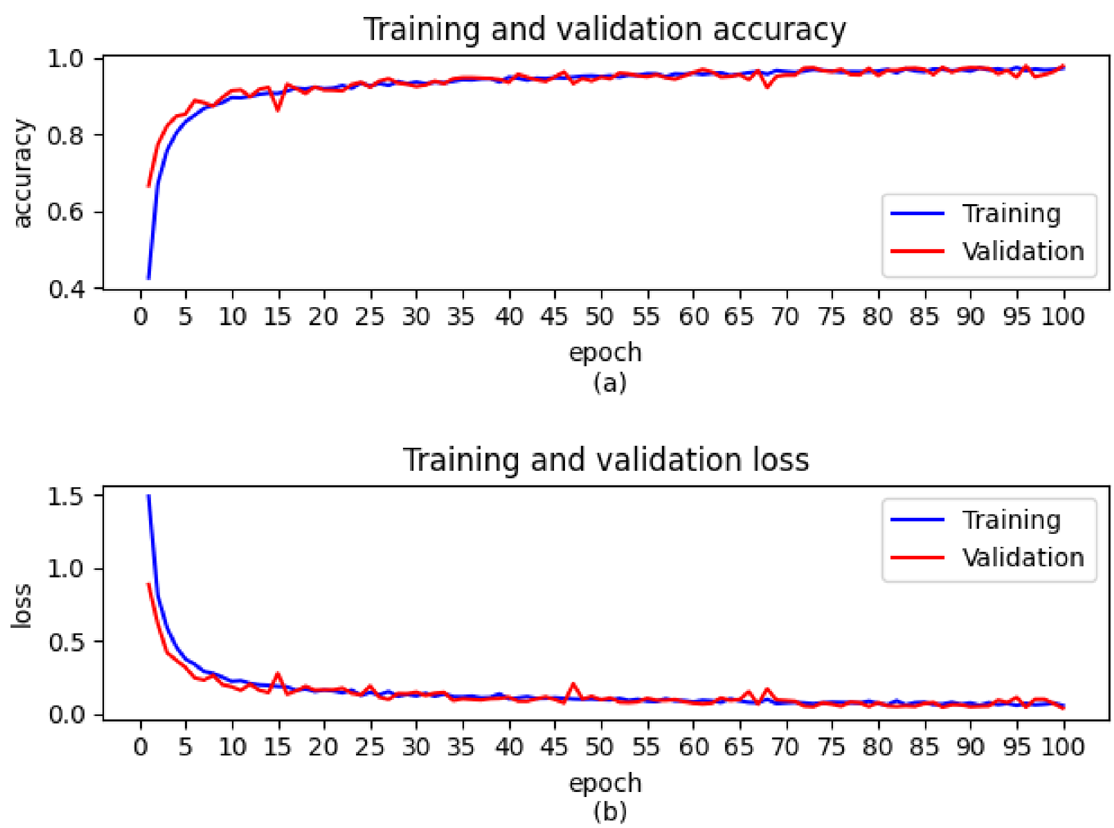

Figure 4.4 Performance of the fault classification by 1D-CNN. (a) accuracy of training and validation. (b) loss of training and validation

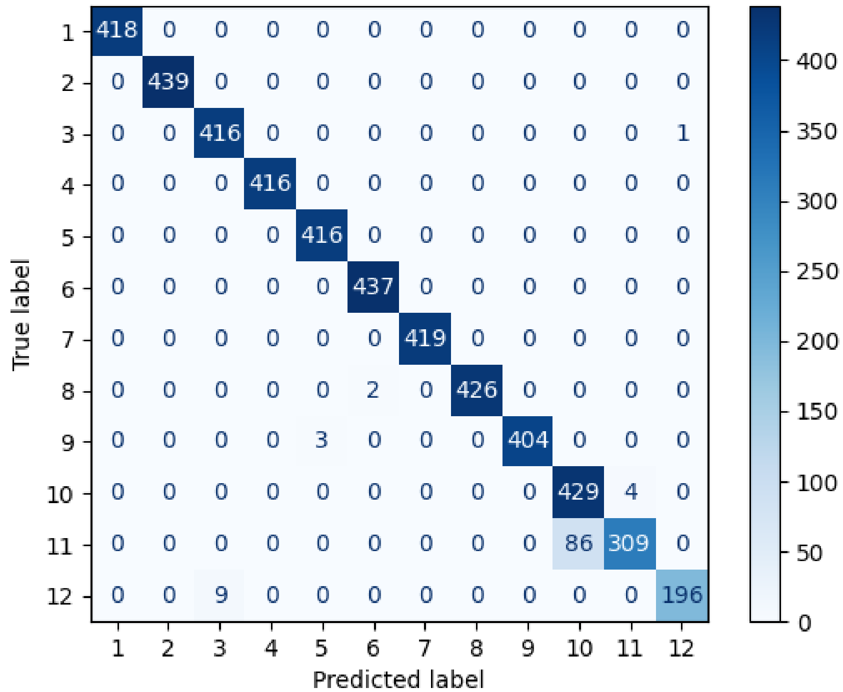

Figure 4.5 Confusion matrix of the proposed CNN

The performance and confusion matrix of the proposed CNN are depicted in Figure 4.4 and Figure 4.5, respectively. Figure 4.4 shows the mislabeled data points of CNN are minor while obtaining high accuracy and low loss at the end of the iterations. Based on the confusion matrix in Figure 4.5, 86 samples were misclassified as TLL-ABC (label 10) when they were actually TLG-ABC (label 11). The model achieved nearly 100% accuracy for all other fault types.

Three other AI (SVM, LSTM, MLP) models are implemented for comparison. The performance of different methods is listed in Table 4.3. We can see that the proposed 1D-CNN based DL method outperforms the other methods with higher accuracy above 97% with low computation cost. Thus, it can effectively process fault features and learn the feature boundary of fault classification. Moreover, the proposed DL method can be used as a fault classification tool for the power system engineer in real-time.

Table 4.3 Accuracy comparison of fault classification

Method	Training set accuracy (%)	Validation set accuracy (%)	Computation Cost/s
SVM (Support Vector Machine)	68.06	68.27	1.03
LSTM (Long Short-Term Memory)	86.06	85.10	0.32
MLP (Multilayer Perceptron)	90.53	89.49	0.22
1D-CNN (one-dimension Convolutional Neural Network)	98.27	97.83	0.29

4.5.2 Fault Events Diagnosis

After the offline training of DL model, we validate the effectiveness of the proposed framework (DSE-based fault detection and DL-based fault classification) on three different fault events of the real-world distribution system.

1) Event 1: A single-phase A to ground fault (SLG-A)

A single-phase A to ground fault with 0.1 Ohms impedance was simulated at bus BPG-146. The electric fault started at 0.5s and was cleared at 0.65s from the recording. The measurements and the results are shown in Figure 4.6. From Figure 4.6, we can see that the confidence level dropped immediately to zero at 0.5s when the fault occurred. Thus, the proposed DSE algorithm can detect the internal fault once it happens while generating a detection signal after 10ms. Note that this delay was caused by the delay time defined by users. Then, the proposed CNN model fit the sample data and output the classification result (fault type 1) that was consistent with the true fault type.

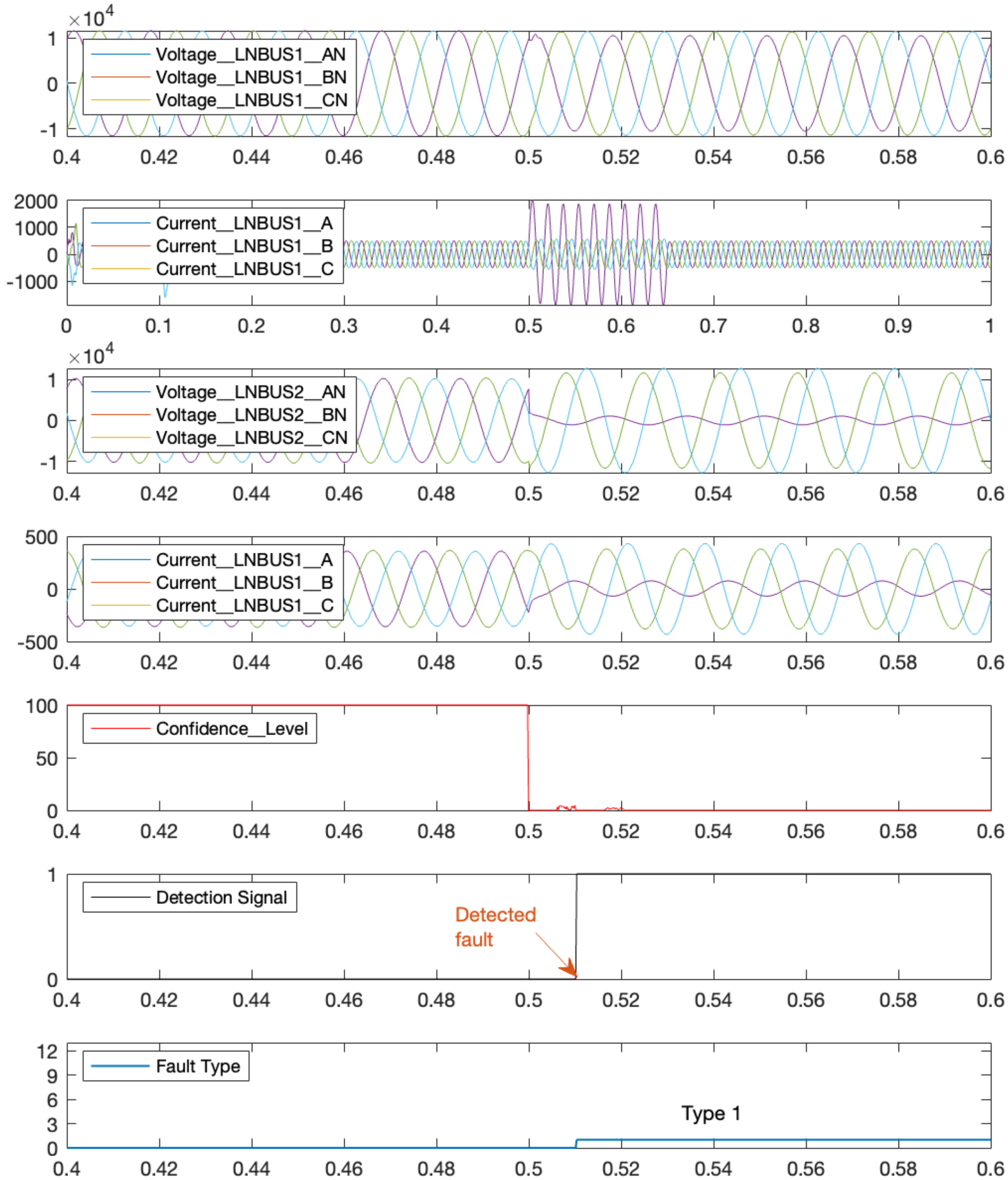

Figure 4.6 Measurements and results of event 1

2) Event 2: Downed conductor fault (SDC)

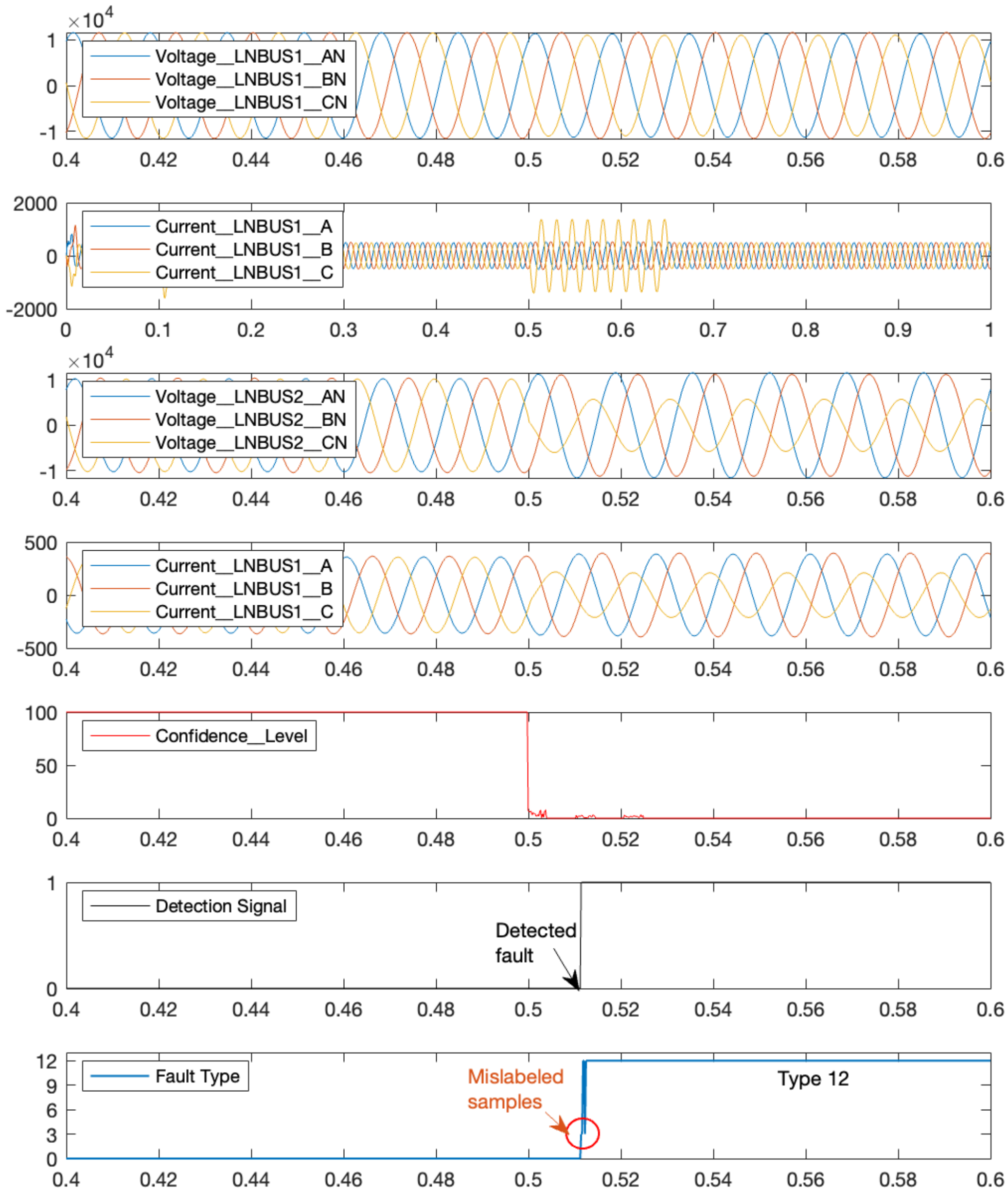

Figure 4.7 Measurements and results of event 2

A single-phase downed conductor fault was simulated at the same location. Similarly, this fault started from 0.5s with a duration of 0.15s. Figure 4.7 shows the results of fault diagnosis. When the fault occurred, it was the disturbance of measurement data that contributed to the fluctuation of confidence level. Still, the proposed DSE algorithm can detect the internal fault once it happens while generating a detection signal. In Figure 4.7, there are two mislabeled samples with predicted type 3 that can be ignored due to bad data or disturbance. On the other hand, the proposed model obtained the correct fault type 12 for all other samples.

3) Event3: External Fault

In this event, a three-phase line-to-line fault with 0.1 Ohms impedance is simulated out of the protection zone at BPG-123. Similarly, this fault started from 0.5s with a duration of 0.15s. Figure 4.8 shows the collected measurements from MUs. Although there were voltage and current fluctuations in the protection zone, the DSE would identify it as an external fault without any detection signal. Unlike Event 1 and Event 2, the confidence level of this event remained 100%. Thus, it indicated that the system was under normal conditions, and the external fault was ignored without any mis-operation.

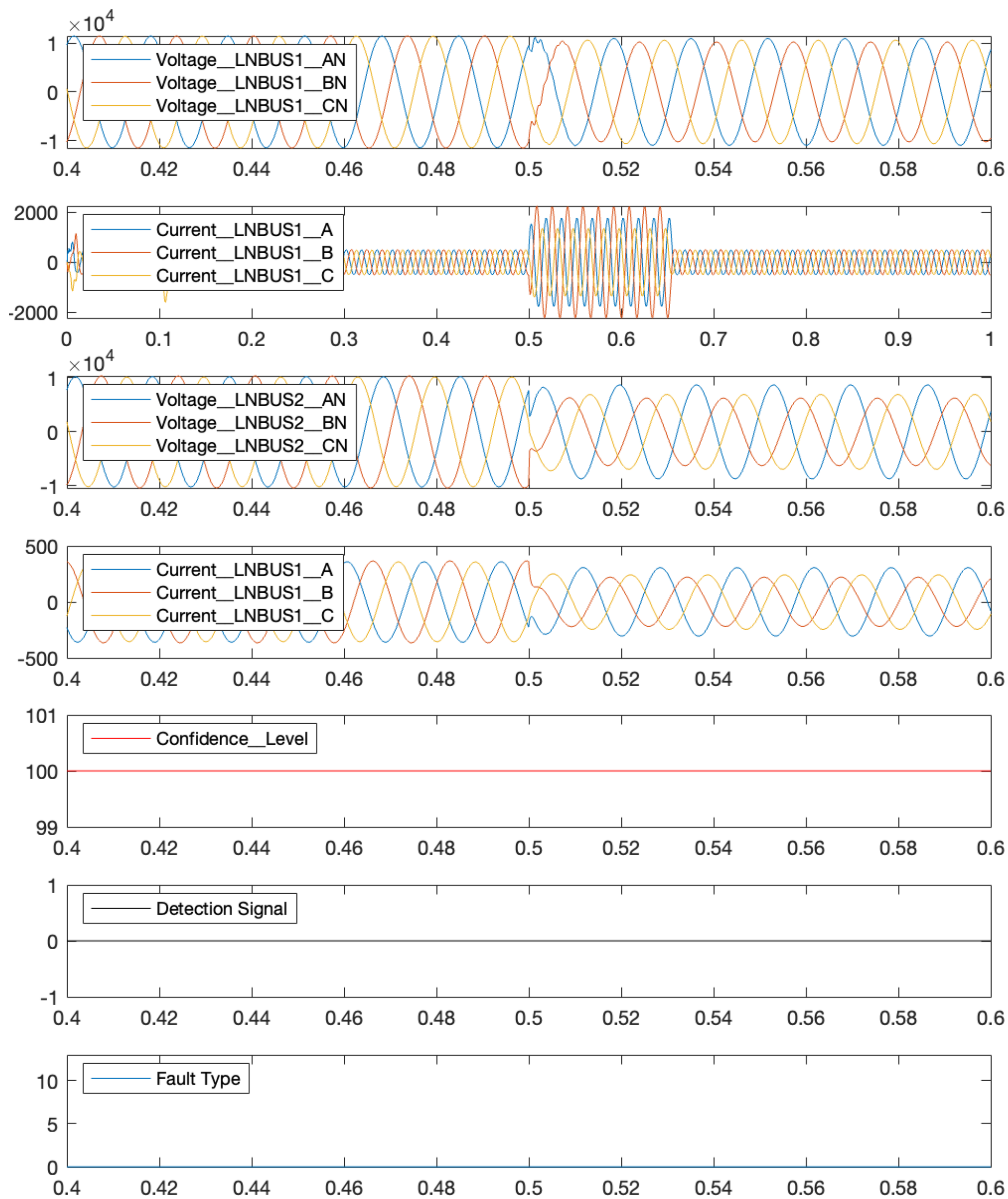

Figure 4.8 Measurements and results of event 3

4.5.3 Results of Fault Locating

The real-world distribution system in Figure 3.3 (a) is used for testing the proposed fault location method in time domain. Specifically, we tested four different scenarios with a fault along the line from BPG-149 to BPG-150 (total length is 2miles) as follows.

- **Scenario A1**: 0.1 ohms bolted phase A-N fault, 0.8 miles from BPG-149.
- **Scenario A2**: 10 ohms impedance phase A-N fault, 0.8 miles from BPG-149.
- **Scenario A3**: 10 ohms impedance phase A-N fault, 1.6 miles from BPG-149.
- **Scenario A4**: 10 ohms impedance phase A-B fault, 1.6 miles from BPG-149.

Figures 4.9 (a)-4.9 (d) depict the fault location results of the proposed method under different scenarios. Additionally, the absolute errors between the estimated and actual value of fault location in these scenarios are shown in Figures 4.10 (a)-4.10 (d). From Figure 4.9 and Figure 4.10, we can observe that the proposed DSE method converges within a few steps, and the absolute estimation error is within an acceptable range. Figure 4.9 (b) and Figure 4.10 (b) show that Scenario A2 has the best performance regarding the absolute error. Even the worst case, Scenario A1, has an absolute estimation error of less than 1%. Furthermore, it can be inferred that higher fault impedances do not lead to increased errors. Moreover, the proposed method has proven effective for different fault types, as observed from Scenario A3 and A4 results. These results indicate that the proposed approach is appropriate for accurately locating faults in real-time distribution systems.

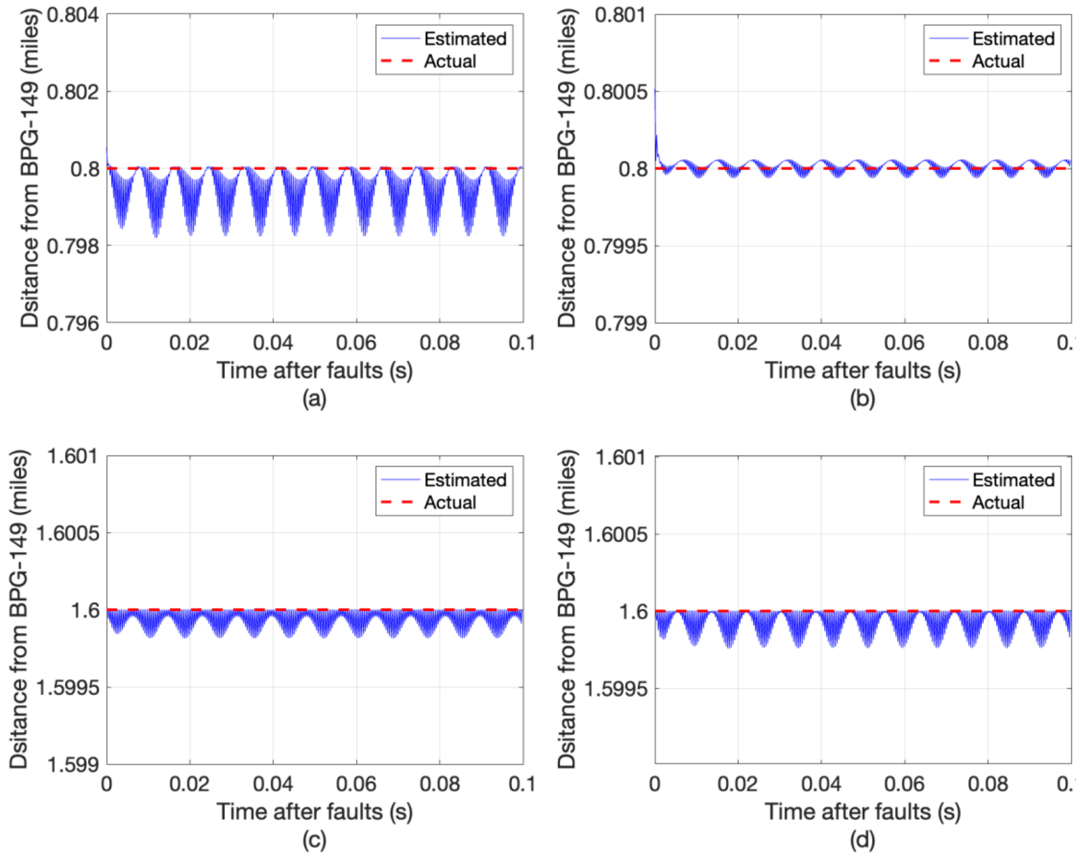

Figure 4.9 Fault location results under various scenarios. (a) Scenario A1; (b) Scenario A2; (c) Scenario A3; (d) Scenario A4

To investigate the impact of measurement errors on the proposed methodology, simulated cases have added mean-zero Gaussian noise with 5% and 6% maximum errors of current and voltage measurements, respectively.

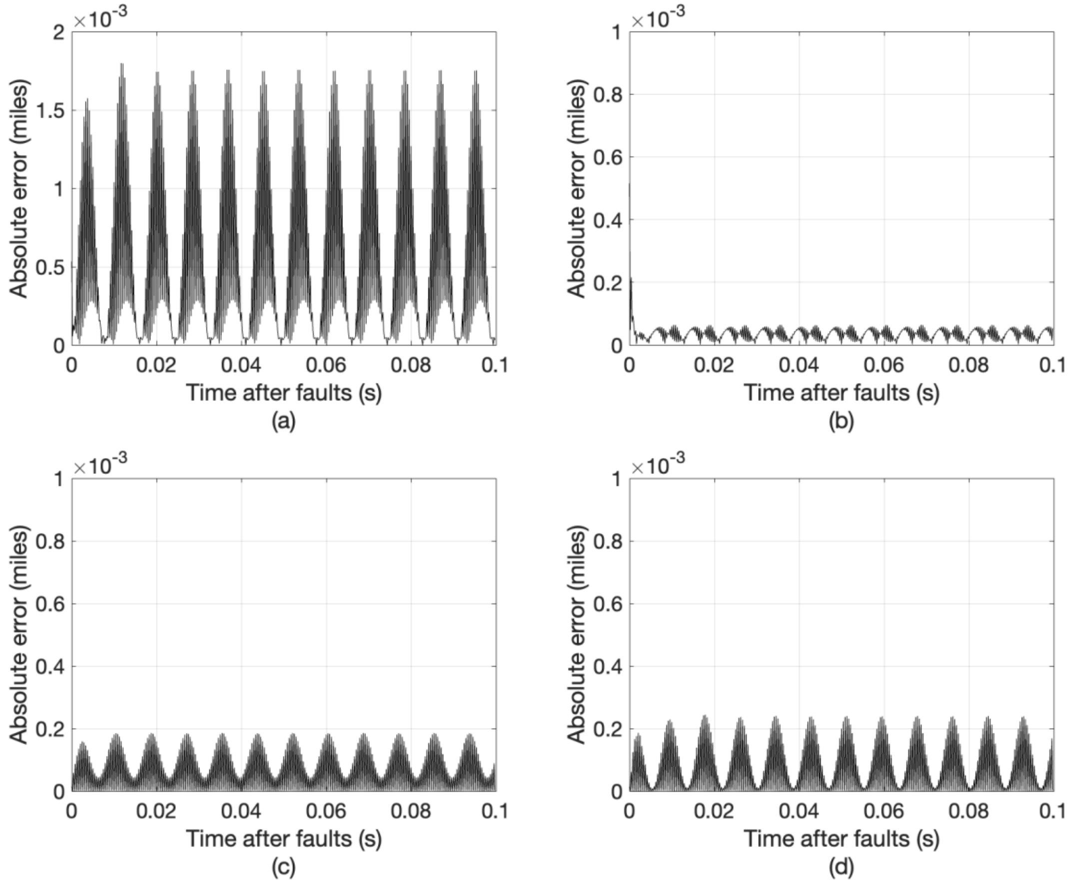

Figure 4.10 Absolute error of various scenarios. (a) Scenario A1; (b) Scenario A2; (c) Scenario A3; (d) Scenario A4

The accuracy of the fault locating method is represented by absolute percentage error (APE):

$$\text{APE} = \left| \frac{l_F - \hat{l}_F}{l_F} \right| \times 100 \tag{4.11}$$

where l_F and $\hat{l}_F$ represent actual and estimated fault location, respectively.

Table 4.4 presents the results of the fault location analysis under two conditions: with and without the presence of measurement noise. This table provides a clear comparison of the fault location performance under both conditions, which shows the proposed method is robust in the presence of measurement noise. Even in the worst-case scenario A1, the APE is only 0.1224%. This indicates that the proposed fault location method has significant potential for real-world applications in distribution systems.

Table 4.4 Results of fault location with measurement noise

Normal Condition			Under Measurement Noise		
Scenario	**Estimated (miles)**	**APE(%)**	**Scenario**	**Estimated (miles)**	**APE(%)**
A1	0.799523	0.0596	A1	0.799021	0.1224
A2	0.800016	0.0020	A2	0.799938	0.0078
A3	1.599844	0.0098	A3	1.599806	0.0121
A4	1.599740	0.0163	A4	1.599697	0.0189

4.6 Summary

This chapter proposes a real-time fault diagnosis framework, which is crucial for maintaining the stability and reliability of ADNs. This data-driven approach analyzes fault information based on recorded measurements from MUs, making it potential for radial distribution systems. Extensive simulations verify the accuracy, efficiency, and robustness of this framework under various fault scenarios, including measurement noise. By focusing on real-time fault diagnosis, this chapter addresses the immediate response to disturbances or faults in the system, a critical aspect of any resilient electrical grid. Thus, this chapter is essential as it sets the stage for understanding how quick response mechanisms and accurate fault diagnosis contribute to the overall robustness of ADNs.

CHAPTER 5. ROBUST REINFORCEMENT LEARNING FOR VOLT-VAR OPTIMIZATION ON DISTRIBUTION SYSTEMS

5.1 Introduction

This chapter introduces a robust deep reinforcement learning (RDRL) framework for Volt-VAR optimization (VVO) in active distribution systems. Unlike other DRL methods for VVO, we consider power injection uncertainties from DERs and load, modeled as adversarial attacks, to ensure safe exploration across action spaces. Section 5.2 covers the basics of reinforcement learning (RL). Section 5.3 presents the general mathematical model of the VVO problem with fast timescale and slow timescale voltage regulation equipment. Section 5.4 outlines the proposed RDRL framework, including RDRL design, uncertainty set quantification, and the proposed robust DDPG algorithm. Section 5.5 demonstrates the numerical results of training and online testing. Finally, section 5.6 concludes the proposed RDRL framework.

5.2 Preliminary

RL is a type of machine learning where agents learn to make decisions to maximize the cumulative reward with the interaction of the environment. Exploitation of maximum reward draws a line between reinforcement learning and classical machine learning settings including supervised and unsupervised learning. Unlike unsupervised learning, RL assumes supervision, which, similar to labels in data for supervised learning, makes it well-suited for real-world decision-making tasks in dynamic and uncertain environments.

Mathematically, the decision-making problem is represented as a Markov Decision Process (MDP), denoted as a tuple $(\mathcal{S},\mathcal{A},\mathbb{T},r,\gamma)$. Specifically, $\mathcal{S}$ is the state space; $\mathcal{A}$ is the action space, which can be discrete or continuous. $\mathbb{T}$ is the transition probability $p\left(s' \middle| s,a\right)$, where $s,s' \in \mathcal{S}, a \in \mathcal{A}$. r is the reward function and $\gamma \in (0,1)$ is the discount factor. As depicted in Figure 5.1, the environment starts with an initial state s_0. At each time $t = \{0,1,\ldots\}$, the agent chooses action a_t based on the current state s_t and the policy $\pi(a \mid s)$, and subsequently receives a reward r_t. The next state s_{t+1} is randomly generated from the transition function $p(s' \mid s,a) = \Pr(s_{t+1} = s' \mid s_t, a_t)$. In most practical problems, the interaction process will come to some sort of an end with a finite length T to reset the environment back to s_0 to start a new interaction. Such interaction cycle from s_0 to the final state is called an episode. Note that the episode length T may vary, but the episodic property holds if the interaction ends after a set maximum time $T_{\max}$.

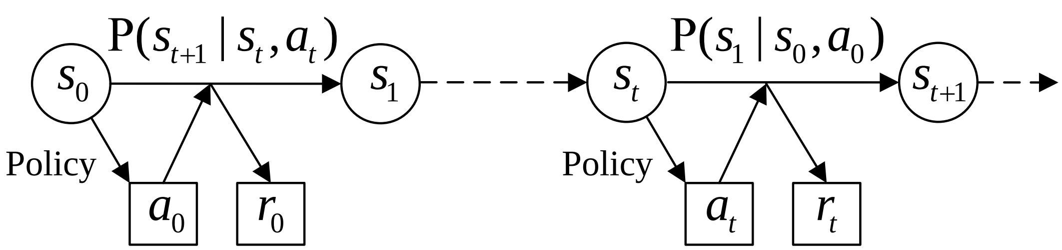

Figure 5.1 Illustration of a Markov decision process

In RL, the agent aims to maximize a cumulative reward during one episode. This cumulative reward, referred to the return, can be expressed as a summation of all received reward signals as follows:

$$R = \sum_{t=1}^{T} r_t \tag{5.1}$$

A policy $\pi(a \mid s): \mathcal{S} \to \mathcal{A}$ is a map from the state to a distribution on the action space, which determines the best action to a given state s. The policy can be deterministic or stochastic, depending on how actions are chosen based on the current state. From the probabilistic perspective, the trajectory distribution can be expressed as:

$$\mathcal{T}_\pi = \prod p(s_{t+1} \mid s_t, a_t)\pi(a_t \mid s_t) \tag{5.2}$$

For given MDP and policy, the discounted expected reward is defined as:

$$J(\pi) = \mathbb{E}_{\mathcal{T}_\pi} \sum_{t=0} \gamma^t r_{t+1} \tag{5.3}$$

The goal of the RL agent is to find an optimal policy π^*, which maximizes the discounted expected reward:

$$\pi^* \in \arg\max_\pi J(\pi) = \mathbb{E}_{\mathcal{T}_\pi} \sum_{t=0} \gamma^t r_{t+1} \tag{5.4}$$

To estimate the efficacy of an agent using a policy π to visit state s, the value function is defined as:

$$V^\pi(s) = \mathbb{E}_{\mathcal{T}_\pi \mid s_0 = s} \sum_{t=0} \gamma^t r_{t+1} \tag{5.5}$$

Similarly, the Q-function is introduced to provide more information about transition probabilities (identify what the state may be the environment's response on certain action in a given state), which is denoted as:

$$Q^\pi(s,a) = \mathbb{E}_{\mathcal{T}_\pi \mid s_0 = s, a_0 = a} \sum_{t=0} \gamma^t r_{t+1} \tag{5.6}$$

By recalling interconnection between value function and Q-function, the *Bellman Equation* in (5.7) shows a recursive relation to compute Q-value.

$$Q^\pi(s,a) = r(s,a) + \gamma \mathbb{E}_{s' \sim \mathbb{P}(\cdot \mid s,a), a' \sim \pi(\cdot \mid s')} Q^\pi(s', a') \tag{5.7}$$

By substituting the optimal (deterministic) policy $\pi^* = \arg\max_a Q^*(s,a)$, we can obtain the *Bellman Optimality Equation*:

$$Q^*(s,a) = r(s,a) + \gamma \mathbb{E}_{s' \sim \mathbb{P}(\cdot|s,a)} \max_{a' \in \mathcal{A}} Q^*(s',a') \tag{5.8}$$

Based on the *Bellman Optimality Equation* in (5.8), the optimal Q-function Q^* and an optimal policy π^* can be solved using dynamic programming (DP) or linear programming (LP) [81].

5.3 VVO in Active Distribution Network

This section introduces the power flow model and problem statement of VVO, using slow time-scale regulation equipment (e.g. regulators and capacitor banks) and fast time-scale regulation equipment (e.g. inverters). Moreover, we reformulate the optimization problem for VVO under uncertainties from load and DERs.

5.3.1 Power Flow Model

We consider an ADN as an undirected graph $\mathcal{G} = (\mathcal{N}, \mathcal{E})$, which consists of a set of nodes $\mathcal{N} = \{0,1,\ldots,n\}$ and a set of branches $\mathcal{E} = (i,j) \in \mathcal{N} \times \mathcal{N}$. Node 0 represents the substation. We use $\mathcal{N}_s$ to denote the set of nodes excluding the substation node. Figure 5.2 presents a 5-bus active distribution network. Let $s_i = p_i + \mathrm{i}q_i$ be the complex power injection on bus i. Also, let v_i denote the voltage magnitude of bus i.

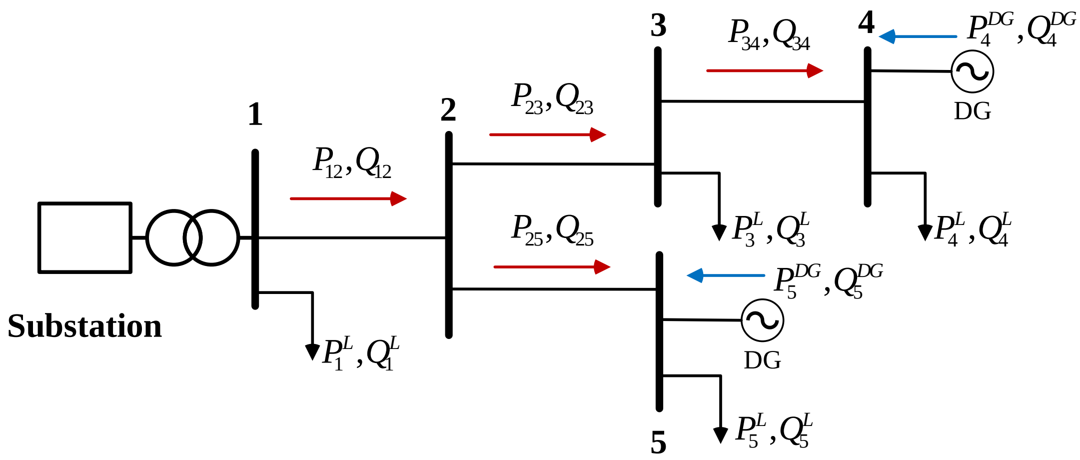

Figure 5.2 A 5-bus radial active distribution network

The power flow equations are as follows:

$$\begin{aligned} p_i &= P_i^G - P_i^L = \sum_{j=1}^{n} |v_i||v_j|[G_{ij}\cos\theta_{ij} + B_{ij}\sin\theta_{ij}] \\ q_i &= Q_i^G - Q_i^L = \sum_{j=1}^{n} |v_i||v_j|[G_{ij}\sin\theta_{ij} - B_{ij}\cos\theta_{ij}] \end{aligned} \tag{5.9}$$

where G_{ij} / B_{ij} represent the real/imaginal parts of the admittance between node i and node j. $\theta_{ij} = \theta_i - \theta_j$ is the phase angle difference between node i and node j. P_i^G / Q_i^G are active/reactive power injection from substation or distributed generation (DG) at node i. P_i^L / Q_i^L are active and reactive power injection from load demand at node i.

The total active and reactive power losses of the system can be calculated by

$$\begin{aligned} P_{loss} &= \sum_{(i,j)\in\mathcal{E}} G_{ij}(v_i^2 + v_j^2 - 2v_i v_j \cos\theta_{ij}) \\ Q_{loss} &= \sum_{(i,j)\in\mathcal{E}} -B_{ij}(v_i^2 + v_j^2 - 2v_i v_j \cos\theta_{ij}) \end{aligned} \tag{5.10}$$

5.3.2 VVO Problem Formulation

Three types of voltage regulation devices are considered: 1) voltage regulator; 2) capacitor bank; 3) smart inverter. We assume that a voltage regulator is installed at the substation. Thus, the reference voltage of the network for discrete time step t is expressed as:

$$v_t^0 = 1\text{p.u.} + u_t^{reg} \cdot M^{reg} \tag{5.11}$$

where u_t^{reg} is the tap position, M^{reg} is the fixed step size.

Similarly, the reactive power output of the capacitor bank at bus i can be computed by

$$q_t^{i,cap} = u_t^{cap} \cdot M^{cap} \cdot (v^i)^2 \tag{5.12}$$

We assume that smart inverters utilize the reactive power control strategy and that the active power outputs of DGs are known. Let $q_t^{i,DG}$ be the reactive power of the DGs regulated by inverters at bus i. Such injected or absorbed reactive power by inverters can be expressed as the following constraint. For example, if the maximum complex power $s_t^{i,DG}$ is 1.1 p.u. of the rated active power, the reactive power output should be no larger than $0.4\left|p_t^{i,DG}\right|$.

The goal of VVC is to regulate the voltage magnitude to the nominal values or stay within an acceptable interval while minimizing the network losses. Thus, the VVC problem can be formulated as an optimization problem with the objective function as follows,

$$
\begin{gathered}
\min f = C_p P_{loss,t} + C_v \sum_{i \in \mathcal{N}} \left[\mathbb{I}\left(v_{i,t} > \overline{v}\right) + \mathbb{I}\left(v_{i,t} < \underline{v}\right) \right] \\
\text{s.t. (5.9)-(5.12)} \\
q_t^{c,i} = q_t^{i,cap} + q_t^{i,DG} \\
\left| q_t^{i,DG} \right| \le \sqrt{\left(s_t^{i,DG}\right)^2 - \left(p_t^{i,DG}\right)^2} \\
\underline{v}^i \le v_t^i \le \overline{v}^i
\end{gathered}
\tag{5.13}
$$

where $P_{loss,t}$ is the active power loss of the network at time t. $\mathbb{I}(.)$ is the indicator functions with 1 for true and 0 otherwise, $v_{i,t}$ denotes a tuple of single-phase voltage magnitude $\left[v_{i,t}^a, v_{i,t}^b, v_{i,t}^c\right]$. C_p and C_v are the active power loss cost and the voltage violation cost when the voltage magnitude of any bus falls outside the acceptable range $[\underline{v} = 0.95\text{p.u.}, \overline{v} = 1.05\text{p.u.}]$, respectively.

5.3.3 Power Injection Uncertainty

VVO computes control settings for a snapshot of the system using forecasted complex loads and active power generation from PVs. These forecasts have some uncertainty, called forecast-type uncertainty, which is the difference between actual and forecasted values. It is essential to note that the VVO system's performance may worsen if the power injections deviate from their forecasted values between the control set-points in the field. This deviation could cause the voltages to operate outside their designated boundaries, leading to practical problems.

Generally, load demand uncertainty can be modeled using the Gaussian probability density functions (PDFs) as follows:

$$
f(S_L \,|\, \mu_L, \sigma_L^2) = \frac{1}{\sqrt{2\pi\sigma_L}} \exp\left[-\frac{(S_L - \mu_L)^2}{2\sigma_L^2} \right] \tag{5.14}
$$

where S_L is the complex power of the load demand. σ_L and μ_L are the standard deviation and mean of the load demand, respectively.

The lognormal probability density is an efficient and precise way to express the distribution of solar irradiance. The PDF of solar irradiance ϕ_s with standard deviation of σ_s and a mean value of μ_s can be computed by

$$f(\phi_s \left| \mu_s, \sigma_s^2 \right.) = \frac{1}{\sqrt{2\pi\sigma_s}} \exp\left[-\frac{(\log(\phi_s) - \mu_s)^2}{2\sigma_s^2} \right] \quad \forall \phi_s > 0 \tag{5.15}$$

The amount of power a PV system generates depends on several factors, including solar irradiance, the location and angle of installation, and the ambient temperature [82]. However, without access to solar farms or small-scale PV plants, obtaining this information can be challenging. To model the uncertainties, we use historical load and PV output records datasets to compute the prediction interval for the forecasted complex loads and active power generation from PVs.

The uncertainty sets of load and PV generation are represented as $\mathbb{U}_L$ and $\mathbb{U}_{PV}$, respectively. To handle such uncertainties, the VVO problem in (5.13) can be rewritten as the min-max optimization problem given by

$$\begin{aligned} \min_{u} \max_{S_L \in \mathbb{U}_L, P_{PV} \in \mathbb{U}_{PV}} & J = f(x, u \mid S_L, P_{PV}) \\ \text{s.t. } & h(x) = 0 \\ & g(x) \geq 0 \end{aligned} \tag{5.16}$$

where u is the control vector of voltage regulation devices. $h(x)$ and $g(x)$ are equality and inequality constraints in (5.13).

5.4 Robust Reinforcement Learning for VVO

This section proposes a robust VVO method where this decision-making problem is modeled as the adversarial state MDP (ASMDP) to handle uncertainties. Next, we present the design of RDRL with the proposed robust DDPG algorithm.

5.4.1 RDRL Design

Definition 5.1. An *adversarial attack* is any perturbation that disrupts the agent's observation, causing it to take suboptimal actions in a 'phony' state.

We proposed a robust deep reinforcement learning (RDRL) algorithm for VVC, accounting for unknown power deviations from IBRs and loads. Like game theory, this algorithm aims to solve a min-max optimization problem corresponding to the worst-case design. Specifically, it involves an agent tasked with minimizing an objective function while simultaneously contending with an adversarial player determined to maximize the same objective. We model the uncertainties as adversarial attacks on the agent's observation. As shown in Figure 5.3, the adversary distorts the agent's perception of the actual states of the environment. Therefore, the agent makes detrimental decisions.

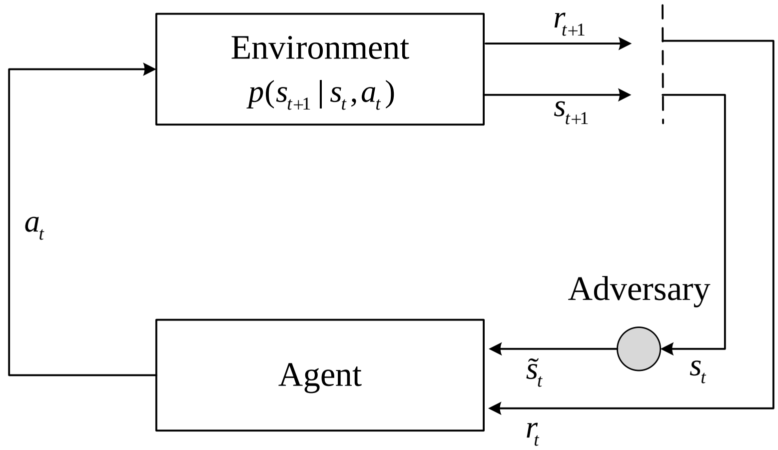

Figure 5.3 Reinforcement learning with perturbed observation

Definition 5.2. *Adversary perturbation set* is defined as $\mathbb{U}(s)$ with bounded perturbations to restrict the power of an adversary, where $\mathbb{U}(s)$ is a set of states and $s \in \mathcal{S}$.

We formulate the VVC as an adversarial state MDP (AS-MDP), which can be represented as a tuple $(\mathcal{S}, \mathcal{A}, \mathbb{U}, r, p, \gamma)$. Given the adversarial states $s_{adv} \in \mathbb{U}(s)$ and fixed π, the Bellman equations for an ASMDP is:

$$\begin{aligned} \tilde{V}^{\pi}(s) &= \mathbb{E}_{a \sim \pi(\cdot|s_{adv})}\left[r(s,a,s') + \gamma \tilde{V}^{\pi}(s') \right] \\ \tilde{Q}^{\pi}(s,a) &= \mathbb{E}_{s' \sim p(\cdot|s,a)}\left[r(s,a,s') + \gamma \mathbb{E}_{a' \sim \pi(\cdot|s_{adv}')} \tilde{Q}^{\pi}(s',a') \right] \end{aligned} \tag{5.17}$$

A robust deep reinforcement learning (DRL) algorithm is proposed for VVO, accounting for uncertainties from PVs and load demands. Like game theory, this algorithm aims to solve a min-max optimization problem corresponding to the worst-case design. Specifically, it involves an agent tasked with minimizing an objective function while simultaneously contending with an adversarial player determined to maximize the same objective. The specific descriptions of elements for VVO are as follows.

1) *Environment and Episode*: In this article, we use OpenDSS to implement the environment. The P/Q setpoints of the PVs and load demands are input into OpenDSS to obtain power loss and node voltages by simulation. Moreover, we have set the episode to terminate automatically at the end of the training process when the maximum timestep is reached.

2) *State*: the state for the VVO is defined as a vector $\mathcal{S} = \{s_t \mid s_t = [p_t, q_t, Tap_{t-1}, t]\}$, where $p_t = \{p_{t-1}^1, \hat{p}_t^i \mid i \in \mathcal{N}\}$ and $q_t = \{q_{t-1}^1, \hat{q}_t^i \mid i \in \mathcal{N}\}$ are the vectors of nodal active/reactive power injections with forecasted active power injection $\hat{p}_t^i$ and reactive power injection $\hat{q}_t^i$ at time t, Tap_{t-1} is the list of status of voltage regulators and capacitor bank at time $t-1$. This state vector includes SCADA measurements that can be readily adopted in practice if the system operator can access SCADA data in real time and the load condition of different regions in the distribution feeder.

3) *Action*: the action space, including tap position of the voltage regulator, the on/off status of the capacitor banks, and the reactive power output of inverters, is expressed as $\mathcal{A} = \{a_t \mid a_t = [u_t^{reg}, u_t^{cap}, q_t^{DG}]\}$. Note that $u_t^{reg}, u_t^{cap}, q_t^{DG}$ are all vectors. It is a hybrid action space referred to a scenario where the agent can take both continuous and discrete actions. Discrete actions are tap changes of regulators and switching status of capacitors, while continuous actions are reactive power output of smart inverters.

4) *Reward*: the objective of VVO is to maintain all voltage magnitudes within a safe operating range while minimizing power loss. The reward function is modified

from the objective function in (5.13) by adding a penalty of switching cost as follows.

$$\begin{aligned} r_t = -C_p P_{loss,t} - C_v \sum_{i \in \mathcal{N}} \left[\mathbb{I}\left(v_{i,t} > \overline{v}\right) + \mathbb{I}\left(v_{i,t} < \underline{v}\right) \right] \\ -C_u \sum_i \left| Tap_{t-1}^i - Tap_t^i \right| \end{aligned} \tag{5.18}$$

where C_u is the switching cost of regulators and capacitors. This design enforces voltage constraints and incentivizes agents to obtain a positive reward. Negative rewards indicate that actions cause voltage violations or increased power loss.

5.4.2 Conformal Prediction for Uncertainty Quantification

Quantifying uncertainty is crucial in statistics and machine learning, usually done by creating prediction intervals. Traditional prediction models provide a single-point estimate, but newer regression methods such as random forest [83], deep neural network (DNN) [84], and ensemble method [85] have been successful in computing prediction intervals (PI). However, computing prediction intervals for dynamic time series data, such as PV generation and load, can be challenging due to their non-stationary nature and high stochasticity with spatial-temporal correlations across different regions [86]. To address this challenge, conformal prediction (CP) provides a measure of confidence or uncertainty associated with the estimate. This measure of confidence is used to handle uncertainty in the subsequent section.

Given an unknown model $f:\mathbb{R}^d \to \mathbb{R}$, where d is the dimension of input vector, we observe that $Y_t = f\left(X_t\right) + \varepsilon_t, t = 1, 2, \ldots$, where ε_t are identically distributed according to a common cumulative distribution function (CDF). $X_t = \{y_t\}_{t=1}^M$ is the history of Y_t with M

sample points. The goal is to construct a sequence of PI $C_{T,t}^{\alpha}$ given a significance α, such that the ground-truth values of the entire time-series trajectory are contained within the intervals.

$$P(Y_t \in C_{T,t}^{\alpha}) \geq 1-\alpha \tag{5.19}$$

The PI at time t can be expressed as follows:

$$C_{T,t}^{\alpha} = \hat{f}_{-t}(x_t) \pm (1-\alpha) \text{ quantile of } \{\hat{\varepsilon}_t\}_{i=t-1}^{t-T} \tag{5.20}$$

where $\hat{f}_{-i}$ denotes the i-th "leave-one-out" (LOO) estimator of model f, whose training data excludes the i-th datapoint (x_i, y_i). Thus, the prediction residual is calculated by

$$\hat{\varepsilon}_i := \left| y_i - \hat{f}_{-i}(x_i) \right| \tag{5.21}$$

In this article, Sequential Distribution-free Ensemble Batch Prediction Intervals (EnbPI) [87] is implemented to construct the PIs of PV generation and load of the form $\left[\hat{y}_{t+h}^{L}, \hat{y}_{t+h}^{U}\right], h \in \{1, \ldots, H\}$, where H is the prediction horizon. Note that such algorithm requires no data-splitting and efficiently constructs $\hat{f}_{-i}$ to avoid model overfitting. The flowchart of the CP process is shown in Figure 5.4. The inputs are observations of individual time-steps within the time-series. The PIs of historical PV generation and load time-series are obtained automatically by EnbPI algorithm.

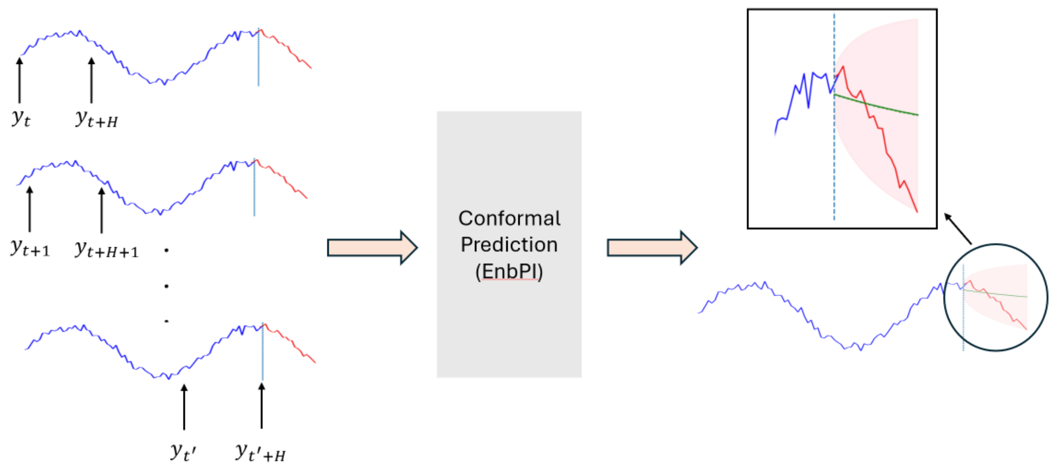

Figure 5.4 Conformal prediction for time-series paradigm

5.4.3 Robust DDPG Algorithm

Unlike other approaches that use only one predicted value for the PV generation and load, we consider the prediction interval part of the adversarial states s_{adv} for training to manage the uncertainty. The modified robust DDPG, depicted in Figure 5.5, is a DRL algorithm that can handle hybrid action spaces and facilitate learning.

1) Actor-Critic Network

DDPG is a model-free off-policy algorithm [91] employed to approximate the policy gradient in our learning process. This algorithm adopts the Actor-Critic framework where the 'Actor' learns to has a deterministic policy function $\mu(s)$ to determine the best action based on a given state, while the 'Critic' evaluates the optimal action-value function $Q(s,a)$ using the Bellman equation. Both the actor and critic are fitted by two deep neural networks (DNNs), referred to as online networks with parameter θ and ω. Another two DNNs are established in the training with a copy: actor target network with parameter θ', critic target network with parameter ω'.

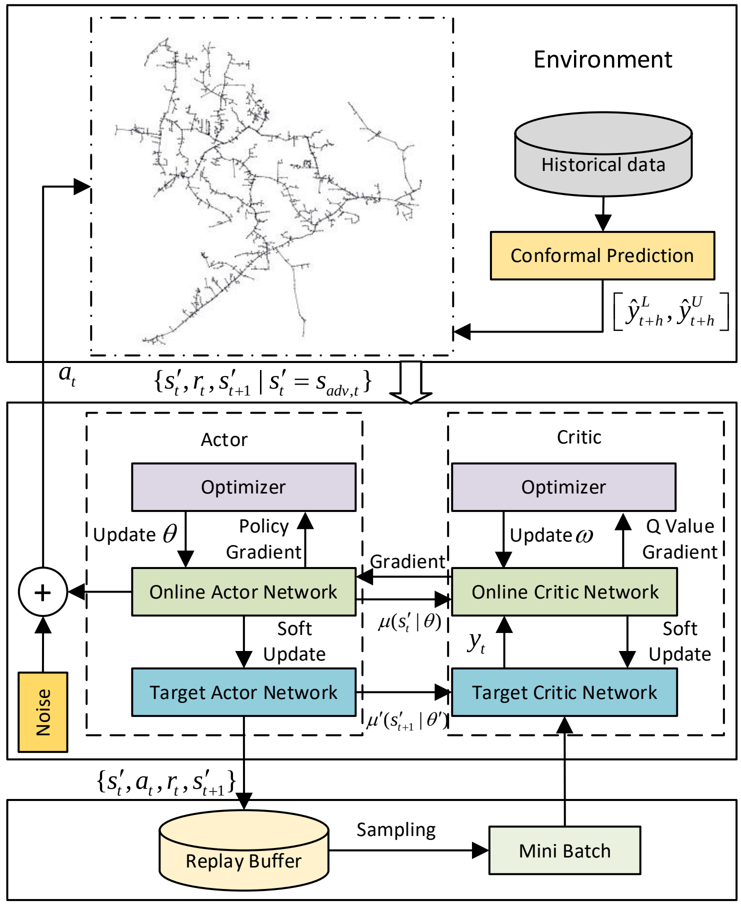

Figure 5.5 Structure of the proposed DDPG algorithm

The proposed approach is to incorporate the uncertainty associated with photovoltaic (PV) generation and load into the state variable for VVO in active distribution systems. Instead of attempting to calculate the worst-case outcome that could potentially disrupt the agent's performance due to this uncertainty, we adjust the state variable to account for it and use it as input for a DNN to learn the optimal policy. Additionally, we can achieve robust online VVO by utilizing real-time data. The description of the adversarial state is as follows:

$$s_{adv} \leftarrow \{s, y^L, y^U \mid s \in \mathcal{S}; y^L, y^U \in \mathcal{U}\} \tag{5.22}$$

where y^L, y^U denote the upper bound and lower bound of the uncertainty set $\mathbb{U}$ (obtained by conformal prediction).

The loss function of the Critic network is expressed by

$$L = \mathbb{E}\left[\left(Q(s_{adv,t}, a_t \mid \omega) - y_t\right)^2\right] \tag{5.23}$$

where,

$$y_t = r_t + \gamma Q\left(s_{adv,t+1}, \mu(s_{adv,t+1}) \mid \omega\right) \tag{5.24}$$

The online Actor network is updated using the chain rule in (9) with its loss gradient stated as:

$$\begin{aligned} \nabla_\theta J &\approx \mathbb{E}\left(\nabla_\theta Q(s_{adv}, a \mid \omega)\big|_{s_{adv}=s'_t, a=\mu(s'_t \mid \theta)}\right) \\ &= \mathbb{E}\left(\nabla_\theta Q(s_{adv}, a \mid \omega)\big|_{s_{adv}=s'_t, a=\mu(s'_t)} \nabla_\theta \mu(s_{adv} \mid \theta)\right) \end{aligned} \tag{5.25}$$

2) Replay Buffer

The proposed algorithm adopts a replay buffer to efficiently avoid sample correlation and make use of hardware optimizations. The replay buffer is a finite-sized cache in the form of a tuple $\{s'_t, a_t, r_t, s'_{t+1}\}$. When the replay buffer reached its maximum capacity, the oldest samples were discarded. After that, the agent chooses B tuples in the buffer to make up a mini-batch. The optimal buffer size is dependent on the nature of the problem being addressed. Inadequate data quantities may result in overfitting, while excessive data amounts may impede learning. To prevent algorithm divergence, the training data must be independently distributed. At each stage, the DNNs are updated through random sampling. This involves selecting a subset of minibatch from the buffer to reduce sample correlations, which enhances the model's accuracy and reliability.

3) Offline Training and Online Testing

In the training process, the Actor network can calculate $\mu(s_t')$ that is an input to the Critic network with the mini-batch $\{s_t', a_t, r_t, s_{t+1}'\}$. The policy gradient can be approximated using the action's and parameter's gradients as follows:

$$\nabla_\theta J \approx \frac{1}{N}\sum_{i\in B}\nabla_u Q(s,a\,|\,\theta^Q)\,|_{s=s_i',a=G_\theta(s_i')}\,\nabla_\theta G(s\,|\,\theta^G)\,|_{s_i'} \tag{5.26}$$

To improve the performance of the policy, the parameters of the Actor network are updated by gradient ascent with a small learning rate lr_a.

$$\theta \leftarrow \theta + lr_a \nabla_\theta J \tag{5.27}$$

Finally, the target networks are updated by

$$\begin{aligned} \theta' &\leftarrow \tau\theta + (1-\tau)\theta' \\ \omega' &\leftarrow \tau\omega + (1-\tau)\omega' \end{aligned} \tag{5.28}$$

where τ is the soft-update rate.

The pseudocode, as shown in Algorithm 5.1, summarizes the offline training process of the proposed algorithm. In our VVO framework, the training process for the RL agent can be summarized as "centralized learning, decentralized execution," where each control device receives the control action from the central coordinator. Different metrics, such as average reward and actor-critic losses, are monitored throughout the training to track the agent's learning progress. Once the training is complete, the trained robust DDPG model is deployed for online testing. During online testing, the agent's performance is evaluated by observing cumulative rewards and success rate metrics. We can improve the agent's performance iteratively by continuously monitoring and gathering feedback. This can be achieved through fine-tuning the existing model or collecting more data for retraining.

Algorithm 5.1: Robust DDPG Training Process for VVO

Input: Historical dataset $\mathcal{D}$, active distribution system model, the state/action space, and the uncertainty set $\mathbb{U}$ of the node power injection (load and PV output)

Output: Actor network with parameters θ^*

Randomly initialize critic network $Q_\omega(s,a|\omega)$, target critic network Q'_ω, actor network $\mu_\theta(s)$, target actor network $\mu'_\theta(s)$, reply buffer B_g with batch size of B, and soft-update rate τ

for t=1: N_{ep} **do**

  Reset the environment and observe the state s_t

  while not terminal or not max time steps per episode reached **do**

    $s'_t \leftarrow s_{adv}$, where s_{adv} is defined in (14) based on the uncertainty set $\mathbb{U}$

    $a_t \leftarrow \mu_\theta(s'_t)$

    Execute action a_t, obtain receive reward r_t and next state s'_{t+1}

    if the replay buffer is not full ($t \le B$) **then**

      Store the new $(s'_t, a_t, r_t, s'_{t+1})$

    else

      Push the new $(s'_t, a_t, r_t, s'_{t+1})$ into the buffer and pop out the oldest one

      Randomly choose M tuples from B_g to form a mini-batch

      Calculate y_t according to (5.24) and update the loss in (5.23)

      Update the parameters of network $Q_\omega(s,a|\omega)$

      Calculate the sampled policy gradient using (18)

      Update the parameters of network $\mu_\theta(s)$: $\theta \leftarrow \theta + lr_a \nabla_\theta J$

      Update the target networks by (5.28)

  end while

end for

For online application, the agent observes the current state, selects the optimal actions using the learned policy (the best state-action pairs $\pi(s,a)$) as the Actor network $\mu_{\theta*}(s)$, and executes these actions in the environment to provide a solution for online system VVO control.

5.5 Numerical Results

Numerical studies are conducted on IEEE 13-bus, 123-bus, and 8500-node test feeders [88]. We have modified these three test feeders with smart inverters as active distribution systems. We then compared our proposed robust VVO method based on DRL with some popular benchmark algorithms to validate its effectiveness. The simulations are performed in OpenDSS under Python 3.11.5. The DRL training process is implemented using PyTorch. Experiments are run on a MacBook Pro with 16GB memory and 8-core CPU and 14-core GPU.

5.5.1 Test Feeder and Data Acquisition

Three PV units with smart inverters have been added to the IEEE 13-bus feeder at bus numbers 634, 680, and 684, as shown in Figure 5.6 (a). The three separate voltage regulator controllers have been merged into a single unit that adjusts the tap positions. The LTCs have 33 tap positions with turns ratios ranging from 0.9 to 1.1. To accommodate the actual operation of the distribution feeder, smart inverters and regulators can be controlled using a single-phase method. Meanwhile, the control capacitors are operated in a three-phase configuration. These capacitors have two statuses, "on" and "off," with capacity values of 100 kVar and 150 kVar. In Figure 5.6 (b), 8 PV units with smart inverters have been added to the 123-bus system at bus {32, 41, 50, 57, 71, 83, 88, 110}. In addition, 20 PVs have been added to the 8500-node system shown in Figure 7. The installed capacity of all these PV units is set to 500kW and their rated complex power is 550kVA. Note that the optimal allocation of these PVs is not the focus of this paper. Table 5.1 shows the summary of three test feeders. In the 123-bus test feeder, regulator 4 has been updated to a gang-controlled

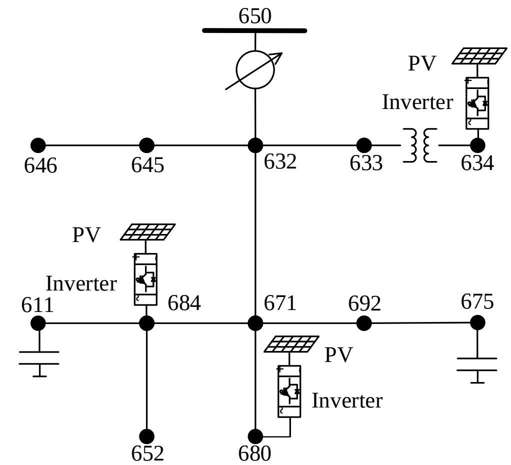

(a)

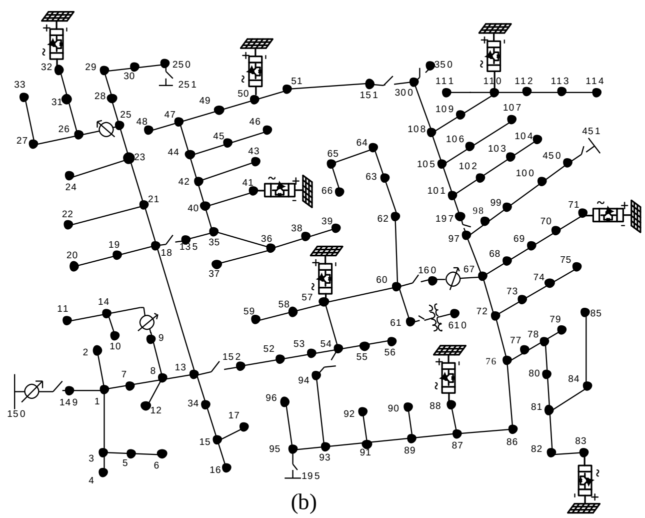

(b)

Figure 5.6 Modified test feeder with PVs: (a) IEEE 13 bus, (b) IEEE 123-bus

Table 5.1 Summary of test feeders

	13-bus	123-bus	8500-node
# of loads	9	85	1177
# of regulators	1	5	12
# of capacitors	2	4	10
# of smart inverters	3	8	20

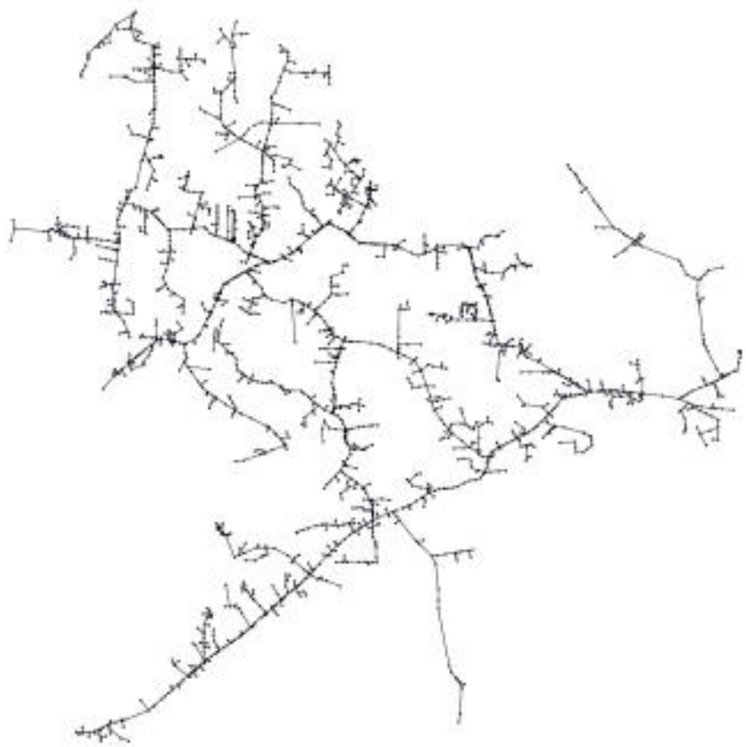

Figure 5.7 Diagram of IEEE 8500-node system

version with a resistance of 0.6 and a reactance of 1.3. Meanwhile, the 8500-node test feeder has no regulator or capacitor control changes. Although capacitor 3 is assumed to be open, the RL algorithm can still manage it. It's important to note that the 8500-node test feeder is designed for balanced scenarios, while the other two are simulated to represent unbalanced distribution systems.

An operational dataset, which includes PV generation, load data, regulator tap and capacitor status, voltage profile, and SCADA information, is generated to train offline RL algorithms for mimicking real-world VVO. The PV generation datasets are collected at the inverter level, with each inverter having multiple lines of solar panels attached. Sensor data is gathered at a plant level, with a single array of sensors optimally placed [89]. The load data (kW and kVAr) for each load at each test feeder is calculated by multiplying the original single snapshot load of the test feeders with a normalized load time series. The load time series was obtained from the London smart meter dataset [90], which includes half-hourly smart meter kWh data for over 5,000 customers from 2011-2014. To ensure synchronization of the PV and load data, we have carefully selected 27,649 half-hourly timestamps for the operational dataset. The OpenDSS static power flow program solves the LTC tap, capacitor status, voltage, and SCADA data. The control logic for LTC and capacitors was discussed in the problem statement. Since the interval is relatively long (30 minutes), each timestamp is treated as an independent power flow analysis. This is achieved by setting the control mode of OpenDSS to STATIC. We split the dataset into a 7:3 ratio, with 70% (19,354 samples) used for offline training and 30% (8,295 samples) used for online testing. Note that the active power loss cost C_p, voltage violation C_v, and switching cost C_u are set as 20.0 $/MWh, 0.1 $/switching, and 1.0 $/p.u., respectively. These values can be selected based on the application's specific requirements in practical scenarios.

5.5.2 Power Injection Uncertainty Quantification

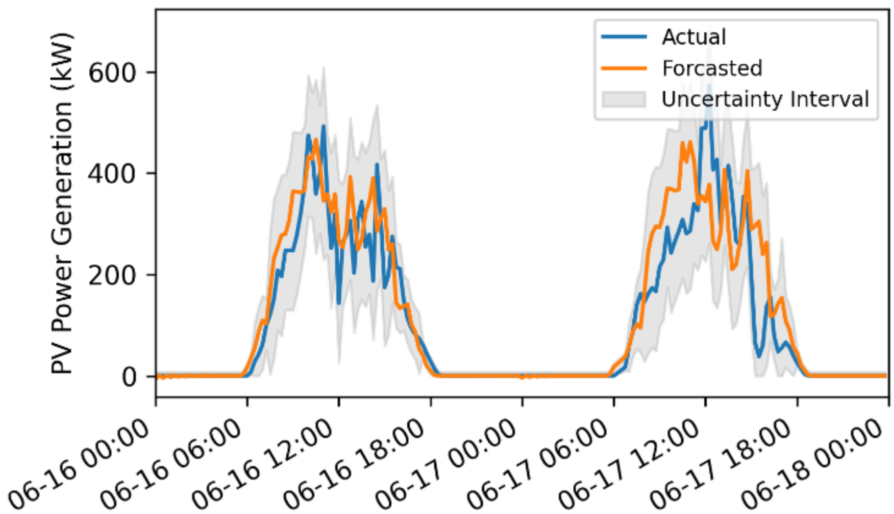

Figure 5.8 Power generation uncertainty interval of a PV unit over two consecutive days

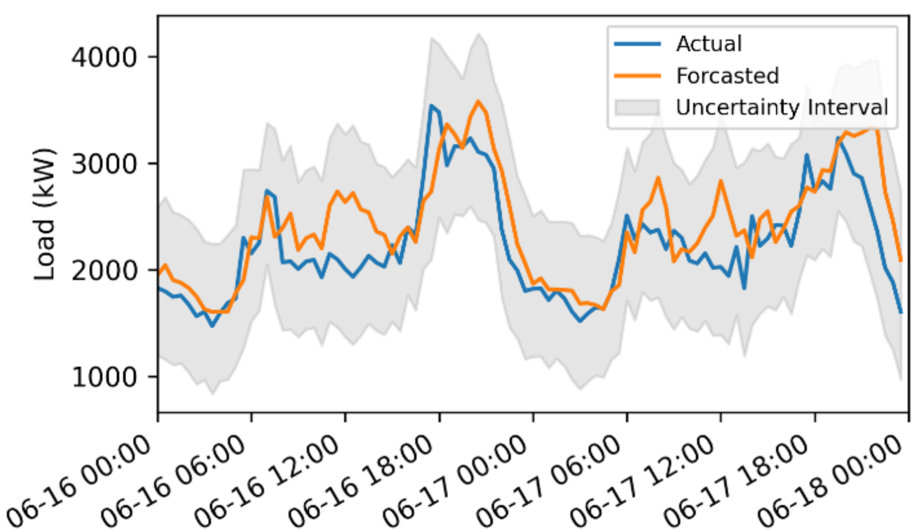

Figure 5.9 The uncertainty interval of total load over two consecutive days

Figure 5.8 displays the forecasted generation output and power generation uncertainty interval of a PV unit for two consecutive days. PV generation follows a predictable daily pattern driven by the sun's position. It ramps up after sunrise, peaks around midday, like 11 AM to 2 PM, and decreases as the sun sets. Weather and seasonal changes influence this pattern but remain consistent with the natural solar cycle. On the other hand, the forecasted value and the uncertainty interval of the total load for two consecutive days are shown in Figure 5.9. Human activities largely influence load demand and follow a different pattern. The demand typically rises in the early morning and stabilizes during the morning and early afternoon. The highest demand occurs in the early evening (6 PM to 9 PM) when people return home, use lights, cook, and engage in other activities that consume electricity. After this peak, demand decreases as people go to bed, reaching its lowest levels late at night and in the early morning hours. This daily cycle of load demand reflects typical residential and commercial usage patterns, creating a challenge when it does not align with the solar generation peak.

From Figure 5.8 and Figure 5.9, we can see that the EnbPI algorithm effectively captures the variability and potential forecast errors in load demand and PV generation. Based on conformal prediction, this algorithm substantially enhances the quantification of PV generation and load uncertainty in response to abrupt disturbances or environmental variations. By defining these uncertainty sets, we can improve the robustness of the RL-based VVO method. This method can utilize uncertainty information to make more informed and resilient decisions, ensuring optimal voltage control despite uncertainties. The quantified uncertainty sets provide a buffer that allows the RL agents to adjust its strategies dynamically, thereby improving the overall reliability and performance of the voltage management.

5.5.3 Algorithm Setup

This subsection provides the hyperparameter setup for the proposed algorithm and three benchmarks. The first benchmark is deep Q-learning network (DQN) [65] using a combined discrete action space, partitioning the continuous control space into 100 linearly distributed discrete control options. The second benchmark is Soft Actor-Critic (SAC) [92], a neural network structure decoupled from devices, scaling linearly with the number of devices rather than exponentially. The third benchmark is DDPG [93] adopting a hybrid action space. It involves utilizing sigmoid activation for discrete actions and tanh activation for continuous actions after the fully connected layer. The hyperparameters are listed in Table 5.2. In Table 5.2, the first section displays the parameters that are shared by all algorithms. Note that when selecting hyperparameters based on the feeder, the parameter will be denoted in curly brackets to indicate the values tailored for the 13-bus, 123-bus, and 8500-node distribution systems, respectively.

This study assumes we have one thousand hours of operational data from the historical dataset before the agent starts interacting with the system. The historical dataset, as described in Section A, contains information on load/DG, voltage, network loss, and corresponding tap positions. This dataset was created to simulate the database of a standard electric utility company. As a result, we can pre-train specific components of the RL-VVC framework, which provides a slightly better initial policy [94]. To facilitate a more thorough demonstration and comparison, we pre-train the proposed and benchmark algorithms using this historical data. Moreover, we assume that the AMI and SCADA data are available for the offline training process, allowing us to use the actual value of load demand and DERs to train the RL agent. However, during the online testing process, due to limited AMI data availability, we utilize forecasted values of load and DER to assess operational conditions under uncertainty and evaluate the performance of the proposed robust DDPG algorithm.

Table 5.2 Algorithm hyperparameters

All	Replay buffer size	3000
	Discount factor γ	{0.95,0.95,0.99}
	Optimizer	Adam
	Pre-train steps	500
	Reward Scale	5
DQN	Hidden layer sizes	{(30,40,80), (40,60,80), (120,120)}
	Hidden activation	tanh-tanh-tanh
	Learning rate	0.0005
	Copy steps C	30
	Epsilon length	500
	Epsilon max	1.0
	Epsilon min	0.02
SAC	Hidden layer sizes	{(30,40,80), (40,60,80), (120,120)}
	Hidden activation (actor-critic)	tanh-relu-relu
	Learning rate (actor-critic)	0.0005
	Temperature parameter α	0.2
	Smoothing coefficient ρ	0.99
	Batch size	64
DDPG	Hidden layer sizes	{(30,40,80), (40,60,80), (120,120)}
	Hidden activation (actor-critic)	relu-relu-relu
	Learning rate (actor-critic)	0.001
	Soft update rate τ	0.005
	Noise	{0.07, 0.05, 0.1}
	Batch size	64
Robust DDPG	Hidden layer sizes	{(30,40,80), (40,60,80), (120,120)}
	Hidden activation (actor-critic)	relu-relu-relu
	Learning rate (actor-critic)	0.001
	Soft update rate τ	0.005
	Confidence level of uncertainty sets	0.95
	Noise	{0.07, 0.05, 0.1}
	Batch size	64

5.5.4 VVO Performance

To demonstrate the effectiveness of the proposed RDRL method by comparing it with other benchmark algorithms and a mixed-integer conic programming (MICP) based VVO method using the DistFlow equation [95] under uncertainties. Specifically, we evaluate the performance using the power loss index and voltage violation ratio (VVR).

VVR: VVR is defined as the fraction of the total node voltage violation across all the testing runs. Mathematically it's defined as:

$$VVR = \frac{\sum_{i=1}^{N_{test}} nVV_i(\varphi)}{N_{test} * nPh} \tag{5.29}$$

where N_{test} is the total number of testing runs, $nVV_i(\varphi)$ is denotes the number of phase voltage violation in i^{th} run, and nPh is the total number of phases in the system.

1) IEEE 13-bus test feeder

Figure 5.10 plots the reward step value during offline training and a plot for maximum voltage magnitude deviation to evaluate the system-wide voltage magnitude flatness. The solid curve represents the average value on independent runs, with shaded regions indicating the corresponding error bounds.

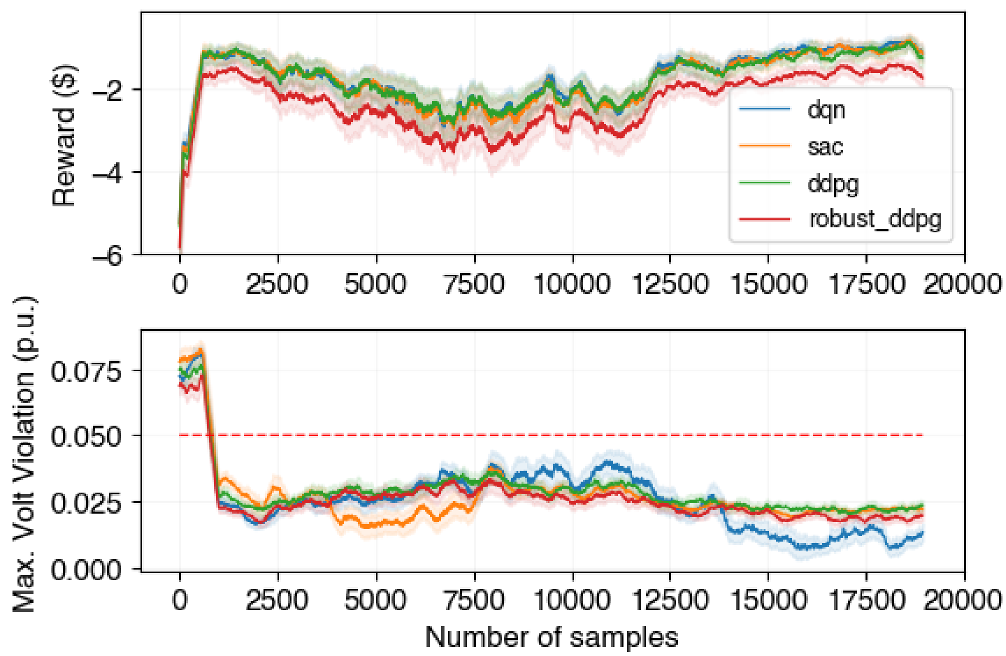

Figure 5.10 Offline training reward and voltage violation of 13-bus feeder

The reward curve in Figure 5.10 indicates that all the model-free DRL-based algorithms can approach a near-zero negative value after 15,000 training samples. DQN shows slight fluctuation, and SAC's exploration is extensive, although it exhibits minor convergence in reward toward the end of training. The proposed robust DDPG demonstrates the lowest reward, potentially compromising power loss to ensure the safety region of the voltage profile. Analyzing the voltage violation curve, we find that SAC tends to outperform DDPG and DQN in terms of both convergence speed and accuracy. The proposed robust DDPG falls between DDPG and SAC, quickly registering the maximum voltage violation within an acceptable threshold.

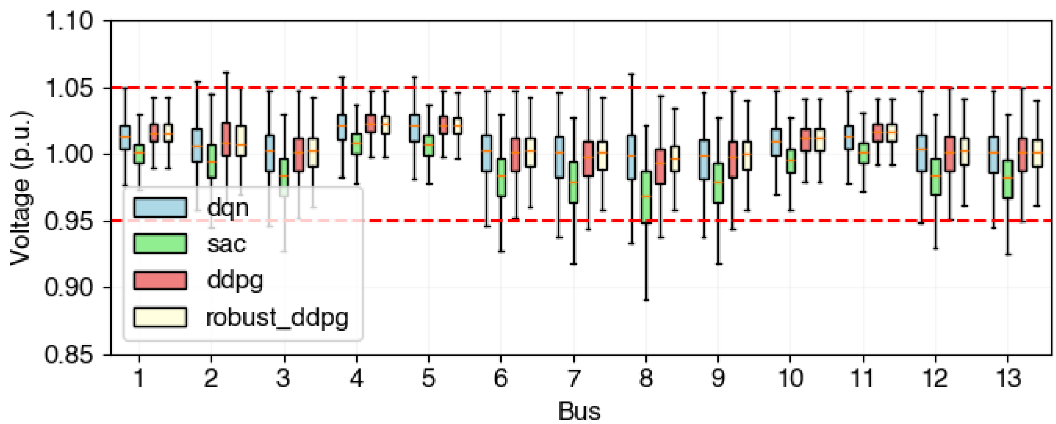

Figure 5.11 Voltage profile of 13-bus feeder in online testing

Table 5.3 Voltage profile comparison of 13-bus system in online application

Algorithm	Voltage mag. profile (p.u.)		
	Min.	Max.	Avg.
MICP	0.9683	1.0283	1.0016
DQN	0.9329	1.0708	1.0053
SAC	0.8908	1.0450	0.9923
DDPG	0.9375	1.0621	1.0068
Robust DDPG	**0.9558**	**1.0484**	1.0082

In the context of online testing, Figure 5.11 displays the voltage profiles of the 13-bus feeder, while Table 5.3 and Table 5.4 provide statistical illustrations of the voltage magnitude profiles and performance comparisons. Additionally, Figure 5.12 showcases the control actions of VVO equipment executed by the proposed RL agent over a day. Note that smart inverters have a single-phase control configuration. However, for simplicity, we only present the balanced Q injection.

Table 5.4 Performance comparison of 13-bus system in online application

Algorithm	Power loss (MW)		VVR
	Mean	Std.	%
MICP	3.60e-2	-	0
DQN	3.50e-2	2.66e-2	2.5
SAC	3.81e-2	2.85e-2	4.37
DDPG	3.80e-2	2.74e-2	2.29
Robust DDPG	4.11e-2	2.74e-2	**0**

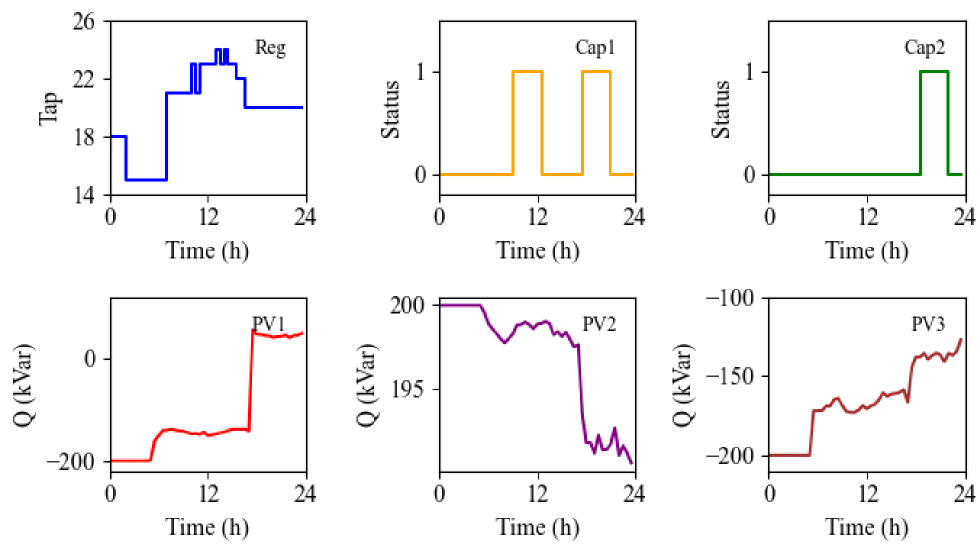

Figure 5.12 Control actions executed by the proposed RL agent over one day

Based on Figure 5.11 and Table 5.3, the proposed robust DDPG algorithm ensures that the voltage profile remains within an acceptable range with minimum and maximum values of 0.9558 and 1.0484 p.u. This outperforms other RL algorithms in terms of safety. Despite exhibiting the highest mean power loss in online testing, the algorithm achieves a zero VVR, indicating its effectiveness in managing uncertainties arising from DERs and load demand. The optimization-based approach using an approximate ADN model also demonstrates excellent performance in this small-scale feeder with zero VVR and low power loss.

We have selected a specific day to demonstrate the control actions of the robust DDPG agent, encompassing the tap position of LTC, the on/off status of capacitors, and the Q injection of intelligent inverters. According to Figure 5.12, after 6 am, the voltage regulator becomes active to set points, restoring voltage levels to normal operating conditions using smart inverter controls as the PV output increases. By 10 am, with a significant rise in load, the first capacitor is activated to inject reactive power and prevent over-voltage. From 6 pm to 10 pm, both capacitor 1 and capacitor 2 are engaged to support reactive power needs as the load demand continues to increase. During this period, the voltage regulator is not active. After 10 pm, as the load demand decreases, smart inverters control reactive power to prevent over-voltage conditions, while the capacitors and voltage regulator are not actively controlled.

2) Large test feeder: IEEE 123-bus and 8500-node

Figure 5.13 and Figure 5.14 illustrate the reward step value and the maximum voltage violation observed during the training phase for the 123-bus system and 8500-node system, respectively. A comprehensive performance comparison during online testing is delineated in Table 5.5. Upon application to larger test feeders, all DRL-based methodologies exhibit lower power losses than MICP. Among these, the proposed robust DDPG notably outperforms DQN, SAC, and traditional DDPG models without any voltage violations. Even though it might lead to a suboptimal solution with increased power loss, it still meets the safety criteria for voltage control. Such outcomes underscore the efficacy of the

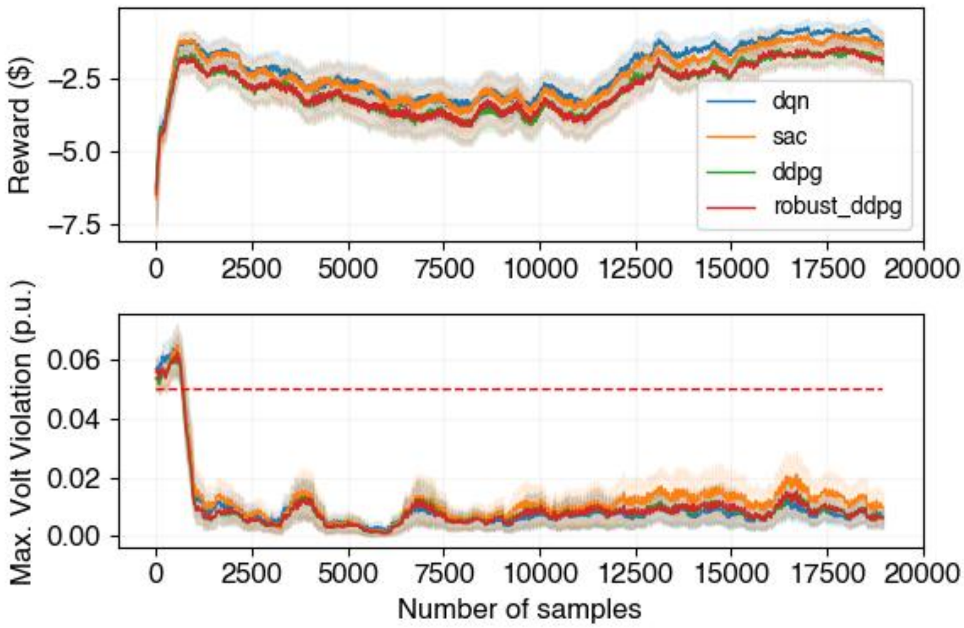

Figure 5.13 Offline training reward and voltage violation of 123-bus feeder

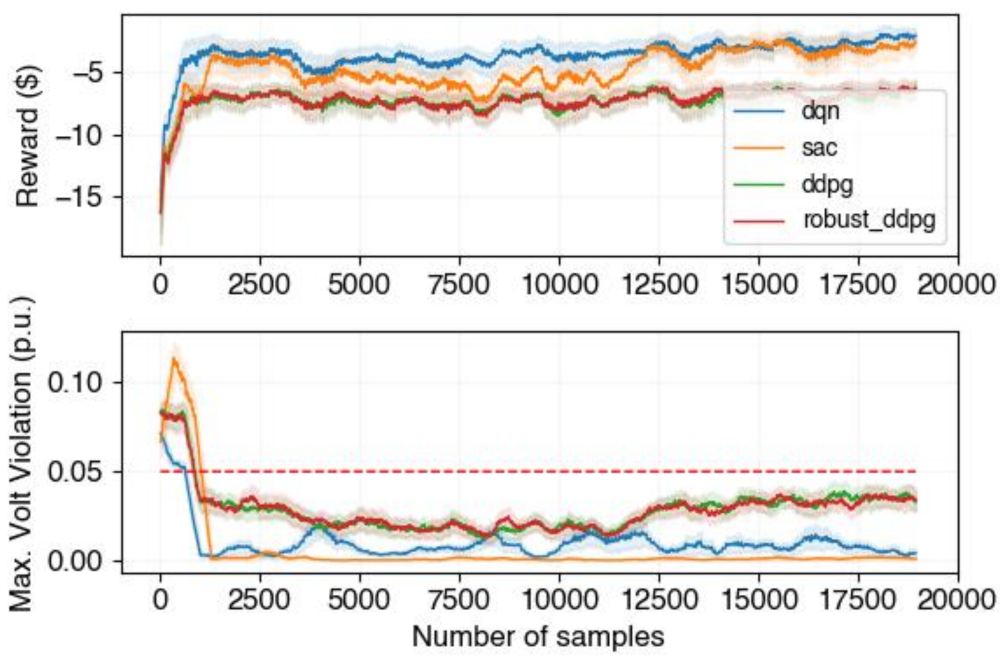

Figure 5.14 Offline training reward and voltage violation of 8500-node feeder

Table 5.5 Performance comparison of larger test feeder in online application

Test System	Algorithm	Power loss (MW)		VVR
		Mean	Std.	%
123-bus	MICP	1.46e-1	-	0
	DQN	1.24e-1	9.01e-2	10.45
	SAC	1.26e-1	8.86e-2	6.57
	DDPG	1.28e-1	9.86e-2	7.61
	Robust DDPG	1.33e-1	**7.53e-2**	**0**
8500-node	MICP	4.51e-1	-	0
	DQN	2.27e-1	2.93e-1	8.39
	SAC	2.30e-1	2.97e-1	8.61
	DDPG	3.5e-1	2.32e-1	6.29
	Robust DDPG	3.92e-1	**2.12e-1**	**0**

proposed approach in enhancing the safety controls of RL agents, offering resilience against uncertainties prevalent in the operational environment.

Traditional optimization-based VVO methods may compromise their performance for large distribution systems due to inaccuracies in modeling without an accurate network model. In contrast, mode-free DRL-based algorithms show more significant potential and are worth considering regardless of complex network topology. The technology for quantifying uncertainties in the proposed method enhances VVO performance in online applications. The robust DDPG algorithm balances exploring the safety region and optimizing the objective function. It's worth noting that while DQN demonstrates excellent offline training, SAC and DDPG are more advantageous for the hybrid action space.

5.5.5 Computation cost

In the online testing, the average executive time of MICP is around 3.7 and 52.2 seconds for the 13-bus and 123-bus systems and more than a half-an-hour for the 8500-node system. However, DQN, SAC, DDPG, and robust DDPG models only take a few milliseconds, as shown in Table 5.6, which promises to meet the real-time implementation requirement in power systems. The proposed algorithm demonstrates high computational efficiency in unbalanced and balanced distribution systems. Moreover, the proposed RDRL method performs well when dealing with a hybrid action space in three-phase distribution systems.

Table 5.6 Computation cost of online application

Algorithm	Average execution time (milliseconds/sample)		
	13-bus	123-bus	8500-node
DQN	2.23	13.61	63.66
SAC	3.39	15.06	68.37
DDPG	2.63	13.80	66.92
Robust DDPG	2.94	14.34	66.02

5.6 Summary

This chapter proposes a novel RDRL framework for VVO in active distribution systems to enable autonomous operation without the knowledge of accurate model parameters. To address the uncertainties in power injections from DERs and load, we formulate the VVO problem as an ASMDP, treating uncertainties as an adversarial attack on the agent's observation. Then, we propose a robust DDPG algorithm that addresses adversarial states by incorporating uncertainty quantification through conformal prediction. Numerical studies on ADNs represented by the modified 13-bus, 123-bus and

8500-node test feeders indicate that the proposed robust DDPG outperforms the traditional optimization-based and DRL-based benchmark methods in the online application. Particularly in larger-scale ADNs, this algorithm can ensure safe voltage control with exceptional efficiency and robustness under uncertainties. Applying the proposed RDRL framework with the robust DDPG algorithm to online VVO for unbalanced ADNs shows excellent promise. Note that the dataset's quality would influence the performance of RL agents during the training. For future work, we plan to create two separate datasets for training and online testing.

CHAPTER 6. ROBUST OPTIMIZATION BASED LOAD MANAGEMENT UNDER CYBERATTACKS

6.1 Introduction

This chapter presents a consumer-level load management system under false data injection (FDI) attack on price of electricity, which is known as real-time pricing integrity attack. Section 6.2 demonstrates the mathematical model of dynamic load demand based on real-time pricing policy. Section 6.3 investigates the impact of such attack of the price-responsive demand and quantifies the economic loss of error of total demand. Moreover, a robust optimization method is proposed to handle the real-time pricing attack as uncertainty to obtain the optimal energy consumption plan based on the preference of consumers. Case study is conducted to verify the effectiveness of the proposed method in Section 6.4, where a comparison with a deterministic method is provided. Section 6.5 concludes the proposed robust load demand system considering cybersecurity.

6.2 Dynamic Load Demand Modeling

With the improvement of smart sensing, communication and control technologies, consumer-level appliances are becoming more intelligent with load management and communication capabilities. As a result, future consumers will engage in managing energy consumption, production, storage with interactive behaviors. Large commercial, industrial, and residential consumers will be able to participate directly in the Transactive Energy Market (TEM) [96]. Therefore, advanced load management system which will use real-time electricity price, consumer preferences to schedule different devices and real-time generation is expected to maximize the benefit of using electricity.

On the customer side, they receive the information of electricity price which is set by the aggregator as a step function based on the total demand $D(t)$ [97]. Real-word electricity pricing policy is modeled as:

$$\lambda(t)=\begin{cases}\lambda_1 & \text{if} \quad 0\le D(t)<d_1 \\ \lambda_n & \text{if} \quad d_1\le D(t)<d_2 \\ \vdots & \vdots \qquad \vdots \\ \lambda_r & \text{if} \quad d_{r-1}\le D(t)\end{cases} \tag{6.1}$$

Generally, the aggregator will increase the price of electricity as demand increases during the time slot. Otherwise, they will decrease. However, a few deterministic mathematical models exist to describe the dynamic relationship between demand and price since the aggregator and the adopted marketing policy govern the electricity price. The real-time price of the electricity will be sent to all the active consumers in contract with the aggregator through the communication channel. Then, based on the current electricity price, the consumers may change a portion of demand to obtain a more economical consumption behavior. Therefore, the transactive energy market's demand profile becomes more complicated and unpredictable. For simplicity, the total demand can be modeled with the following:

$$D(t)=F(t)+\xi(\lambda(t)) \tag{6.2}$$

where, $F(t)$ is the baseline load demand that is independent of the real-time price. For instance, for a household, the baseline demand can be the minimum necessary power usage as cooking, illumination, and refrigerators. $\lambda(t)$ denotes the controllable load also referred as the price-responsive demand. This demand is a decreasing function of $\lambda(t)$. Obviously, if the real-time price is neglectable, $D(t)=F(t)$.

ISO utilizes historical total demand data as valuable input for advanced Machine Learning algorithms to make accurate predictions regarding future energy consumption patterns. However, with the increasing application of intelligent meters and home-side IoT systems, observing human-induced responses towards real-time price is crucial. We assume that the fixed demand is known at the interval by prediction. The price-responsive demand has been represented by the constant elasticity of own-price (CEO) model [98]. The CEO model is expressed as:

$$\xi(\lambda(t)) = \beta \cdot \lambda(t)^{\epsilon} \tag{6.3}$$

where, β and ϵ are positive and negative constants, respectively. ϵ is within (-1,0).

6.3 Robust Load Management System

6.3.1 Impact Analysis of Cyberattacks

The attack model is designed as the data integrity attack towards the real-time electricity price, which is presented in Figure 6.1. Attacks are implemented over the communication channel to manipulate the real-time electricity price at any given time. By alternating electricity price signal from the aggregator to the consumer, the adversary may impact the energy consumption of active consumers resulting in a change in total demand. Without knowing the risk of being attacked, those active consumers may make incorrect decisions that may lead to economic loss. For example, the adversary modifies the price to a low value when the price is high. As a result, the active consumers would increase their power consumption, which exceeds the expected demand by the power supplier. To be worse, it may degrade the operating condition like instability of price-responsive demand and voltage violations leading to cascading failures and outages.

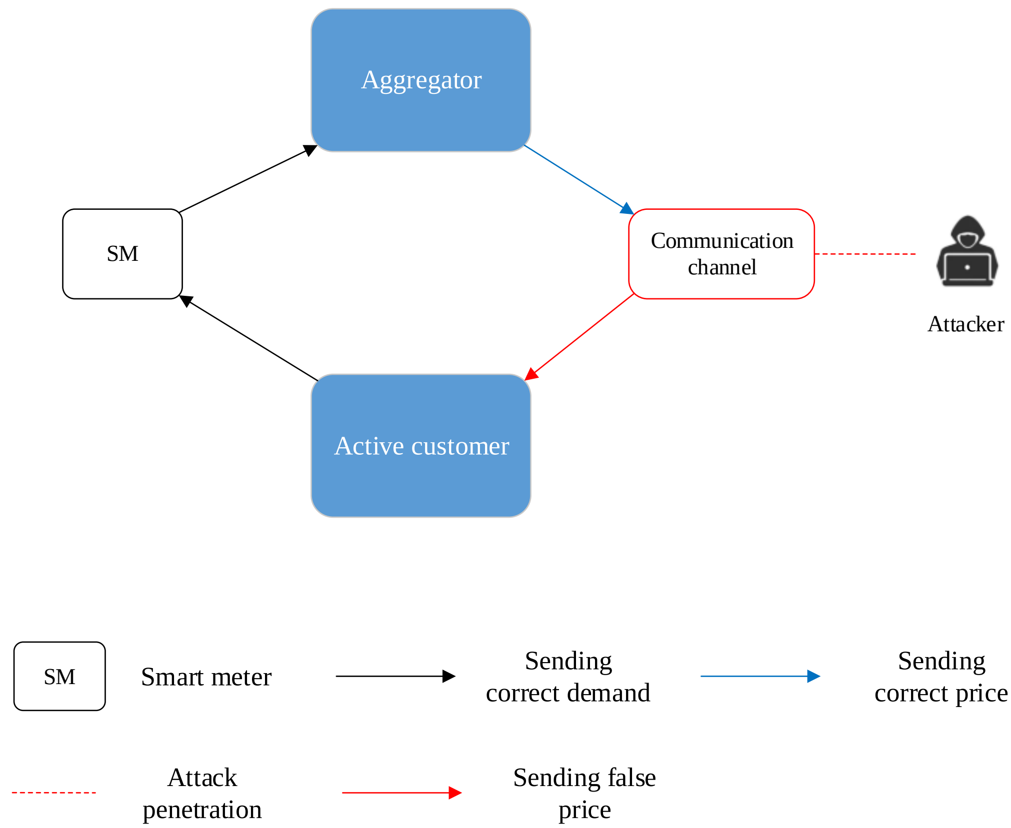

Figure 6.1 Real-time pricing attack scheme

Let $\hat{D}(t)$ denotes the demand based on the manipulated price $\hat{\lambda}(t)$, then it is represented as:

$$\hat{D}(t) = F(t) + \xi(\hat{\lambda}(t)) = F(t) + \beta \cdot \hat{\lambda}(t)^{\epsilon} \tag{6.4}$$

The error of demand is characterized as $e_D(t)$ that is $e_D(t) = D(t) - \hat{D}(t)$ given by

$$e_D(t) = \beta \cdot (\lambda(t)^{\epsilon} - \hat{\lambda}(t)^{\epsilon}) \tag{6.5}$$

Therefore, the economic loss for consumer can be computed by

$$\ell = \int e_D(t)\lambda(t)dt \tag{6.6}$$

6.3.2 Consumer-oriented Load Management Model

At the consumer level, a preference variable B is conducted to describe the benefit of power consumption, which is set artificially. For example, industrial consumers who are more profitable have higher value of B. On the other hand, the preference variable for residential consumption is lower. But it may be different for different time even for the same consumer. Consider the active consumers aim to maximize the benefit of power consumption by dispatching the controllable load over time-period T. The normal deterministic linear problem is formulated below.

$$\max \sum_{t=1}^{T}(B-\lambda_t)(F_t+u_t)$$

$$\begin{aligned} &\text{subject to} \\ &\quad D_t = F_t + u_t \\ &\quad \underline{U}^h \le D_t \le \bar{U}^h \\ &\quad \sum_{t=1}^{T} D_t \le \bar{U}^d \\ &\quad \sum_{t=1}^{T} D_t \ge \underline{U}^d \\ &\quad u_t \ge 0 \end{aligned} \tag{6.7}$$

where, λ_t is real-time electricity price at time *t*, D_t is the total demand at time *t*, F_t is the fixed demand which is assumed to be known at time *t*, u_t is the controllable demand at time *t*, $\underline{U}^h$ and $\bar{U}^h$ are minimum and maximum level of hourly demand. $\underline{U}^d$ and $\bar{U}^d$ are minimum and maximum total energy consumption, respectively.

6.3.3 Robust Optimization Method

Under data integrity attack, the real-time price is manipulated as $\hat{\lambda}_t$, which can be considered as uncertain parameters. It's assumed that every $\hat{\lambda}_t$ takes value in the interval $[\lambda_t, \lambda_t + d_t]$, where d_t denotes the deviation from the correct price. In addition, an integer control parameter $\Gamma \in [0, |J_0|]$ is defined, where $J_0 = \{t \mid d_t > 0\}$. If $\Gamma = 0$, the impact of the cost deviations in the objective function is disregarded. If $\Gamma = |J_0|$, all cost deviations are considered, corresponding to the worst-case scenario.

The objective function of the robust optimization problem can be stated as:

$$\max \sum_{t=1}^{T} B(F_t + u_t) - \min \sum_{t=1}^{T} \lambda_t (F_t + u_t) \tag{6.8}$$

The above min-max structure can be reformulated equivalently as the inner problem:

$$\begin{aligned} & \min \sum_{t=1}^{T} (\lambda_t - z\tilde{\lambda}_t) \times (F_t + u_t) \\ & \text{suject to} \\ & \qquad z \le 1 \\ & \qquad \sum_{t=1}^{T} z \le \Gamma \\ & \qquad z \ge 0 \end{aligned} \tag{6.9}$$

Finally, this problem can be reformulated into the consumer-oriented robust optimization problem as:

$$\begin{aligned}
&\min\ -\sum_{t=1}^{T}(B-\lambda_t)(F_t+u_t)+z\Gamma+\sum_{t=1}^{T}q_t \\
&\text{suject to} \\
&\quad D_t = F_t + u_t \\
&\quad \underline{U}^h \le D_t \le \bar{U}^h \\
&\quad \sum_{t=1}^{T} D_t \le \bar{U}^d \\
&\quad \sum_{t=1}^{T} D_t \ge \underline{U}^d \\
&\quad D_t \ge 0 \\
&\quad z + q_t \ge d_t y_t \\
&\quad q_t \ge 0 \\
&\quad z \ge 0 \\
&\quad D_t \le y_t
\end{aligned} \tag{6.10}$$

where, z and q_t are dual variables of the constraints related to the deviation of cost coefficients and level of robustness, y_t is an auxiliary variable corresponding to linear expressions [99].

6.4 Case Study

According to Georgia electricity market price, the time-varying price model for case study is shown in Figure 6.2, where $P_1 = 0.057\$/\text{kWh}$, $P_2 = 0.094\$/\text{kWh}$ and $P_3 = 0.097\$/\text{kWh}$.

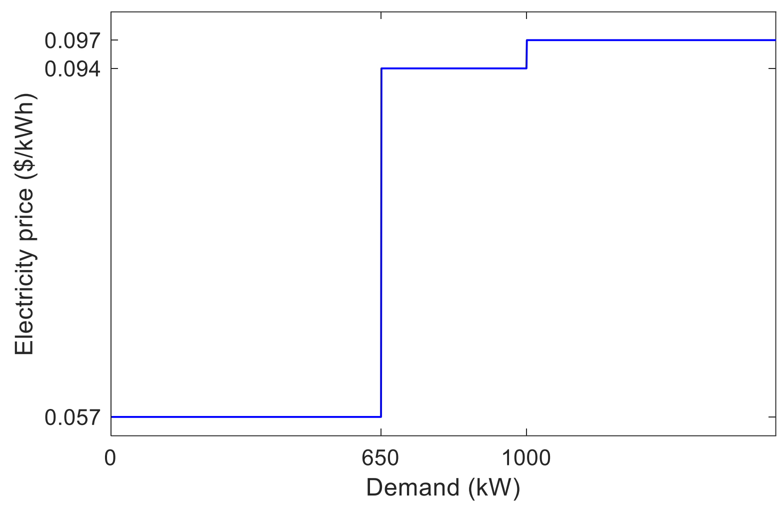

Figure 6.2 Electricity price based on different levels of demand

Figure 6.3 represents price-responsive demand with three different ϵ . From the figure, we can see that if ϵ increases, the demand decreases.

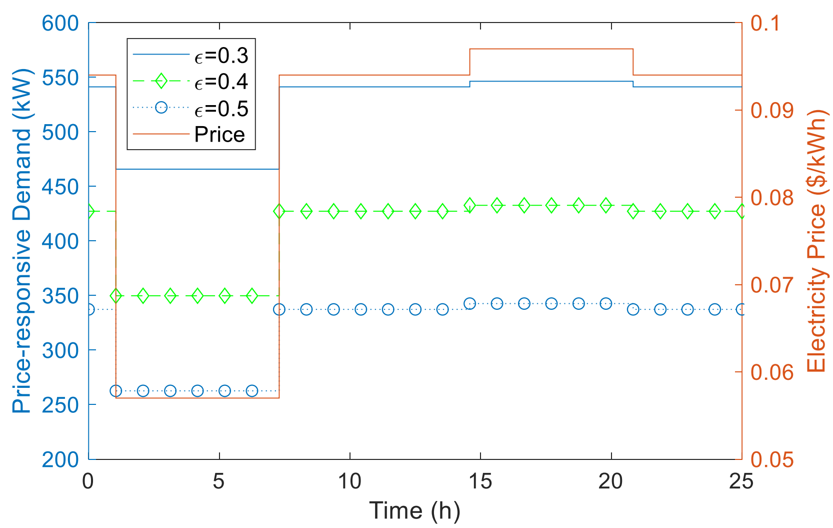

Figure 6.3 Price-responsive demand based on real-time price

The time window of case study is 24 h. Moreover, other parameters are shown in Table 4.1. The described problem is solved with a code developed in MATLAB.

Table 6.1 Parameters of benefit and constraints

B	0.2 $/kWh	$\underline{U}^d$	8 MWh
Γ	24	$\bar{U}^d$	16.5 MWh

Time	Electricity price ($/kWh)	Fixed demand (kW)	$\underline{U}^h$ (kW)	$\bar{U}^h$ (kW)
0	0.094	50	650	1000
1	0.057	50	0	650
2	0.057	75	0	650
3	0.057	100	0	650
4	0.057	125	0	650
5	0.057	100	0	650
6	0.057	350	0	650
7	0.094	250	650	1000
8	0.094	350	650	1000
9	0.094	350	650	1000
10	0.094	450	650	1000
11	0.094	300	650	1000
12	0.094	250	650	1000
13	0.094	400	650	1000
14	0.097	400	1000	3000
15	0.097	300	1000	3000
16	0.097	400	1000	3000
17	0.097	350	1000	3000
18	0.097	350	1000	3000
19	0.097	400	1000	3000
20	0.094	300	650	1000
21	0.094	150	650	1000
22	0.094	100	650	1000
23	0.094	50	650	1000

6.4.1 Impact of Real-time pricing attack

Cyberattack scenario: For t in [8,12], the price is manipulated as 0.057$/kWh instead of 0.094$/kWh by the attacker. Without noticing the real-time price being attacked, the consumers maintain their demand based on the incorrect price signal. In this case, they would keep high demand since they receive lower price than the correct one, resulting in paying more money when they receive the bill. After t=12, they receive the correct price and take the appropriate action. The attacked price compared with the correct are depicted in Figure 6.4 (a), where ϵ is -0.4. The error of the total demand caused by the attack is shown in Figure 6.4 (b).

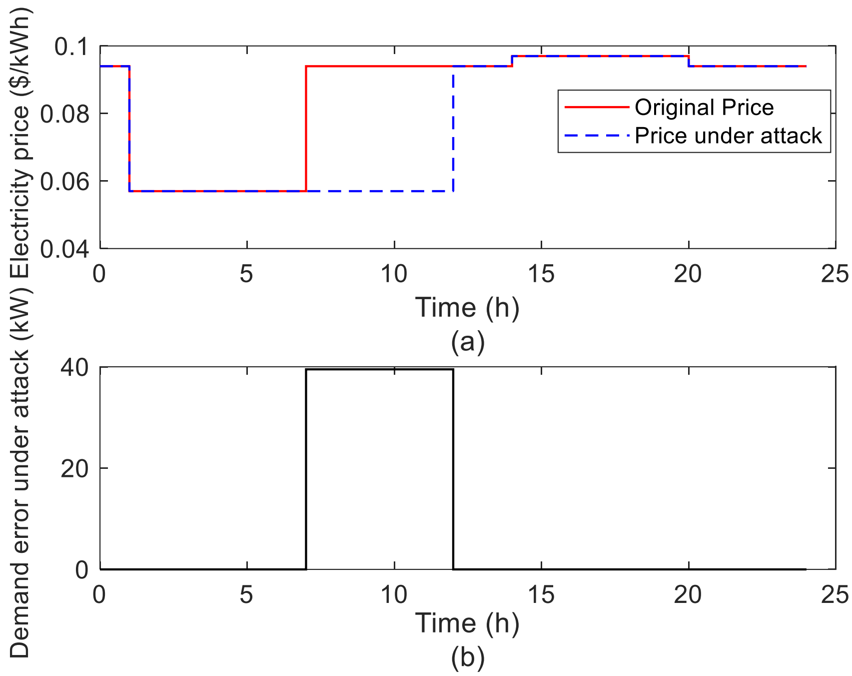

Figure 6.4 (a) Correct electricity price and attacked price, (b) Error in demand under attack.

As the consumer maintain high demand for t in [8,12], the economic loss of the customer is $\ell = 148.52\$$ in this case. Imagine that there are 2,000 units of active consumers in one area, the daily loss can be 297,040$. Such enormous loss increases the concern towards the detection and mitigation of the real-time pricing attack. Hence, a robust and secure load management model is highly required.

6.4.2 Performance of Optimization

The simulation results of deterministic optimization and robust optimization are shown in Figure 6.5 and Figure 6.6, respectively. In Figure 6.5, load demand of deterministic optimization method without attack during 24h period is obtained, which is compared with the condition under attack. It's obvious that consumers would like to use more electricity when the price is hacked (t in [8,11]), which may lead to economic loss. The result of the proposed robust optimization method in Figure 6.6 shows the optimal decision of demand management in each time-period without the detailed information of the attack signal. From Figure 6.5 and Figure 6.6, we can see that the robust optimization will have the same small amount of consumption when the price is high in the afternoon, while deterministic method obtains zero-energy planning at that period. Moreover, the demand bar graph in Figure 6.6 is flatter than that in Figure 6.5 under real-time pricing attack during [8h,11h], contributing to a more stable, reliable, and economical grid operation.

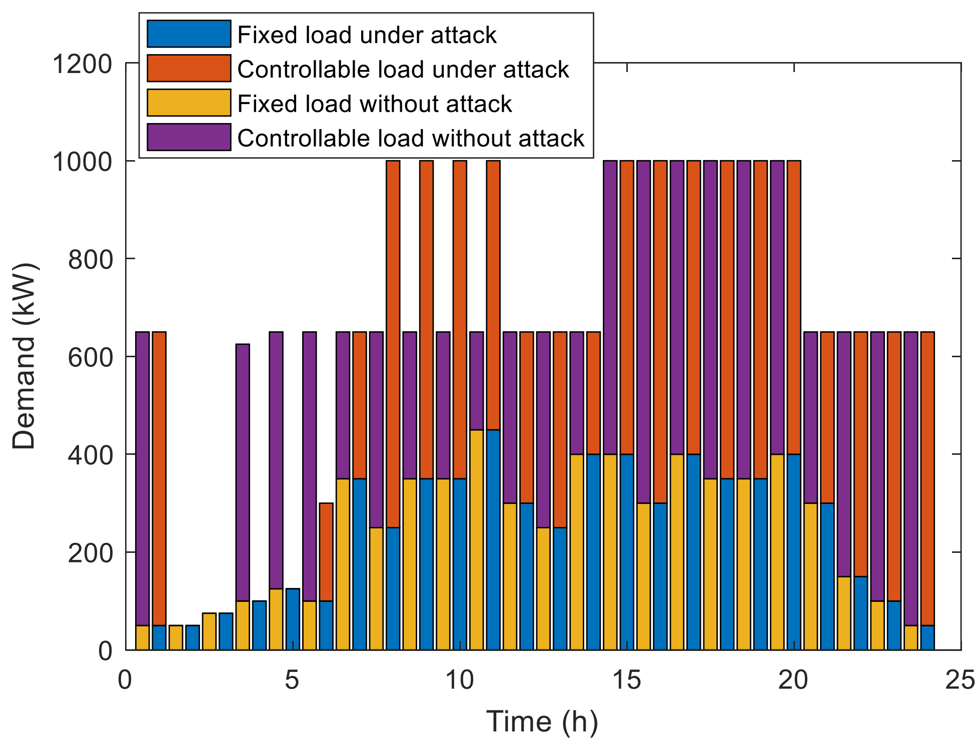

Figure 6.5 Load demand of deterministic optimization method without/under attack

The deterministic method assumes no uncertainty in the electricity price as well as the robust budget is zero. Table 6.2 compares the maximum profit under attack using deterministic and robust optimization methods. When the robust budget is considered within 24 hours, the maximum profit is $1819.8, close to the normal condition ($1830.9) and better than the deterministic method under attack ($1779.1). Thus, the proposed robust optimization method enables consumers to make secure and cost-effective energy consumption decisions even if attackers try to manipulate the power market price.

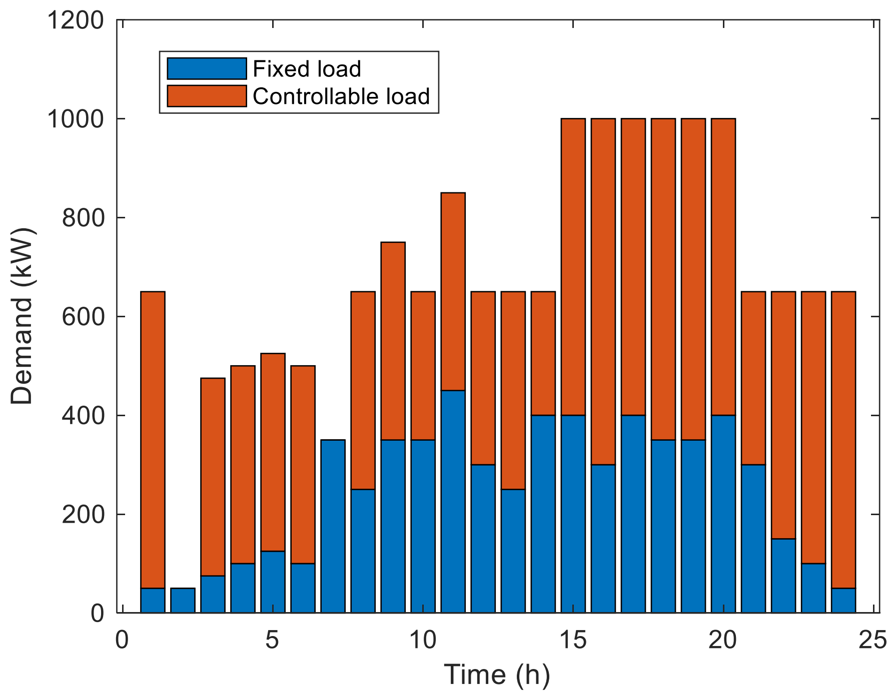

Figure 6.6 Load demand of robust optimization method under attack.

Table 6.2 Comparison of deterministic method and robust optimization method

	Deterministic method without attack ($\Gamma = 0$)	Deterministic method under attack ($\Gamma = 0$)	Robust optimization method under attack ($\Gamma = 24$)
Maximum Profit ($)	1830.9	1779.1	1819.8

6.5 Summary

This chapter proposes a robust optimization load management system to make optimal decisions of energy consumption where the real-time pricing is modeled as uncertain parameters. In the case study, the impact of cyberattacks on the pricing signal is analyzed based on a realistic real-time pricing policy and the loss of consumer level is quantified. The results show that when robust budget is considered in 24h, the maximum profit is $1819.8 under such attacks, which can save more than 2% economic loss compared with the traditional deterministic method. Therefore, the proposed method is better than comparable deterministic methods and can be used in consumer-oriented load management to reduce economic loss under real-time pricing attacks.

This approach primarily focuses on mitigating integrity attacks. However, a valuable research direction involves proactively detecting these attacks and developing strategies to disrupt the methods attackers use for deployment. For instance, deep learning models [103] and Kalman filter-based estimators [104] have been applied to identify cyber threats. Consequently, anomaly detection is a critical concern for large-scale industrial systems, such as bulk electric power grids.

CHAPTER 7. CONCLUSION AND FUTURE WORK

7.1 Conclusion

This dissertation investigates new approaches to improve Distribution Automation (DA) in response to the increasing challenges of integrating DERs. These approaches offer solutions to bolster the resilience of distribution systems by enabling more effective protection, fault diagnosis, voltage control, and load management. The main contributions are as follows. (1) A new distribution system Dynamic State Estimation Based Protection (EBP) scheme has been proposed. This protection scheme is reliable and secure with power electronics interfaces like inverters. (2) A real-time fault diagnosis framework based on DSE and DL has been proposed, which is accurate and robust to measurement noises. (3) A robust Volt-VAR optimization (VVO) method has been proposed. The proposed robust deep reinforcement learning (RDRL) framework can handle uncertainty better than standard DRL methods. (4) A robust optimization-based load management system has been proposed, providing customers with solutions to mitigate cyberattacks with reduced losses.

The proposed EBP scheme in Chapter 3 provides a systematic diagram for distribution protection from dynamic modeling of distribution systems to monitoring and control using DSE. It outperforms legacy protection functions due to the following benefits: (a) the simple settings of the protection without coordination issues, (b) the higher accuracy and fast response time, (c) its immunity to the impact of IBRs, and (d) the ability to detect high impedance faults.

The real-time diagnosis framework presented in Chapter 4 addresses the need for real-time fault detection, classification, and locating using physics-based and learning-based methods. The proposed deep learning-based fault classification using the 1D-CNN model can effectively process fault features and learn the feature boundary of fault classification with low computation cost. Additionally, the Dynamic State Estimation Based Fault Locating (EBFL) method effectively estimates fault location using just two sample values and is robust under measurement noise. In summary, this fault framework lays the groundwork for understanding how quick response mechanisms and accurate fault diagnosis contribute to the overall robustness of ADNs, which can be applied for real-time applications.

Towards the VVO problem for distribution systems, the proposed Robust Deep Reinforcement Learning (RDRL) method is compared with traditional optimization-based and DRL methods. The proposed RDRL has the following advantages: (a) it utilizes the "centralized training and decentralized deployment" framework, enabling fast and slow time-scale control; (b) it applies conformal prediction to establish uncertainty sets of PV output and load, which are inputs in the proposed robust DDPG algorithm; and (c) it has low computation cost and can ensure safe voltage control while having high sample efficiency and robustness under uncertainties.

For the load management system, we consider the real-time pricing policy to make optimal energy consumption decisions that fit the future energy market. The proposed robust optimization-based method is better than comparable deterministic methods and can be used in consumer-oriented load management to reduce economic loss under real-time pricing attacks. This system can be applied to dynamic electricity price scenarios by introducing an integer control parameter to improve robustness. Moreover, it’s immune to cyberattacks, providing a secure solution for load demand management of active consumers.

7.2 Future work

The dissertation focuses on tasks for advancing DA, which uses DSE and ML methods to deploy accurate and fast protection and fault diagnosis, including fault detection, classification, and locating. It also involves VVO for distribution systems and load management. We briefly discuss future work in the following areas to enhance the robustness and resilience of ADNs:

- **Smart sensors and data acquisition.** Advanced Metering Infrastructure (AMI) technologies, including Measurement Units (MUs), enable significant enhancements in real-time monitoring of distribution systems. Investigating how data from field sensors can be leveraged to facilitate advanced distribution system analytics is a promising research direction. Additionally, exploring the optimal placement of MUs, along with assessing the effects of various sampling rates and data update frequencies, could provide valuable insights into improving DSE performance—particularly in applications related to distribution protection and control.
- **Topology and network parameter identification.** Topology change is a noticeable phenomenon in distribution systems, whether it encounters faults with forwarding system reconfigurations or adopting different penetration of DERs. Distribution system operators (DSOs) may lack knowledge of network topologies, especially the connectivity of DERs in secondary distribution networks, as the utilities may not own them. Additionally, network parameter identification matters

since we need to consider dynamic parameters to ensure the accuracy of DSE and its applications, such as EBP and EBFL. Thus, further exploration of how topology and network parameter changes impact our proposed algorithm for real-time fault diagnosis is needed.

- **Training efficiency and scalability of ML.** Regarding DL and RL, there is an open question: "How can we improve learning efficiency with limited sample data and lead to a scalable method?". For example, as the network scale and number of controllable devices change in the VVO problem, the state/action space size varies accordingly. Authors in [100] define different Q-functions for different actions to get the scalable issue resolved. Moreover, we can utilize transfer learning [101] to pre-train the network parameters for better scalability. Note that real-world data is a rare and crucial element in power systems, significantly impacting the accuracy of the learning process. Thus, we can employ generative models [102] to acquire sufficient "virtual" data points and real-world data for training the DL/RL model.
- **Electric vehicles integration.** As a matter of fact, the increasing number of electric vehicles (EVs) will affect load demand, operation, energy management systems, and the energy market. By analyzing EV charging patterns alongside distribution system data, we can thoroughly examine the effect of uncoordinated EV charging on distribution grids. Additionally, we can explore the peer-to-peer electricity transaction when there are abundant battery energy storage systems (BESS) and EVs. It would be beneficial to discuss how to design regulation policies, control algorithms, and multi-vector energy centers for the future energy market.

APPENDIX A. DYNAMIC DEVICE MODEL OF DISTRIBUTION SYSTEMS

This appendix presents a high-fidelity modeling method, which can be expressed in a standard format as QDM and SCAQCF. These dynamic device models are derived to form a network model for simulation. Moreover, the critical components of active distribution systems are discussed, where the modeling of Inverter-Based Resources (IBRs) is represented in detail.

A.1 Compact Model, QDM and SCAQCF

A compact device model includes several mathematical equations, which can be grouped into three equation sets: terminal equation set, linear differential equation set, and nonlinear equation set, representing the physical circuit of the device.

Take the three-phase distribution line as an example, whose circuit model is shown in Figure A.1. The compact distribution line model derived from this circuit is given with the following equations:

$$
\begin{aligned}
&i_1(t) = C \cdot \frac{dv_1(t)}{dt} + i_L(t) + G \cdot L \cdot \frac{di_L(t)}{dt} \\
&i_2(t) = C \cdot \frac{dv_2(t)}{dt} - i_L(t) - G \cdot L \cdot \frac{di_L(t)}{dt} \\
&0 = -v_1(t) + v_2(t) + R \cdot (i_L(t) + G \cdot L \cdot \frac{di_L(t)}{dt}) + L \cdot \frac{di_L(t)}{dt}
\end{aligned}
$$

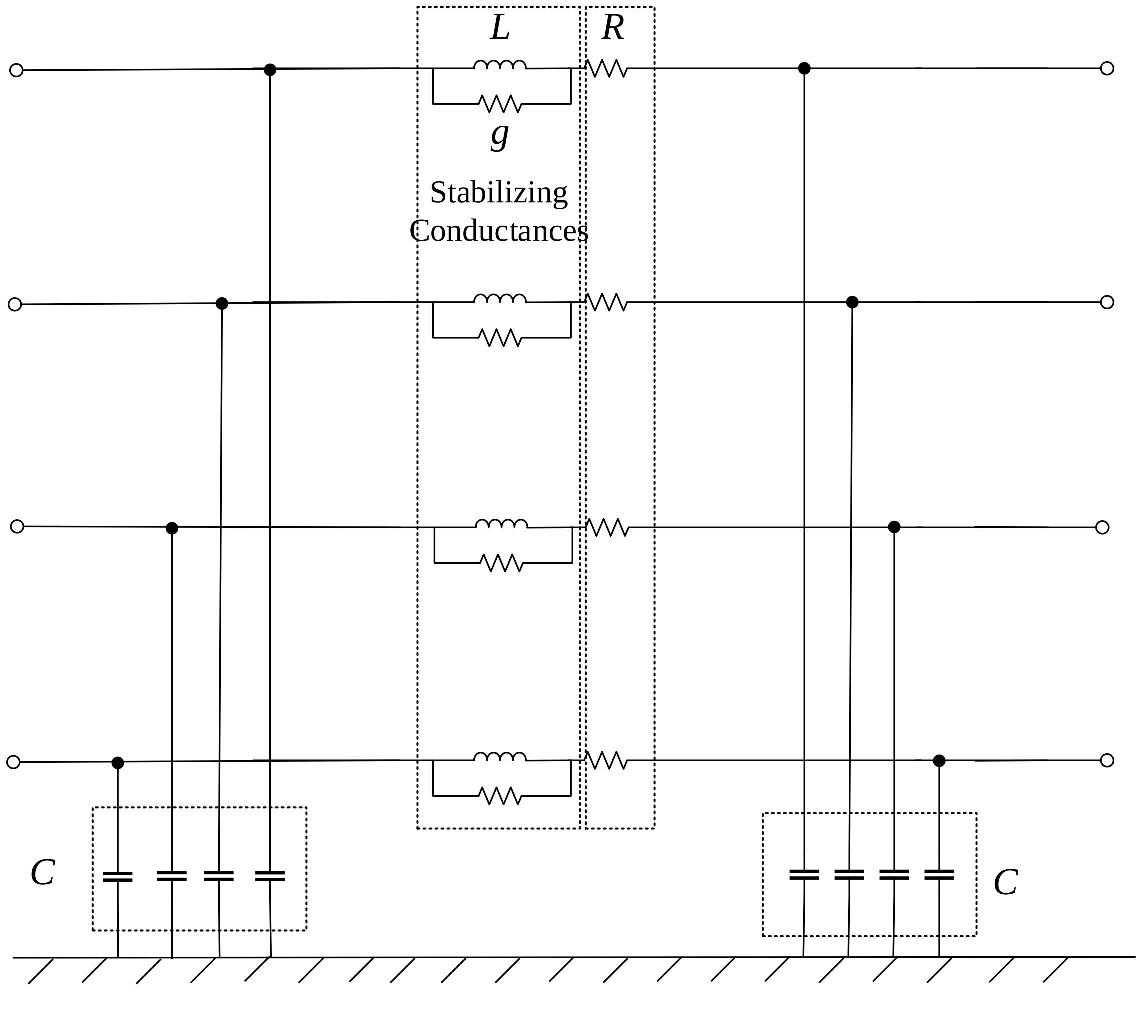

Figure A.1 Three Phase Distribution Line Model, where dashed boxes show the mutual couplings

The time domain state and control quadratized device model (SCQDM) is the basis of a standardized method with which the behavior of any power system device is rigorously defined. It consists of a set of differential equations with terms of first or second order. The standardized equation form is as follows:

$$i(t) = Y_{eqx1}x(t) + Y_{equ1}u(t) + D_{eqxd1}\frac{dx(t)}{dt} + C_{eqc1}$$

$$0 = Y_{eqx2}x(t) + Y_{equ2}u(t) + D_{eqxd2}\frac{dx(t)}{dt} + C_{eqc2}$$

$$0 = Y_{eqx3}x(t) + Y_{equ3}u(t) + \begin{Bmatrix} \vdots \\ x(t)^T \left\langle F^i_{eqxx3} \right\rangle x(t) \\ \vdots \end{Bmatrix} + \begin{Bmatrix} \vdots \\ u(t)^T \left\langle F^i_{equu3} \right\rangle u(t) \\ \vdots \end{Bmatrix} + C_{eqc3}$$

Constraints:

$$\mathbf{h}(\mathbf{x},\mathbf{u}) = Y_{hfeqx}\mathbf{x}(t) + Y_{hfequ}\mathbf{u}(t) + \begin{Bmatrix} \vdots \\ \mathbf{x}(t)^T \left\langle F^i_{hfeqxx} \right\rangle \mathbf{x}(t) \\ \vdots \end{Bmatrix}$$

$$+ \begin{Bmatrix} \vdots \\ \mathbf{u}(t)^T \left\langle F^i_{hfequu} \right\rangle \mathbf{u}(t) \\ \vdots \end{Bmatrix} + C_{hfeqc} \leq 0$$

$$\mathbf{u}_{hmin} \leq \mathbf{u}(t) \leq \mathbf{u}_{hmax}$$

$$\left|\mathbf{d}(t)\right| \leq \mathbf{u}_{hllim}$$

As the distribution line model is linear, the quadratized model is identical to the compact model. In compact matrix form, QDM of the distribution line model is:

In compact matrix form, the model is:

$$\begin{bmatrix} i(t) \\ 0 \end{bmatrix} = A \cdot \begin{bmatrix} v(t) \\ i_L(t) \end{bmatrix} + B \cdot \frac{d}{dt}\begin{bmatrix} v(t) \\ i_L(t) \end{bmatrix}$$

Where: $i(t) = \begin{bmatrix} i_1(t) \\ i_2(t) \end{bmatrix}, v(t) = \begin{bmatrix} v_1(t) \\ v_2(t) \end{bmatrix}$

$$A = \begin{bmatrix} 0 & 0 & I \\ 0 & 0 & -I \\ -I & I & R \end{bmatrix}, B = \begin{bmatrix} C & 0 & G \cdot L \\ 0 & C & -G \cdot L \\ 0 & 0 & R \cdot G \cdot L + L \end{bmatrix}$$

R, L, C: are the line section resistance, inductance and capacitance matrices (Note that the terms in the matrices are resistance, inductance and capacitance values). G is the matrix of stabilizing conductances.

Quadratic Integration: To obtain the QDM, the quadratic integration method is adopted to eliminate the differential terms. Assume that a linear system can be expressed as $\dot{x} = Ax$, where A is a constant square matrix and x is the state vector.

Let $t_m = t - \frac{h}{2}$. For integration over time interval $[t-h, t_m]$:

$$\int_{t-h}^{t_m} x(T)dT = \int_0^{\frac{h}{2}} x(\tau)d\tau = \frac{5h}{24}x(t-h) + \frac{h}{3}x(t_m) - \frac{h}{24}x(t)$$

For integration over time interval $[t-h, t]$:

$$\int_{t-h}^{t} x(T)dT = \int_0^{h} x(\tau)d\tau = \frac{h}{6}x(t-h) + \frac{2h}{3}x(t_m) + \frac{h}{6}x(t)$$

For integration over time interval $[t_m, t]$:

$$\int_{t_m}^{t} x(T)dT = \int_{h/2}^{h} x(\tau)d\tau = -\frac{h}{24}x(t-h) + \frac{h}{3}x(t_m) + \frac{5h}{24}x(t)$$

The algebraic companion form model is derived after quadratic integration of the quadratized model with a time step h. Then, according to (3.2), the SCAQCF of distribution line model is:

$$\begin{bmatrix} i(t) \\ 0 \\ i(t_m) \\ 0 \end{bmatrix} = E \cdot F_1 \cdot \begin{bmatrix} v(t) \\ i_L(t) \\ v(t_m) \\ i_L(t_m) \end{bmatrix} - b_{eq}$$

where $b_{eq} = E \cdot F_2 \cdot \begin{bmatrix} v(t-h) \\ i_L(t-h) \end{bmatrix} + E \cdot F_3 \cdot \begin{bmatrix} i(t-h) \\ 0 \end{bmatrix}$

$$E=\begin{bmatrix} \frac{h}{6}I & 0 & \frac{2h}{3}I & 0 \\ 0 & 0 & 0 & 0 \\ -\frac{h}{24}I & 0 & \frac{h}{3}I & 0 \\ 0 & 0 & 0 & 0 \end{bmatrix}^{-1} = \begin{bmatrix} \frac{4}{h}I & 0 & -\frac{8}{h}I & 0 \\ 0 & I & 0 & 0 \\ \frac{1}{2h}I & 0 & \frac{2}{h}I & 0 \\ 0 & 0 & 0 & I \end{bmatrix}$$

$$F_1=\begin{bmatrix} \frac{h}{6}A+B & \frac{2h}{3}A \\ -\frac{h}{24}A & \frac{h}{3}A+B \end{bmatrix}, F_2=\begin{bmatrix} B-\frac{h}{6}A \\ B-\frac{5h}{24}A \end{bmatrix}, F_3=\begin{bmatrix} \frac{h}{6}I & 0 \\ 0 & 0 \\ \frac{5h}{24}I & 0 \\ 0 & 0 \end{bmatrix}$$

A.2 Devices in Active Distribution Systems

The growing integration of renewable energy into power distribution systems is transforming how electricity is generated, distributed, and consumed. Solar and wind energy, in particular, are being increasingly connected to both transmission and distribution networks. For example, Germany's Energiewende (energy transition) initiative has successfully integrated over 50% renewable energy into its grid, yet it relies on advanced energy storage, grid modernization, and smart systems to handle fluctuating solar and wind outputs. Similarly, California has aggressively deployed rooftop solar and wind farms, but it also depends on advanced forecasting, energy storage systems like Tesla's Powerwall, and demand-response programs to ensure grid reliability during peak demand or low generation periods. Corresponding, the active distribution network (ADN) concept was proposed to enhance power system's stability, reliability, and resilience. Unlike the traditional "passive" distribution system, ADN allows bidirectional power flow and varied operation modes by adapting intelligent control and operation strategies. Figure A.2 shows power distribution system with integration of renewable energy with bidirectional power flow.

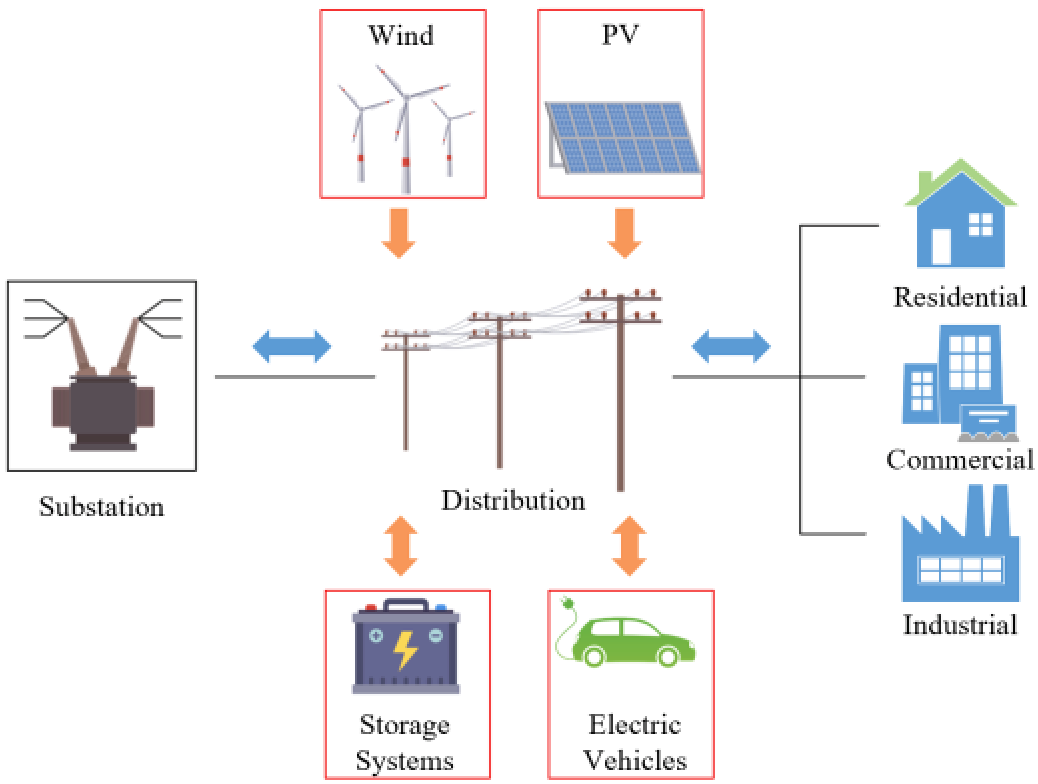

Figure A.2 Power distribution system with integration of renewable energy

Table A.1 shows the critical devices in distribution systems, including transformers, distribution line sections, three-phase loads, capacitors, and inverters etc. In addition to those common, modern power distribution systems must incorporate several other critical elements: energy storage systems for balancing supply and demand, communication networks and automation systems (such as SCADA), demand response systems, electric vehicle charging infrastructure, and power quality management, especially with the growing integration of renewable energy. However, we focus on the high-fidelity modeling and simulation of IBR dominated distribution system for protection and control applications in chapter 3 and chapter 4. Other applications of DA will be considered in other chapters.

Table A.1 Critical devices in distribution systems

Device	Description
Switch/breaker	Automatically isolate faults and restore power, improving the resilience and reliability of the distribution system.
Transformer	Steps up or steps down voltage levels to enable efficient power transmission and distribution, ensuring that the voltage is suitable for the consumers or other parts of the grid.
Distribution line section	Transfers electrical power from substations to consumers through overhead or underground lines.
Single-phase /three-phase load	Electrical devices or systems that consume power in either single-phase (for small loads) or three-phase (for larger, industrial loads) configurations.
Capacitor	Improves power factor by reducing reactive power in the system, helping to stabilize voltage and improve overall efficiency.
Smart inverter	Convert DC from DERs (like solar panels) into AC and provide additional services such as voltage and frequency regulation, as well as reactive power support.
Voltage regulator	Maintains a constant voltage level in the distribution network to ensure reliable operation of electrical devices.

A.3 IBR Modeling

This section presents the quasi-dynamic domain model of a voltage source converter (VSC), which is one way to model IBRs. The block diagram of the quasi-dynamic domain voltage source converter is shown in Figure A.3. The block diagram provides the AC and DC terminals and control signals coming from the controller. The control signals are the modulation index, modulation angle and frequency.

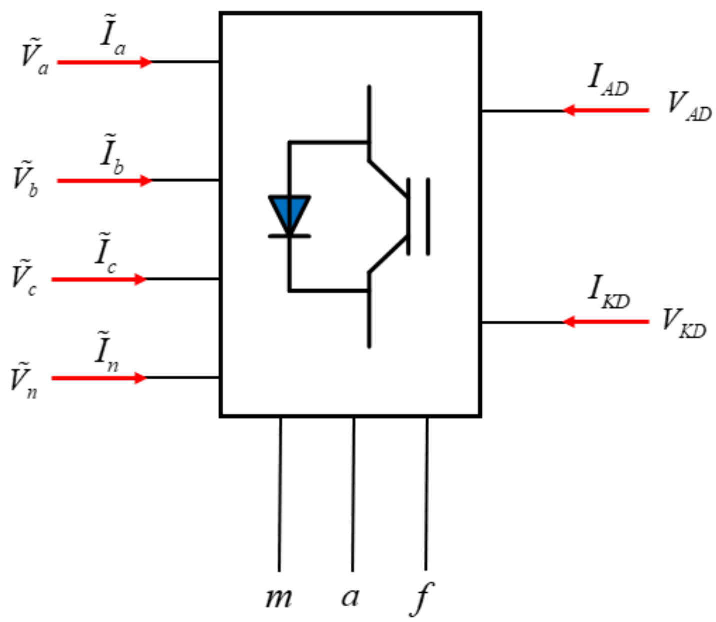

Figure A.3 Block diagram of the quasi-dynamic domain VSC model

Figure A.4 illustrates the overall system of an AC-DC VSC. An AC-DC VSC consists of six valves, each valve contains an IGBT, a diode, snubber circuits and current limiting circuits, capacitors at both AC and DC sides, and smoothing/filter inductors at DC and AC side. These components are interconnected to yield the AC-DC converter topology.

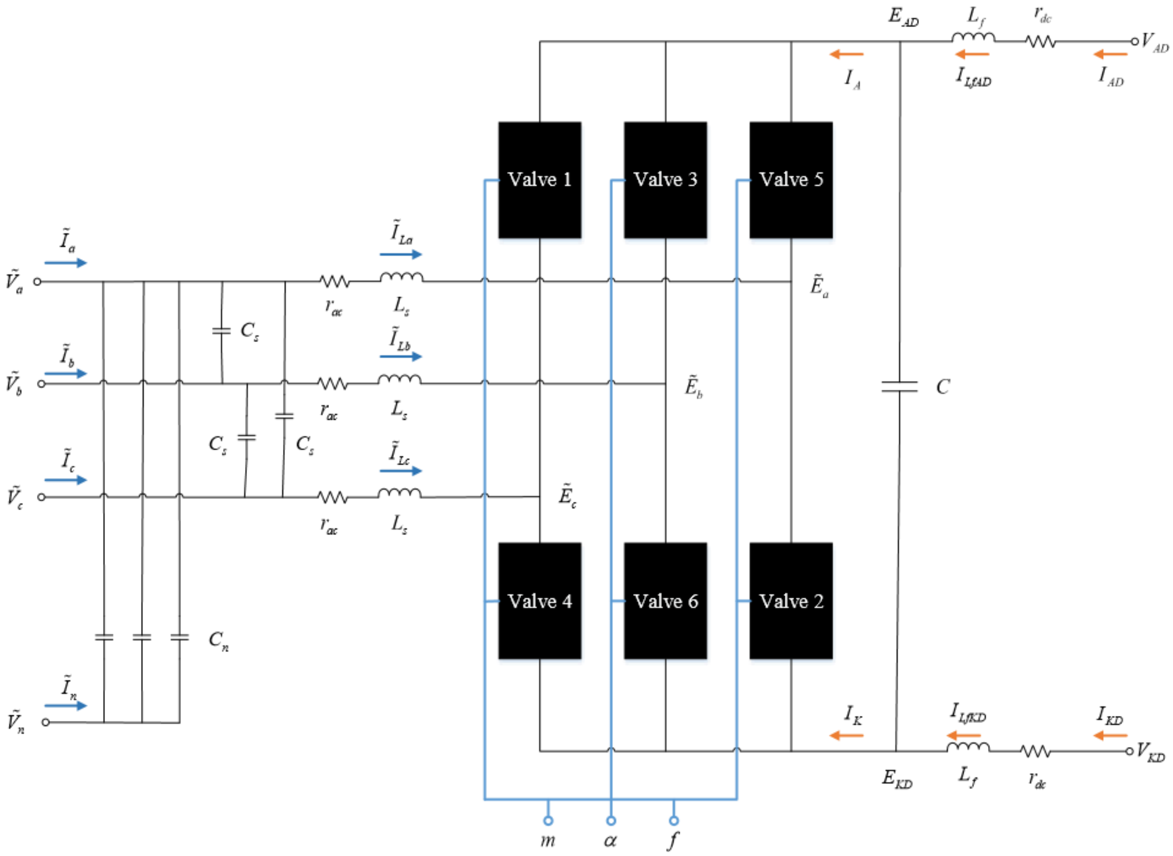

Figure A.4 Circuit diagram of DC-AC inverter

Depending on the operating state of valves, there are 8 different operating modes. The switch conditions for each operating mode are shown in Table A.2.

Table A.2 Inverter operating modes with corresponding switching conditions

Mode	Valve 1	Valve 2	Valve 3	Valve 4	Valve 5	Valve 6
0	OFF	OFF	OFF	ON	ON	ON
1	ON	ON	OFF	OFF	OFF	ON
2	ON	ON	ON	OFF	OFF	OFF
3	OFF	ON	ON	ON	OFF	OFF
4	OFF	OFF	ON	ON	ON	OFF
5	ON	OFF	OFF	OFF	ON	ON
6	ON	OFF	ON	OFF	ON	OFF
7	OFF	ON	OFF	ON	OFF	ON

The **compact model** of the inverter is given by:

$$I_{AD} = I_{LfAD} \tag{A.1}$$

$$I_{KD} = I_{LfKD} \tag{A.2}$$

$$\tilde{I}_a = \tilde{I}_{La} + j4\pi fC_s\tilde{V}_a - j2\pi fC_s\tilde{V}_b - j2\pi fC_s\tilde{V}_c + j2\pi fC_n\tilde{V}_a - j2\pi fC_n\tilde{V}_n \tag{A.3}$$

$$\tilde{I}_b = \tilde{I}_{Lb} + j4\pi fC_s\tilde{V}_b - j2\pi fC_s\tilde{V}_a - j2\pi fC_s\tilde{V}_c + j2\pi fC_n\tilde{V}_b - j2\pi fC_n\tilde{V}_n \tag{A.4}$$

$$\tilde{I}_c = \tilde{I}_{Lc} + j4\pi fC_s\tilde{V}_c - j2\pi fC_s\tilde{V}_a - j2\pi fC_s\tilde{V}_b + j2\pi fC_n\tilde{V}_c - j2\pi fC_n\tilde{V}_n \tag{A.5}$$

$$\tilde{I}_n = j6\pi fC_n\tilde{V}_n - j2\pi fC_n\tilde{V}_a - j2\pi fC_n\tilde{V}_b - j2\pi fC_n\tilde{V}_c \tag{A.6}$$

$$I_m = 0 \quad \text{(terminal m)} \tag{A.7}$$

$$I_\alpha = 0 \quad \text{(terminal a)} \tag{A.8}$$

$$I_f = 0 \quad \text{(terminal f)} \tag{A.9}$$

$$0 = \tilde{V}_a - \tilde{E}_a - j2\pi fL_s\tilde{I}_{La} - L_s\frac{d\tilde{I}_{La}}{dt} - r_{ac}\tilde{I}_{La} \tag{A.10}$$

$$0 = \tilde{V}_b - \tilde{E}_b - j2\pi fL_s\tilde{I}_{Lb} - L_s\frac{d\tilde{I}_{Lb}}{dt} - r_{ac}\tilde{I}_{Lb} \tag{A.11}$$

$$0 = \tilde{V}_c - \tilde{E}_c - j2\pi fL_s\tilde{I}_{Lc} - L_s\frac{d\tilde{I}_{Lc}}{dt} - r_{ac}\tilde{I}_{Lc} \tag{A.12}$$

$$0 = V_{AD} - E_{AD} - L_f\frac{dI_{LfAD}}{dt} - r_{dc}I_{LfAD} \tag{A.13}$$

$$0 = V_{KD} - E_{KD} - L_f\frac{dI_{LfKD}}{dt} - r_{dc}I_{LfKD} \tag{A.14}$$

$$0 = \frac{m}{2\sqrt{2}}\left(E_{AD} - E_{KD}\right)e^{j\alpha} - j2\pi fL_s\tilde{I}_{La} - L_s\frac{d\tilde{I}_{La}}{dt} - \tilde{E}_a \tag{A.15}$$

$$0=\frac{m}{2\sqrt{2}}\left(E_{AD}-E_{KD}\right)e^{j\left(\alpha-\frac{2\pi}{3}\right)}-j2\pi fL_s\tilde{I}_{Lb}-L_s\frac{d\tilde{I}_{Lb}}{dt}-\tilde{E}_b \tag{A.16}$$

$$0=\frac{m}{2\sqrt{2}}\left(E_{AD}-E_{KD}\right)e^{j\left(\alpha+\frac{2\pi}{3}\right)}-j2\pi fL_s\tilde{I}_{Lc}-L_s\frac{d\tilde{I}_{Lc}}{dt}-\tilde{E}_c \tag{A.17}$$

$$0=C\frac{dE_{AD}}{dt}-C\frac{dE_{KD}}{dt}+I_A-I_{LfAD} \tag{A.18}$$

$$0=-C\frac{dE_{AD}}{dt}+C\frac{dE_{KD}}{dt}+I_K-I_{LfKD} \tag{A.19}$$

$$0=I_{Lar}+I_{Lbr}+I_{Lcr}+I_A+I_k \tag{A.20}$$

$$0=\underbrace{\mathrm{Re}\left(\tilde{E}_a\tilde{I}_{La}^*+\tilde{E}_b\tilde{I}_{Lb}^*+\tilde{E}_c\tilde{I}_{Lc}^*\right)}_{AC\ \text{Power}}+\underbrace{E_{AD}I_A}_{DC\ \text{Power}}+\underbrace{E_{KD}I_K}_{DC\ \text{Power}} \tag{A.21}$$

The through variables are: $i^T=\left[I_{AD}\quad I_{KD}\quad \tilde{I}_a\quad \tilde{I}_b\quad \tilde{I}_c\quad \tilde{I}_n\quad I_m\quad I_\alpha\quad I_f\right]^T$

The state variables are:

$$x^T=\left[V_{AD}\quad V_{KD}\quad \tilde{V}_a\quad \tilde{V}_b\quad \tilde{V}_c\quad \tilde{V}_n\quad m\quad \alpha\quad f\quad \tilde{E}_a\quad \tilde{E}_b\quad \tilde{E}_c\quad E_{AD}\quad E_{KD}\quad \tilde{I}_{La}\quad \tilde{I}_{Lb}\quad \tilde{I}_{Lc}\right.$$
$$\left.I_{LfAD}\quad I_{LfKD}\quad I_A\quad I_K\right]$$

There is no control variable in the model.

The compact model has 21 equations and 21 state variables.

Normalization Factors (for all the states x):

StateNormFactor:

$$[V_{DCrated},V_{DCrated},V_{ACrated},V_{ACrated},V_{ACrated},1.0,1.0,60.0,V_{DCrated},V_{DCrated},V_{DCrated},I_{DCrated},I_{DCrated},$$
$$I_{ACrated},I_{ACrated},I_{ACrated},V_{ACrated},V_{ACrated},V_{ACrated},S_{rated}]$$

Normalization Factors (for all the through variables and equations):

ThroughNormFactor:

$$[I_{DCrated}, I_{DCrated}, I_{ACrated}, I_{ACrated}, I_{ACrated}, 1.0, 1.0, 60.0, V_{DCrated}, V_{DCrated}, V_{DCrated}, I_{DCrated}, I_{DCrated}, V_{ACrated}, V_{ACrated}, V_{ACrated}, V_{ACrated}, V_{ACrated}, V_{ACrated}, S_{rated}]$$

where,

$$V_{ACrated} = \frac{V_{LL\_ACrated}}{\sqrt{3}}, I_{ACrated} = \frac{S_{rated}}{\sqrt{3}V_{LL\_ACrated}}, I_{DCrated} = \frac{S_{rated}}{V_{DCrated}}$$

$S_{rated}, V_{LL\_ACrated}, V_{DCrated}$ are obtained from the user inteface.

ControlNormFactor: this model does not have control variables.

Equations (A.1) to (A.11) and (A.14) to (A.16) reflect the physical properties of the VSC circuit. Equations (A.17) to (A.19) present the relationship between the AC side and DC side voltages by modulation index and phase angle. Equations (A.12), (A.13) and (A.20) simulate the dynamic of DC side capacitor by the active power flow in the VSC and current inflow of the capacitor.

Quasi-dynamic domain QDM:

The compact device model is quadratized to provide the quadratized device model (QDM). For the quasi-dynamic domain, the phasor quantities are split into real and imaginary components. Any terms that have nonlinearities great than two, they are converted into quadratic terms by the introduction of additional state variables.

Note that equation sets 1 and 2 must be linear. This means that it may be necessary to introduce additional variables to meet this requirement. In this case, equation set 1 includes nonlinear equations. The following additional state variables are introduced to convert these equations into linear.

$$\tilde{Y}_1(t) = f(t)\tilde{V}_a(t)$$
$$\tilde{Y}_2(t) = f(t)\tilde{V}_b(t)$$
$$\tilde{Y}_3(t) = f(t)\tilde{V}_c(t)$$
$$\tilde{Y}_4(t) = f(t)\tilde{V}_n(t)$$
$$\tilde{Z}_1(t) = f(t)\tilde{I}_{La}(t)$$
$$\tilde{Z}_2(t) = f(t)\tilde{I}_{Lb}(t)$$
$$\tilde{Z}_3(t) = f(t)\tilde{I}_{Lc}(t)$$

Upon substitution of above, equation set 1 becomes linear.

Subsequently, all the complex equations in the resulting model are split into real and imaginary.

Any remaining nonlinear equations are quadratized. For this model the following equation needs to be quadratized (A.20), (A.21) and (A.22). Consider equation (A.20):

$$0 = \frac{m}{2\sqrt{2}}\left(E_{AD} - E_{KD}\right)e^{j\alpha} - j2\pi fL_s\tilde{I}_{La} - L_s\frac{d\tilde{I}_{La}}{dt} - \tilde{E}_a$$

First, the equation is split into real and imaginary parts.

$$0 = \frac{m}{2\sqrt{2}}\left(E_{AD} - E_{KD}\right)\cos\alpha + 2\pi fL_s I_{Lai} - L_s\frac{dI_{Lar}}{dt} - E_{ar}$$
$$0 = \frac{m}{2\sqrt{2}}\left(E_{AD} - E_{KD}\right)\sin\alpha - 2\pi fL_s I_{Lar} - L_s\frac{dI_{Lai}}{dt} - E_{ai}$$

Subsequently, we introduce eight new variables

$$cs = \cos\alpha \quad \rightarrow \quad \frac{dcs}{dt} = -ss\frac{d\alpha}{dt}$$

$$ss = \sin\alpha \quad \rightarrow \quad \frac{dss}{dt} = cs\frac{d\alpha}{dt}$$

$$x_1 = \left(E_{AD} - E_{KD}\right)cs$$

$$x_2 = \left(E_{AD} - E_{KD}\right)ss$$

$$x_3 = \frac{d\alpha}{dt}$$

$$x_4 = \frac{dcs}{dt}$$

$$x_5 = \frac{1}{2\sqrt{2}}mx_1$$

$$x_6 = \frac{1}{2\sqrt{2}}mx_2$$

Using the new variables, the quadratized equation becomes

$$0 = x_5 + 2\pi fL_s I_{Lai} - L_s\frac{dI_{Lar}}{dt} - E_{ar}$$

$$0 = x_6 - 2\pi fL_s I_{Lar} - L_s\frac{dI_{Lai}}{dt} - E_{ai}$$

$$0 = x_1 - \left(E_{AD} - E_{KD}\right)cs$$

$$0 = x_2 - \left(E_{AD} - E_{KD}\right)ss$$

$$0 = x_3 - \frac{d\alpha}{dt}$$

$$0 = x_4 - \frac{dcs}{dt}$$

$$0 = x_4 + ss.x_3$$

$$0 = cs^2 + ss^2 - 1$$

$$0 = x_5 - \frac{1}{2\sqrt{2}}mx_1$$

$$0 = x_6 - \frac{1}{2\sqrt{2}}mx_2$$

Similarly, the equations for phase b and phase c become:

$$0=-\frac{1}{2}x_5+\frac{\sqrt{3}}{2}x_6+2\pi fL_sI_{Lbi}-L_s\frac{dI_{Lbr}}{dt}-E_{br}$$
$$0=-\frac{\sqrt{3}}{2}x_5-\frac{1}{2}x_6-2\pi fL_sI_{Lbr}-L_s\frac{dI_{Lbi}}{dt}-E_{bi}$$
$$0=-\frac{1}{2}x_5-\frac{\sqrt{3}}{2}x_6+2\pi fL_sI_{Lci}-L_s\frac{dI_{Lcr}}{dt}-E_{cr}$$
$$0=\frac{\sqrt{3}}{2}x_5-\frac{1}{2}x_6-2\pi fL_sI_{Lcr}-L_s\frac{dI_{Lci}}{dt}-E_{ci}$$

Note that the quadratization has introduced a number of new variables and an equal number of additional equations. This way the mathematical consistency is maintained.

The quadratized equations are listed as follows:

Equation Set 1:

$$I_{AD}=I_{LfAD}$$

$$I_{KD}=I_{LfKD}$$

$$I_{ar}=I_{Lar}-2\pi\left(2C_s+C_n\right)Y_{1i}+2\pi C_sY_{2i}+2\pi C_sY_{3i}+2\pi C_nY_{4i}$$

$$I_{ai}=I_{Lai}+2\pi\left(2C_s+C_n\right)Y_{1r}-2\pi C_sY_{2r}-2\pi C_sY_{3r}-2\pi C_nY_{4r}$$

$$I_{br}=I_{Lbr}-2\pi\left(2C_s+C_n\right)Y_{2i}+2\pi C_sY_{1i}+2\pi C_sY_{3i}+2\pi C_nY_{4i}$$
$$I_{bi}=I_{Lbi}+2\pi\left(2C_s+C_n\right)Y_{2r}-2\pi C_sY_{1r}-2\pi C_sY_{3r}-2\pi C_nY_{4r}$$

$$I_{cr}=I_{Lcr}-2\pi\left(2C_s+C_n\right)Y_{3i}+2\pi C_sY_{1i}+2\pi C_sY_{2i}+2\pi C_nY_{4i}$$
$$I_{ci}=I_{Lci}+2\pi\left(2C_s+C_n\right)Y_{3r}-2\pi C_sY_{1r}-2\pi C_sY_{2r}-2\pi C_nY_{4r}$$

$$I_{nr}=-6\pi C_nY_{4i}+2\pi C_nY_{1i}+2\pi C_nY_{2i}+2\pi C_nY_{3i}$$
$$I_{ni}=6\pi C_nY_{4r}-2\pi C_nY_{1r}-2\pi C_nY_{2r}-2\pi C_nY_{3r}$$

$$I_m=0\ \text{(Terminal m)}$$

$$I_\alpha=0\ (\text{Terminal}\ \alpha)$$

$I_f = 0$ (Terminal f)

Equation Set 2:

$$0 = V_{ar} - E_{ar} + 2\pi L_s Z_{1i} - L_s \frac{dI_{Lar}}{dt} - r_{ac} I_{Lar}$$
$$0 = V_{ai} - E_{ai} - 2\pi L_s Z_{1r} - L_s \frac{dI_{Lai}}{dt} - r_{ac} I_{Lai}$$

$$0 = V_{br} - E_{br} + 2\pi L_s Z_{2i} - L_s \frac{dI_{Lbr}}{dt} - r_{ac} I_{Lbr}$$
$$0 = V_{bi} - E_{bi} - 2\pi L_s Z_{2r} - L_s \frac{dI_{Lbi}}{dt} - r_{ac} I_{Lbi}$$

$$0 = V_{cr} - E_{cr} + 2\pi L_s Z_{3i} - L_s \frac{dI_{Lcr}}{dt} - r_{ac} I_{Lcr}$$
$$0 = V_{ci} - E_{ci} - 2\pi L_s Z_{3r} - L_s \frac{dI_{Lci}}{dt} - r_{ac} I_{Lci}$$

$$0 = V_{AD} - E_{AD} - L_f \frac{dI_{LfAD}}{dt} - r_{dc} I_{LfAD}$$

$$0 = V_{KD} - E_{KD} - L_f \frac{dI_{LfKD}}{dt} - r_{dc} I_{LfKD}$$

$$0 = x_5 + 2\pi L_s Z_{1i} - L_s \frac{dI_{Lar}}{dt} - E_{ar}$$
$$0 = x_6 - 2\pi L_s Z_{1r} - L_s \frac{dI_{Lai}}{dt} - E_{ai}$$

$$0 = -\frac{1}{2} x_5 + \frac{\sqrt{3}}{2} x_6 + 2\pi L_s Z_{2i} - L_s \frac{dI_{Lbr}}{dt} - E_{br}$$
$$0 = -\frac{\sqrt{3}}{2} x_5 - \frac{1}{2} x_6 - 2\pi L_s Z_{2r} - L_s \frac{dI_{Lbi}}{dt} - E_{bi}$$
$$0 = -\frac{1}{2} x_5 - \frac{\sqrt{3}}{2} x_6 + 2\pi L_s Z_{3i} - L_s \frac{dI_{Lcr}}{dt} - E_{cr}$$
$$0 = \frac{\sqrt{3}}{2} x_5 - \frac{1}{2} x_6 - 2\pi L_s Z_{3r} - L_s \frac{dI_{Lci}}{dt} - E_{ci}$$

$$0 = C \frac{dE_{AD}}{dt} - C \frac{dE_{KD}}{dt} + I_A - I_{LfAD}$$

$$0 = -C\frac{dE_{AD}}{dt} + C\frac{dE_{KD}}{dt} + I_K - I_{LfKD}$$

$$0 = I_{Lar} + I_{Lbr} + I_{Lcr} + I_A + I_k$$

$$0 = x_3 - \frac{d\alpha}{dt}$$

$$0 = x_4 - \frac{dcs}{dt}$$

Equation Set 3:

$$0 = Y_{1r} - fV_{ar}$$

$$0 = Y_{1i} - fV_{ai}$$

$$0 = Y_{2r} - fV_{br}$$

$$0 = Y_{2i} - fV_{bi}$$

$$0 = Y_{3r} - fV_{cr}$$

$$0 = Y_{3i} - fV_{ci}$$

$$0 = Y_{4r} - fV_{nr}$$

$$0 = Y_{4i} - fV_{ni}$$

$$0 = Z_{1r} - fI_{Lar}$$

$$0 = Z_{1i} - fI_{Lai}$$

$$0 = Z_{2r} - fI_{Lbr}$$

$$0 = Z_{2i} - fI_{Lbi}$$

$$0 = Z_{3r} - fI_{Lcr}$$

$$0 = Z_{3i} - fI_{Lci}$$

$$0 = x_1 - \left(E_{AD} - E_{KD}\right)cs$$
$$0 = x_2 - \left(E_{AD} - E_{KD}\right)ss$$
$$0 = x_4 + ss \cdot x_3$$
$$0 = cs^2 + ss^2 - 1$$
$$0 = x_5 - \frac{1}{2\sqrt{2}} m x_1$$
$$0 = x_6 - \frac{1}{2\sqrt{2}} m x_2$$

$$0 = E_{ar} I_{Lar} + E_{ai} I_{Lai} + E_{br} I_{Lbr} + E_{bi} I_{Lbi} + E_{cr} I_{Lcr} + E_{ci} I_{Lci} + E_{AD} I_A + E_{KD} I_K$$

Note, the SCQDM has 53 states and 53 equations as follows: 13 through equations, 19 internal linear equations and 21 internal non-linear equations.

The through variables are:

$$i^T = \; I_{AD},\; I_{KD}, I_{ar},\; I_{ai},\; I_{br}, I_{bi},\; I_{cr}, I_{ci},\; I_{nr}, I_{ni}, I_m,\; I_\alpha,\; I_f$$

The states are:

$$x^T = \; V_{AD},\; V_{KD},\; V_{ar}, V_{ai},\; V_{br}, V_{bi},\;\; V_{cr}, V_{ci},\; V_{nr}, V_{ni},\; m,\; \alpha,\; f,$$

$$E_{ar}, E_{ai},\; E_{br}, E_{bi}, E_{cr}, E_{ci},\quad E_{AD}, E_{KD},\quad I_{Lar}, I_{Lai}, I_{Lbr}, I_{Lbi}, I_{Lcr}, I_{Lci}\quad I_{LfAD}, I_{LfKD}, I_A, I_K,$$

$$x_3, x_4, Y_{1r}, Y_{1i}, Y_{2r}, Y_{2i}, Y_{3r}, Y_{3i}, Y_{4r}, Y_{4i}, Z_{1r}, Z_{1i}, Z_{2r}, Z_{2i}, Z_{3r}, Z_{3i},\quad x_1, x_2, cs, ss, x_5, x_6$$

The matrices appearing in the standard SCQDM from are:

Matrix Y_{eqx1} non zero terms:

$Y_{eqx1}[0][27] = 1.0;$

$Y_{eqx1}[1][28] = 1.0;$

$Y_{eqx1}[2][21] = 1.0, Y_{eqx1}[2][34] = -2\pi(2C_s + C_n), Y_{eqx1}[2][36] = 2\pi C_s,$

$Y_{eqx1}[2][38] = 2\pi C_s, Y_{eqx1}[2][40] = 2\pi C_n;$

$Y_{eqx1}[3][22] = 1.0, Y_{eqx1}[3][33] = 2\pi(2C_s + C_n), Y_{eqx1}[3][35] = -2\pi C_s,$

$Y_{eqx1}[3][37] = -2\pi C_s, Y_{eqx1}[3][39] = -2\pi C_n;$

$Y_{eqx1}[4][23] = 1.0, Y_{eqx1}[4][36] = -2\pi(2C_s + C_n), Y_{eqx1}[4][34] = 2\pi C_s,$

$Y_{eqx1}[4][38] = 2\pi C_s, Y_{eqx1}[4][40] = 2\pi C_n;$

$Y_{eqx1}[5][24] = 1.0, Y_{eqx1}[5][35] = 2\pi(2C_s + C_n), Y_{eqx1}[5][33] = -2\pi C_s,$

$Y_{eqx1}[5][37] = -2\pi C_s, Y_{eqx1}[5][39] = -2\pi C_n;$

$Y_{eqx1}[6][25] = 1.0, Y_{eqx1}[6][38] = -2\pi(2C_s + C_n), Y_{eqx1}[6][34] = 2\pi C_s,$

$Y_{eqx1}[6][36] = 2\pi C_s, Y_{eqx1}[6][40] = 2\pi C_n;$

$Y_{eqx1}[7][26] = 1.0, Y_{eqx1}[7][37] = 2\pi(2C_s + C_n), Y_{eqx1}[7][33] = -2\pi C_s,$

$Y_{eqx1}[7][35] = -2\pi C_s, Y_{eqx1}[7][39] = -2\pi C_n;$

$Y_{eqx1}[8][40] = -6\pi C_n, Y_{eqx1}[8][34] = 2\pi C_n, Y_{eqx1}[8][36] = 2\pi C_n,$

$Y_{eqx1}[8][38] = 2\pi C_n;$

$Y_{eqx1}[9][39] = 6\pi C_n, Y_{eqx1}[9][33] = -2\pi C_n, Y_{eqx1}[9][35] = -2\pi C_n,$

$Y_{eqx1}[9][37] = -2\pi C_n;$

Matrix Y_{eqx2} non zero terms:

$Y_{eqx2}[0][2] = 1.0, Y_{eqx2}[0][13] = -1.0, Y_{eqx2}[0][42] = 2\pi L_s, Y_{eqx2}[0][21] = -r_{ac};$

$Y_{eqx2}[1][3] = 1.0, Y_{eqx2}[1][14] = -1.0, Y_{eqx2}[1][41] = -2\pi L_s, Y_{eqx2}[1][22] = -r_{ac};$

$Y_{eqx2}[2][4] = 1.0, Y_{eqx2}[2][15] = -1.0, Y_{eqx2}[2][44] = 2\pi L_s, Y_{eqx2}[2][23] = -r_{ac};$

$Y_{eqx2}[3][5] = 1.0, Y_{eqx2}[3][16] = -1.0, Y_{eqx2}[3][43] = -2\pi L_s, Y_{eqx2}[3][24] = -r_{ac};$

$Y_{eqx2}[4][6] = 1.0, Y_{eqx2}[4][17] = -1.0, Y_{eqx2}[4][46] = 2\pi L_s, Y_{eqx2}[4][25] = -r_{ac};$

$Y_{eqx2}[5][7] = 1.0, Y_{eqx2}[5][18] = -1.0, Y_{eqx2}[5][45] = -2\pi L_s, Y_{eqx2}[5][26] = -r_{ac};$

$Y_{eqx2}[6][0] = 1.0, Y_{eqx2}[6][19] = -1.0, Y_{eqx2}[6][27] = -r_{dc};$

$Y_{eqx2}[7][1] = 1.0, Y_{eqx2}[7][20] = -1.0, Y_{eqx2}[7][28] = -r_{dc};$

$Y_{eqx2}[8][51]=1.0, Y_{eqx2}[8][42]=2\pi L_s, Y_{eqx2}[8][13]=-1.0;$

$Y_{eqx2}[9][52]=1.0, Y_{eqx2}[9][41]=-2\pi L_s, Y_{eqx2}[9][14]=-1.0;$

$Y_{eqx2}[10][51]=-\frac{1}{2}, Y_{eqx2}[10][52]=\frac{\sqrt{3}}{2}, Y_{eqx2}[10][44]=2\pi L_s, Y_{eqx2}[10][15]=-1.0;$

$Y_{eqx2}[11][51]=-\frac{\sqrt{3}}{2}, Y_{eqx2}[11][52]=-\frac{1}{2}, Y_{eqx2}[11][43]=-2\pi L_s, Y_{eqx2}[11][16]=-1.0;$

$Y_{eqx2}[12][51]=-\frac{1}{2}, Y_{eqx2}[12][52]=-\frac{\sqrt{3}}{2}, Y_{eqx2}[12][46]=2\pi L_s, Y_{eqx2}[12][17]=-1.0;$

$Y_{eqx2}[13][51]=\frac{\sqrt{3}}{2}, Y_{eqx2}[13][52]=-\frac{1}{2}, Y_{eqx2}[13][45]=-2\pi L_s, Y_{eqx2}[13][18]=-1.0;$

$Y_{eqx2}[14][29]=1.0, Y_{eqx2}[14][27]=-1.0;$

$Y_{eqx2}[15][30]=1.0, Y_{eqx2}[15][28]=-1.0;$

$Y_{eqx2}[16][21]=1.0, Y_{eqx2}[16][23]=1.0, Y_{eqx2}[16][25]=1.0, Y_{eqx2}[16][29]=1.0,$

$Y_{eqx2}[16][30]=1.0;$

$Y_{eqx2}[17][31]=1.0;$

$Y_{eqx2}[18][32]=1.0$

Matrix D_{eqx2} non zero terms:

$D_{eqx2}[0][21]=-L_s;$

$D_{eqx2}[1][22]=-L_s;$

$D_{eqx2}[2][23]=-L_s;$

$D_{eqx2}[3][24]=-L_s;$

$D_{eqx2}[4][25]=-L_s;$

$D_{eqx2}[5][26]=-L_s;$

$D_{eqx2}[6][27]=-L_f;$

$D_{eqx2}[7][28]=-L_f;$

$D_{eqx2}[8][21]=-L_s;$

$D_{eqx2}[9][22]=-L_s;$

$D_{eqx2}[10][23] = -L_s;$

$D_{eqx2}[11][24] = -L_s;$

$D_{eqx2}[12][25] = -L_s;$

$D_{eqx2}[13][26] = -L_s;$

$D_{eqx2}[14][19] = C, D_{eqx2}[14][20] = -C;$

$D_{eqx2}[15][19] = -C, D_{eqx2}[15][20] = C;$

$D_{eqx2}[17][11] = -1.0;$

$D_{eqx2}[18][49] = -1.0$

Matrix Y_{eqx3} non zero terms:

$Y_{eqx3}[0][33] = 1.0;$

$Y_{eqx3}[1][34] = 1.0;$

$Y_{eqx3}[2][35] = 1.0;$

$Y_{eqx3}[3][36] = 1.0;$

$Y_{eqx3}[4][37] = 1.0;$

$Y_{eqx3}[5][38] = 1.0;$

$Y_{eqx3}[6][39] = 1.0;$

$Y_{eqx3}[7][40] = 1.0;$

$Y_{eqx3}[8][41] = 1.0;$

$Y_{eqx3}[9][42] = 1.0;$

$Y_{eqx3}[10][43] = 1.0;$

$Y_{eqx3}[11][44] = 1.0;$

$Y_{eqx3}[12][45] = 1.0;$

$Y_{eqx3}[13][46] = 1.0;$

$Y_{eqx3}[14][47] = 1.0;$

$Y_{eqx3}[15][48] = 1.0;$

$Y_{eqx3}[16][32] = 1.0;$

$Y_{eqx3}[18][51] = 1.0;$

$Y_{eqx3}[19][52] = 1.0;$

Matrix F_{eqxx3} non zero terms:

$F_{eqxx3}[0][12][2] = -1.0;$
$F_{eqxx3}[1][12][3] = -1.0;$
$F_{eqxx3}[2][12][4] = -1.0;$
$F_{eqxx3}[3][12][5] = -1.0;$
$F_{eqxx3}[4][12][6] = -1.0;$
$F_{eqxx3}[5][12][7] = -1.0;$
$F_{eqxx3}[6][12][8] = -1.0;$
$F_{eqxx3}[7][12][9] = -1.0;$
$F_{eqxx3}[8][12][21] = -1.0;$
$F_{eqxx3}[9][12][22] = -1.0;$
$F_{eqxx3}[10][12][23] = -1.0;$
$F_{eqxx3}[11][12][24] = -1.0;$
$F_{eqxx3}[12][12][25] = -1.0;$
$F_{eqxx3}[13][12][26] = -1.0;$
$F_{eqxx3}[14][19][49] = -1.0, F_{eqxx3}[14][20][49] = 1.0;$
$F_{eqxx3}[15][19][50] = -1.0, F_{eqxx3}[15][20][50] = 1.0;$
$F_{eqxx3}[16][50][31] = 1.0;$
$F_{eqxx3}[17][49][49] = 1.0, F_{eqxx3}[17][50][50] = 1.0;;$
$F_{eqxx3}[18][10][47] = -\frac{1}{2\sqrt{2}};$
$F_{eqxx3}[19][10][48] = -\frac{1}{2\sqrt{2}};$
$F_{eqxx3}[20][13][21] = 1.0, F_{eqxx3}[20][14][22] = 1.0,$
$F_{eqxx3}[20][15][23] = 1.0, F_{eqxx3}[20][16][24] = 1.0;$
$F_{eqxx3}[20][17][25] = 1.0, F_{eqxx3}[20][18][26] = 1.0,$
$F_{eqxx3}[20][19][29] = 1.0, F_{eqxx3}[20][20][30] = 1.0$

Matrix C_{eqc3} non zero terms:

$C_{eqc3}[17] = -1.0.$

APPENDIX B. FAULTED DISTRIBUTION LINE MODEL FOR FAULT LOCATING

This appendix describes QDM and SCAQCF of distribution lines for EBFL application, especially for a two-terminal distribution line integrated with a fault.

B.1 Model Description

We model the fault based on the fault type accordingly. For instance, consider a phase A to neutral fault occurs on a two-terminal line (between bus j and k) which is l_F miles from bus j. The fault impedance is R_F which is usually unknown.

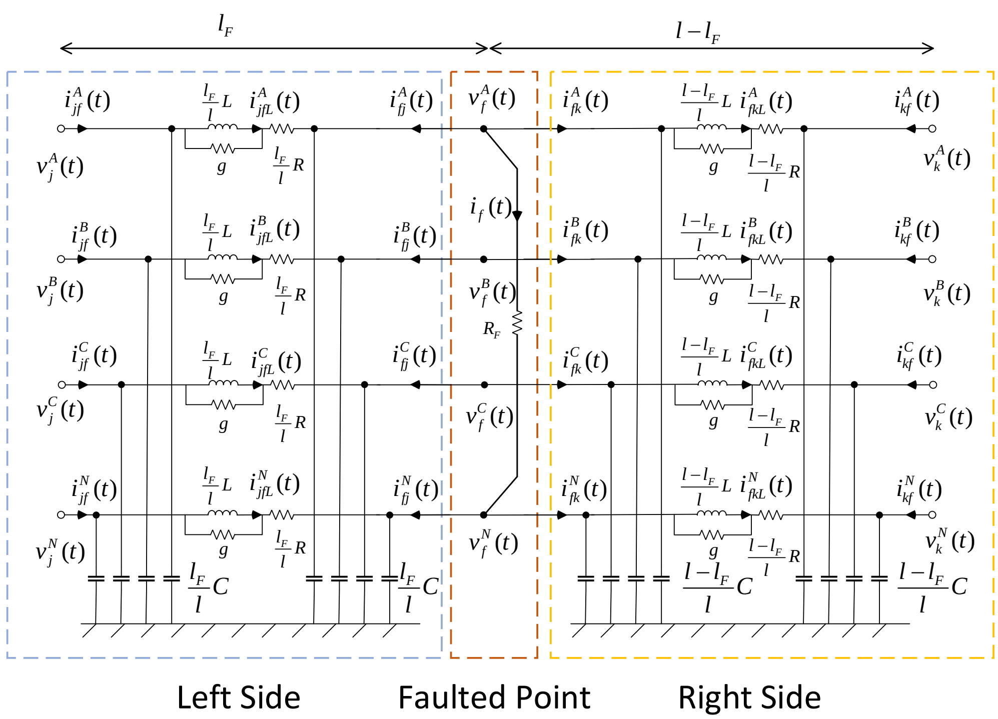

Figure B.1 Two-terminal faulted distribution line model

The model is shown in Figure B.1 where the distribution line models are divided into the left side and right side represented by a π-equivalent short line model.

For the left side of the distribution line model, we can obtain the following equations:

$$\begin{bmatrix} i_{jf}^{A}(t) \\ i_{jf}^{B}(t) \\ i_{jf}^{C}(t) \\ i_{jf}^{N}(t) \end{bmatrix} = \frac{l_F}{l} C \frac{d}{dt} \begin{bmatrix} v_{j}^{A}(t) \\ v_{j}^{B}(t) \\ v_{j}^{C}(t) \\ v_{j}^{N}(t) \end{bmatrix} + \begin{bmatrix} i_{jfL}^{A}(t) \\ i_{jfL}^{B}(t) \\ i_{jfL}^{C}(t) \\ i_{jfL}^{N}(t) \end{bmatrix} + g \frac{l_F}{l} L \frac{d}{dt} \begin{bmatrix} i_{jfL}^{A}(t) \\ i_{jfL}^{B}(t) \\ i_{jfL}^{C}(t) \\ i_{jfL}^{N}(t) \end{bmatrix}$$

$$[0] = -\begin{bmatrix} v_{j}^{A}(t) \\ v_{j}^{B}(t) \\ v_{j}^{C}(t) \\ v_{j}^{N}(t) \end{bmatrix} + \frac{l_F}{l} L \frac{d}{dt} \begin{bmatrix} i_{jfL}^{A}(t) \\ i_{jfL}^{B}(t) \\ i_{jfL}^{C}(t) \\ i_{jfL}^{N}(t) \end{bmatrix} + \frac{l_F}{l} R \left(\begin{bmatrix} i_{jfL}^{A}(t) \\ i_{jfL}^{B}(t) \\ i_{jfL}^{C}(t) \\ i_{jfL}^{N}(t) \end{bmatrix} + g \frac{l_F}{l} L \frac{d}{dt} \begin{bmatrix} i_{jfL}^{A}(t) \\ i_{jfL}^{B}(t) \\ i_{jfL}^{C}(t) \\ i_{jfL}^{N}(t) \end{bmatrix} \right) + \begin{bmatrix} v_{f}^{A}(t) \\ v_{f}^{B}(t) \\ v_{f}^{C}(t) \\ v_{f}^{N}(t) \end{bmatrix}$$

$$\begin{bmatrix} i_{fj}^{A}(t) \\ i_{fj}^{B}(t) \\ i_{fj}^{C}(t) \\ i_{fj}^{N}(t) \end{bmatrix} = \frac{l_F}{l} C \frac{d}{dt} \begin{bmatrix} v_{f}^{A}(t) \\ v_{f}^{B}(t) \\ v_{f}^{C}(t) \\ v_{f}^{N}(t) \end{bmatrix} - \begin{bmatrix} i_{jfL}^{A}(t) \\ i_{jfL}^{B}(t) \\ i_{jfL}^{C}(t) \\ i_{jfL}^{N}(t) \end{bmatrix} - g \frac{l_F}{l} L \frac{d}{dt} \begin{bmatrix} i_{jfL}^{A}(t) \\ i_{jfL}^{B}(t) \\ i_{jfL}^{C}(t) \\ i_{jfL}^{N}(t) \end{bmatrix}$$

where R, C, g, L are 4×4 matrices.

Similarly, for the right side, the equations are:

$$\begin{bmatrix} i_{fk}^{A}(t) \\ i_{fk}^{B}(t) \\ i_{fk}^{C}(t) \\ i_{fk}^{N}(t) \end{bmatrix} = \frac{l-l_F}{l} C \frac{d}{dt} \begin{bmatrix} v_{f}^{A}(t) \\ v_{f}^{B}(t) \\ v_{f}^{C}(t) \\ v_{f}^{N}(t) \end{bmatrix} + \begin{bmatrix} i_{fkL}^{A}(t) \\ i_{fkL}^{B}(t) \\ i_{fkL}^{C}(t) \\ i_{fkL}^{N}(t) \end{bmatrix} + g \frac{l-l_F}{l} L \frac{d}{dt} \begin{bmatrix} i_{fkL}^{A}(t) \\ i_{fkL}^{B}(t) \\ i_{fkL}^{C}(t) \\ i_{fkL}^{N}(t) \end{bmatrix}$$

$$[0] = -\begin{bmatrix} v_{f}^{A}(t) \\ v_{f}^{B}(t) \\ v_{f}^{C}(t) \\ v_{f}^{N}(t) \end{bmatrix} + \frac{l-l_F}{l} L \frac{d}{dt} \begin{bmatrix} i_{fkL}^{A}(t) \\ i_{fkL}^{B}(t) \\ i_{fkL}^{C}(t) \\ i_{fkL}^{N}(t) \end{bmatrix} + \frac{l-l_F}{l} R \left(\begin{bmatrix} i_{fkL}^{A}(t) \\ i_{fkL}^{B}(t) \\ i_{fkL}^{C}(t) \\ i_{fkL}^{N}(t) \end{bmatrix} + g \frac{l-l_F}{l} L \frac{d}{dt} \begin{bmatrix} i_{fkL}^{A}(t) \\ i_{fkL}^{B}(t) \\ i_{fkL}^{C}(t) \\ i_{fkL}^{N}(t) \end{bmatrix} \right) + \begin{bmatrix} v_{k}^{A}(t) \\ v_{k}^{B}(t) \\ v_{k}^{C}(t) \\ v_{k}^{N}(t) \end{bmatrix}$$

$$\begin{bmatrix} i_{kf}^A(t) \\ i_{kf}^B(t) \\ i_{kf}^C(t) \\ i_{kf}^N(t) \end{bmatrix} = \frac{l-l_F}{l} C \frac{d}{dt} \begin{bmatrix} v_k^A(t) \\ v_k^B(t) \\ v_k^C(t) \\ v_k^N(t) \end{bmatrix} - \begin{bmatrix} i_{fkL}^A(t) \\ i_{fkL}^B(t) \\ i_{fkL}^C(t) \\ i_{fkL}^N(t) \end{bmatrix} - g \frac{l-l_F}{l} L \frac{d}{dt} \begin{bmatrix} i_{fkL}^A(t) \\ i_{fkL}^B(t) \\ i_{fkL}^C(t) \\ i_{fkL}^N(t) \end{bmatrix}$$

At the faulted point we can write the Kirchhoff's Current Law as follow:

$$0 = \begin{bmatrix} i_{fj}^A(t) \\ i_{fj}^B(t) \\ i_{fj}^C(t) \\ i_{fj}^N(t) \end{bmatrix} + \begin{bmatrix} i_{fk}^A(t) \\ i_{fk}^B(t) \\ i_{fk}^C(t) \\ i_{fk}^N(t) \end{bmatrix} + D \begin{bmatrix} v_f^A(t) \\ v_f^B(t) \\ v_f^C(t) \\ v_f^N(t) \end{bmatrix}$$

where $D = \frac{1}{R_F} \begin{bmatrix} 1 & 0 & 0 & -1 \\ 0 & 0 & 0 & 0 \\ 0 & 0 & 0 & 0 \\ -1 & 0 & 0 & 1 \end{bmatrix}$

Note that the fault location is a constant, thus we have another equation: $0 = \frac{dl_F(t)}{dt}$.

For simplicity, we define the following variables as the three phase and neutral current/voltage:

$$i_{jf}(t)^T = \begin{bmatrix} i_{jf}^A(t) \\ i_{jf}^B(t) \\ i_{jf}^C(t) \\ i_{jf}^N(t) \end{bmatrix}, i_{fj}(t)^T = \begin{bmatrix} i_{fj}^A(t) \\ i_{fj}^B(t) \\ i_{fj}^C(t) \\ i_{fj}^N(t) \end{bmatrix}, i_{fk}(t)^T = \begin{bmatrix} i_{fk}^A(t) \\ i_{fk}^B(t) \\ i_{fk}^C(t) \\ i_{fk}^N(t) \end{bmatrix} i_{kf}(t)^T = \begin{bmatrix} i_{kf}^A(t) \\ i_{kf}^B(t) \\ i_{kf}^C(t) \\ i_{kf}^N(t) \end{bmatrix}, i_f(t)^T = \begin{bmatrix} i_f^A(t) \\ i_f^B(t) \\ i_f^C(t) \\ i_f^N(t) \end{bmatrix},$$

$$i_{jfL}(t)^T = \begin{bmatrix} i_{jfL}^A(t) \\ i_{jfL}^B(t) \\ i_{jfL}^C(t) \\ i_{jfL}^N(t) \end{bmatrix}, i_{fkL}(t)^T = \begin{bmatrix} i_{fkL}^A(t) \\ i_{fkL}^B(t) \\ i_{fkL}^C(t) \\ i_{fkL}^N(t) \end{bmatrix}, v_j(t)^T = \begin{bmatrix} v_j^A(t) \\ v_j^B(t) \\ v_j^C(t) \\ v_j^N(t) \end{bmatrix}, v_k(t)^T = \begin{bmatrix} v_k^A(t) \\ v_k^B(t) \\ v_k^C(t) \\ v_k^N(t) \end{bmatrix}, v_f(t)^T = \begin{bmatrix} v_f^A(t) \\ v_f^B(t) \\ v_f^C(t) \\ v_f^N(t) \end{bmatrix}$$

To sum up, the compact model (QDM) is

$$i_{jf}(t)=\frac{l_F(t)}{l}C\frac{dv_j(t)}{dt}+i_{jfL}(t)+g\frac{l_F(t)}{l}L\frac{di_{jfL}(t)}{dt} \tag{B.1}$$

$$i_{kf}(t)=C\frac{dv_k(t)}{dt}-\frac{l_F(t)}{l}C\frac{dv_k(t)}{dt}-i_{fkL}(t)-gL\frac{di_{fkL}(t)}{dt}+\frac{l_F(t)}{l}L\frac{di_{fkL}(t)}{dt} \tag{B.2}$$

$$0=-i_{fj}(t)+\frac{l_F}{l}C\frac{dv_f(t)}{dt}-i_{jfL}(t)-g\frac{l_F}{l}L\frac{di_{jfL}(t)}{dt} \tag{B.3}$$

$$0=-i_{fk}(t)+\frac{l-l_F}{l}C\frac{dv_f(t)}{dt}+i_{fkL}(t)+g\frac{l-l_F}{l}L\frac{di_{fkL}(t)}{dt} \tag{B.4}$$

$$0=-v_j(t)+\frac{l_F(t)}{l}L\frac{di_{jfL}(t)}{dt}+\frac{l_F(t)}{l}R\left(i_{jfL}(t)+g\frac{l_F(t)}{l}L\frac{di_{jfL}(t)}{dt}\right)+v_f(t) \tag{B.5}$$

$$0=-v_f(t)+\frac{l-l_F(t)}{l}L\frac{di_{fkL}(t)}{dt}+\frac{l-l_F(t)}{l}R\left(i_{fkL}(t)+g\frac{l-l_F(t)}{l}L\frac{di_{fkL}(t)}{dt}\right)+v_k(t) \tag{B.6}$$

$$0=i_{fj}(t)+i_{kj}(t)+Dv_f(t) \tag{B.7}$$

$$0=\frac{dl_F(t)}{dt} \tag{B.8}$$

The through variables are $i(t)=\begin{bmatrix} i_{jf}(t) & i_{kf}(t)\end{bmatrix}^T$.

The states are:

$$x(t)=\begin{bmatrix} v_j(t) & v_k(t) & v_f(t) & i_{fj}(t) & i_{fk}(t) & i_{jfL}(t) & i_{fkL}(t) & l_F(t)\end{bmatrix}^T$$

To quadratize the compact model, several variables are introduce shown as:

$$
\begin{aligned}
y_{vj}(t) &= \frac{dv_j(t)}{dt}, \\
y_{vk}(t) &= \frac{dv_k(t)}{dt}, \\
y_{vf}(t) &= \frac{dv_f(t)}{dt}, \\
y_{ijL}(t) &= \frac{di_{jfL}(t)}{dt}, \\
y_{ikL}(t) &= \frac{di_{fkL}(t)}{dt}, \\
z_{lj}(t) &= l_F(t) y_{vj}(t), \\
z_{lk}(t) &= l_F(t) y_{vk}(t), \\
z_{lij}(t) &= l_F(t) y_{ijL}(t), \\
z_{lik}(t) &= l_F(t) y_{ikL}(t), \\
\ell(t) &= l_F(t) l_F(t)
\end{aligned}
$$

Then, the QDM model in SCQDM format is:

$$
i_{jf}(t) = \frac{C}{l} z_{lj}(t) + i_{jfL}(t) + \frac{gL}{l} z_{lij}(t)
$$

$$
i_{kf}(t) = C y_{vk}(t) - \frac{C}{l} z_{lk}(t) - i_{fkL}(t) - gL y_{ikL}(t) + \frac{L}{l} z_{lik}(t)
$$

$$
\begin{aligned}
0 &= y_{vj}(t) - \frac{dv_j(t)}{dt} \\
0 &= y_{vk}(t) - \frac{dv_k(t)}{dt} \\
0 &= y_{vf}(t) - \frac{dv_f(t)}{dt} \\
0 &= y_{ijL}(t) - \frac{di_{jfL}(t)}{dt} \\
0 &= y_{ikL}(t) - \frac{di_{fkL}(t)}{dt} \\
0 &= i_{fj}(t) + i_{kj}(t) + D v_f(t) \\
0 &= \frac{dl_F(t)}{dt}
\end{aligned}
$$

$$
0 = -i_{fj}(t) + \frac{C}{l} l_F(t) y_{vf}(t) - i_{jfL}(t) - \frac{gL}{l} z_{lij}(t)
$$

$$0=-i_{fk}(t)+Cy_{vf}(t)-\frac{C}{l}l_F(t)y_{vf}(t)+i_{fkL}(t)+gLy_{ikL}(t)-\frac{gL}{l}z_{lik}(t)$$

$$0=-v_j(t)+\frac{L}{l}z_{lij}(t)+\frac{R}{l}l_F(t)i_{jfL}(t)+\frac{RgL}{l^2}\ell(t)y_{ijL}(t)+v_f(t)$$

$$0=-v_f(t)+(RgL+L)y_{ikL}(t)-\left(\frac{L}{l}+\frac{2RgL}{l}\right)z_{lik}+$$
$$Ri_{fkL}(t)-\frac{R}{l}l_F(t)i_{fkL}(t)+\frac{RgL}{l^2}\ell(t)y_{ikL}(t)+v_k(t)$$

$$\begin{aligned}
0&=z_{lj}(t)-l_F(t)y_{vj}(t)\\
0&=z_{lk}(t)-l_F(t)y_{vk}(t)\\
0&=z_{lij}(t)-l_F(t)y_{ijL}(t)\\
0&=z_{lik}(t)-l_F(t)y_{ikL}(t)\\
0&=\ell(t)-l_F(t)l_F(t)
\end{aligned}$$

The through variables are $i(t)=\begin{bmatrix} i_{jf}(t) & i_{kf}(t)\end{bmatrix}^T$.

The states are:

$$\begin{aligned}x(t)=\big[&v_j(t)\quad v_k(t)\quad v_f(t)\quad i_{fj}(t)\quad i_{fk}(t)\quad i_{jfL}(t)\quad i_{fkL}(t)\\
&y_{vj}(t)\quad y_{vk}(t)\quad y_{vf}(t)\quad y_{ijL}(t)\quad y_{ikL}(t)\quad z_{lj}(t)\quad z_{lk}(t)\quad z_{lij}(t)\quad z_{lik}(t)\quad \ell(t)\quad l_F(t)\big]^T\end{aligned}$$

There is no control variable in the model.

For simplicity, the model can be rewritten into a standard algebraic companion form (ACF) as:

$$\begin{bmatrix} i(t)\\ 0\end{bmatrix}=A\cdot x(t)+B\cdot\frac{dx(t)}{dt}+x^T(t)\cdot F_{xx}\cdot x(t)$$

where,

$$Y_{eqx1}=\begin{bmatrix} 0 & I_4 & & & & C/l & & gL/l & & 0 \\ 0 & & -I_4 & C & -gL & & -C/l & & L/l & 0 \end{bmatrix}$$

$$Y_{eqx2}=\begin{bmatrix} 0 & & & I_4 & & & & & 0 \\ 0 & & & & I_4 & & & & 0 \\ 0 & & & & & I_4 & & & 0 \\ 0 & & & & & & I_4 & & 0 \\ 0 & & & & & & & I_4 & 0 \\ 0 & T & T & & & & & & 0 \\ 0 & & & & & & & & 0 \end{bmatrix}$$

$$Y_{eqx3}=\begin{bmatrix} 0 & & & -I_4 & & -I_4 & & & & & & & & & 0 \\ 0 & & & & -I_4 & & I_4 & C & gL & & & & & & 0 \\ -I_4 & & I_4 & & & & & & & & & L/l & & & 0 \\ 0 & I_4 & -I_4 & & & & R & & RgL+L & & & & \dfrac{-L-2RgL}{l} & & 0 \\ 0 & & & & & & & & & I_4 & & & & & 0 \\ 0 & & & & & & & & & & I_4 & & & & 0 \\ 0 & & & & & & & & & & & I_4 & & & 0 \\ 0 & & & & & & & & & & & & I_4 & & 0 \\ 0 & & & & & & & & & & & & & 1 & 0 \end{bmatrix}$$

$$A=\begin{bmatrix} Y_{eqx1} \\ Y_{eqx2} \\ Y_{eqx3} \end{bmatrix}$$

$$B=\left[\begin{array}{ccccccc} \multicolumn{7}{c}{0} \\ \hline -I_4 & & & & & & 0 \\ 0 & -I_4 & & & & & 0 \\ 0 & & -I_4 & & & & 0 \\ 0 & & & -I_4 & & & 0 \\ 0 & & & & -I_4 & & 0 \\ 0 & & & & & & 0 \\ 0 & & & & & & 1 \\ \hline \multicolumn{7}{c}{0} \end{array}\right]$$

$$F_{eqxx}[i+33][66][j+36]=C_{i+1,j}/l, F_{eqxx}[i+33][66][j+40]=-(gL)_{i+1,j}/l, i=0\sim 3,\ j=1\sim 4;$$
$$F_{eqxx}[i+37][66][j+36]=-C_{i+1,j}/l, F_{eqxx}[i+37][66][j+44]=-(gL)_{i+1,j}/l, i=0\sim 3,\ j=1\sim 4;$$
$$F_{eqxx}[i+41][66][j+20]=R_{i+1,j}/l, F_{eqxx}[i+41][65][j+40]=(RgL)_{i+1,j}/l^2, i=0\sim 3,\ j=1\sim 4;$$
$$F_{eqxx}[i+45][66][j+24]=-R_{i+1,j}/l, F_{eqxx}[i+45][65][j+44]=(RgL)_{i+1,j}/l^2, i=0\sim 3,\ j=1\sim 4;$$
$$F_{eqxx}[i+49][66][i+29]=-1, i=0\sim 3;$$
$$F_{eqxx}[i+53][66][i+33]=-1, i=0\sim 3;$$
$$F_{eqxx}[i+57][66][i+41]=-1, i=0\sim 3;$$
$$F_{eqxx}[i+61][66][i+45]=-1, i=0\sim 3;$$
$$F_{eqxx}[65][66][66]=-1.$$

Note that I_4 is a 4×4 identity matrix, other zero elements of the above matrices are not shown.

B.2 SCAQCF

When applying the proposed quadratic integration, the SCAQCF model can be rewritten as the standard format:

$$\begin{bmatrix} i(t) \\ 0 \\ i(t_m) \\ 0 \end{bmatrix} = E\cdot F_1\cdot\begin{bmatrix} x(t) \\ x(t_m) \end{bmatrix} + \left\{ \begin{bmatrix} x(t) \\ x(t_m) \end{bmatrix}^T \begin{matrix} \vdots \\ F_{eqxx} \\ \vdots \end{matrix} \begin{bmatrix} x(t) \\ x(t_m) \end{bmatrix} \right\} - B_{eq}$$

$$B_{eq} = E\cdot F_2\cdot\left[x(t-h)\right] + E\cdot F_3\cdot\begin{bmatrix} i(t-h) \\ 0 \end{bmatrix}$$

where,

$$E=\begin{bmatrix} \frac{4}{h}*I & 0 & -\frac{8}{h}*I & 0 \\ 0 & I & 0 & 0 \\ \frac{1}{2h}*I & 0 & \frac{2}{h}*I & 0 \\ 0 & 0 & 0 & I \end{bmatrix}$$

$$F_1 = \begin{bmatrix} \frac{h}{6} \times A + B & \frac{2h}{3} \times A \\ -\frac{h}{24} \times A & \frac{h}{3} \times A + B \end{bmatrix}$$

$$F_2 = \begin{bmatrix} B - \frac{h}{6} \times A \\ B - \frac{5h}{24} \times A \end{bmatrix}$$

$$F_3 = \begin{bmatrix} \frac{h}{6} \times I & 0 \\ 0 & 0 \\ \frac{5h}{24} \times I & 0 \\ 0 & 0 \end{bmatrix}$$

Note that the above quadratic integration can be implemented to generate the SCAQCF model automatically. Then, we will obtain the measurement model based on the setting of MUs.

REFERENCES

[1] M.F. Akorede, H. Hizam, and E. Pouresmaeil. "Distributed energy resources and benefits to the environment." *Renewable and Sustainable Energy Reviews*, vol. 14, no. 2, pp. 724-734, 2010.

[2] E. Fasching and S. Ray, "U.S. power grid added 20.2 GW of generating capacity in the first half of 2024," https://www.eia.gov/todayinenergy/detail.php?id=62864 (Accessed Sep 18, 2024).

[3] C. D'Adamo, S. Jupe, and C. Abbey, "Global survey on planning and operation of active distribution networks—Update of CIGRE C6.11 working group activities," *CIRED 2009-20th international conference and exhibition on electricity distribution*, pp. 1–4, 2009.

[4] J. Keller and B. Kroposki, "Understanding fault characteristics of inverter-based distributed energy resources," National Renewable Energy Laboratory (NREL), Golden, CO, USA, Tech. Rep. TP-550-46 698, Jan. 2010.

[5] R. Yan, N. A. Masood, T. Kumar Saha, F. Bai and H. Gu, "The Anatomy of the 2016 South Australia Blackout: A Catastrophic Event in a High Renewable Network," *IEEE Transactions on Power Systems*, vol. 33, no. 5, pp. 5374-5388, 2018.

[6] E. Targett, "Internal Data Stolen, Leaked, in REvil Attack on Electricity Market's Elexon," Computer Business Review, 1 June 2020, https://www.cbronline.com/news/elexon-hack-ransomware-revil (Accessed Oct 1, 2023).

[7] EPRI, "Enhancing distribution resiliency: opportunities for applying innovative technologies," Palo Alto, CA, USA, Tech. Rep. 1026889, Jan 2013.

[8] M.L, Tuballa and M.L. Abundo. "A review of the development of Smart Grid technologies," *Renewable and Sustainable Energy Reviews*, 59, pp.710-725, 2016.

[9] K.M. Muttaqi, J. Aghaei, V. Ganapathy, and A.E. Nezhad, "Technical challenges for electric power industries with implementation of distribution system automation in smart grids," *Renewable and Sustainable Energy Reviews*, 46, pp.129-142, 2015.

[10] V. Madani, *et al*., "Distribution Automation Strategies Challenges and Opportunities in a Changing Landscape," *IEEE Transactions on Smart Grid*, vol. 6, no. 4, pp. 2157-2165, July 2015.

[11] C.L. Smallwood and J. Wennermark. "Benefits of distribution automation," *IEEE Industry Applications Magazine*, vol. 16, no. 1: 65-73, 2009.

[12] S. Pirouzi, et al, "Hybrid planning of distributed generation and distribution automation to improve reliability and operation indices," *International Journal of Electrical Power & Energy Systems*, 135, p.107540, 2022.

[13] J. Zheng, W. Gao, and L. Lin, "Smart meters in smart grid: An overview," IEEE green technologies conference (GreenTech), pp. 57-64. IEEE, 2013.

[14] A. Sami, SCADA (Supervisory Control and Data Acquisition), 2019.

[15] K.M. Muttaqi, A.E. Nezhad, J. Aghaei, and V. Ganapathy, "Control issues of distribution system automation in smart grids," *Renewable and Sustainable Energy Reviews*, 37, pp.386-396, 2014.

[16] Standard for Interconnecting Distributed Resources with Electric Power Systems, IEEE Standard 1547, 2003.

[17] A. Haddadi, M. Zhao, I. Kocar, U. Karaagac, K. W. Chan and E. Farantatos, “Impact of Inverter-Based Resources on Negative Sequence Quantities-Based Protection Elements,” *IEEE Transactions on Power Delivery*, 2021, vol. 36, no. 1, pp. 289-298.
[18] R. Chowdhury and N. Fischer, “Transmission Line Protection for Systems with Inverter-Based Resources – Part I: Problems,” *IEEE Transactions on Power Delivery*, vol. 36, no. 4, pp. 2416-2425, Aug. 2021.
[19] L. Huang, C. Wu, D. Zhou and F. Blaabjerg, “A Double-PLLs-Based Impedance Reshaping Method for Extending Stability Range of Grid-Following Inverter Under Weak Grid,” *IEEE Transactions on Power Electronics*, vol. 37, no. 4, pp. 4091-4104, April 2022.
[20] R. H. Lasseter, Z. Chen and D. Pattabiraman, “Grid-Forming Inverters: A Critical Asset for the Power Grid,” *IEEE Journal of Emerging and Selected Topics in Power Electronics*, vol. 8, no. 2, pp. 925-935, June 2020.
[21] M. J. Reno, S. Brahma, A. Bidram and M. E. Ropp, “Influence of Inverter-Based Resources on Microgrid Protection: Part 1: Microgrids in Radial Distribution Systems,” *IEEE Power and Energy Magazine*, vol. 19, no .3, pp. 36-46, 2021.
[22] K. Jia, Z. Yang, Y. Fang, T. Bi and M. Sumner, “Influence of Inverter Interfaced Renewable Energy Generators on Directional Relay and an Improved Scheme,” in *IEEE Transactions on Power Electronics*, 2019, vol. 34, no. 12, pp. 11843-11855.
[23] H. Jafarabadi Ashtiani, H. Samet, and T. Ghanbari, “Evaluation of directional relay algorithms in the presence of FCL,” *IET Science, Measurement & Technology*, vol. 11, no. 6, pp. 713-722, Sep. 2017.
[24] A. Hooshyar, M. A. Azzouz, and E. F. El-Saadany, “Distance protection of lines emanating from full-scale converter-interfaced renewable energy power plants—Part I: Problem statement,” *IEEE Trans. Power Delivery*, vol. 30, no. 4, pp. 1770–1780, Aug. 2015.
[25] Y. Fang, K. Jia, Z. Yang, Y. Li and T. Bi, “Impact of Inverter-Interfaced Renewable Energy Generators on Distance Protection and an Improved Scheme,” *IEEE Transactions on Industrial Electronics*, vol. 66, no. 9, pp. 7078-7088, Sept. 2019.
[26] B. Han, H. Li, G. Wang, D. Zeng, and Y. Liang, “A virtual multiterminal current differential protection scheme for distribution networks with inverter-interfaced distributed generators,” *IEEE Transactions on Smart Grid*, vol. 9, no. 5, pp. 5418–5431, Sep. 2015.
[27] A. Haddadi, E. Farantatos, I. Kocar, U. Karaagac, “Impact of inverter based resources on system protection,” *Energies*, vol. 14, no. 4, pp. 1050, 2021.
[28] A. P. Meliopoulos, et al., “Dynamic State Estimation-Based Protection: Status and Promise,” *IEEE Transactions on Power Delivery*, vol. 32, no. 1, pp. 320-330, Feb. 2017.
[29] B. Xie, et al., “Dynamic State Estimation Based Unit Protection,” *2019 IEEE Power Energy Society General Meeting (PESGM)*, 2019, pp. 1-5.
[30] K. Liu, A. P. Sakis Meliopoulos, B. Xie, C. Zhong and J. Xie, “Dynamic State Estimation-Based Protection of Distribution Systems with High Penetration of DERs,” *2020 IEEE Power Energy Society General Meeting (PESGM)*, 2020, pp. 1-5.
[31] S. Cai, Z. Chen, Z. Yang, G. Ilunga, A. P. S. Meliopoulos and G. Wilson, “Modeling and Protection of Real-world PV Integrated Distribution System,” *2022 North American Power Symposium (NAPS)*, Salt Lake City, UT, USA, 2022, pp. 1-6.

[32] K. Chen, C. Huang, and J. He, “Fault detection, classification and location for transmission lines and distribution systems: a review on the methods,” *High voltage*, vol. 1, no. 1, pp. 25-33, 2016.

[33] Z. He, L. Fu, S. Lin and Z. Bo, “Fault Detection and Classification in EHV Transmission Line Based on Wavelet Singular Entropy,” *IEEE Transactions on Power Delivery*, vol. 25, no. 4, pp. 2156-2163, Oct. 2010.

[34] S. El Safty, and A. El-Zonkoly, “Applying wavelet entropy principle in fault classification,” *International Journal of Electrical Power & Energy Systems*, vol. 31, no. 10, pp. 604-607, 2009.

[35] M. U. Usman, J. Ospina, and M. O. Faruque, “Fault classification and location identification in a smart distribution network using ANN,” *IEEE power & energy society general meeting (PESGM)*, pp. 1-6, August. 2018.

[36] P. K. Dash, S. R. Samantaray, and G. Panda, “Fault classification and section identification of an advanced series-compensated transmission line using support vector machine,” *IEEE transactions on power delivery*, vol. 22, no. 1, pp. 67-73, 2006.

[37] R.N. Mahanty and P.D. Gupta, “A fuzzy logic based fault classification approach using current samples only,” *Electric power systems research*, vol. 77, no. 5-6, pp.501-507, 2007.

[38] S.R. Samantaray, “A systematic fuzzy rule based approach for fault classification in transmission lines,” *Applied soft computing*, vol. 13, no. 2, pp.928-938, 2013.

[39] S. Belagoune, N. Bali, A. Bakdi, B. Baadji, and K. Atif, “Deep Learning through LSTM Classification and Regression for Transmission Line Fault Detection, Diagnosis and Location in Large-Scale Multi-Machine Power Systems,” *Measurement*, 177, June 2021.

[40] J. Hu et al., “Fault Location and Classification for Distribution Systems Based on Deep Graph Learning Methods,” *Journal of Modern Power Systems and Clean Energy*, vol. 11, no. 1, pp. 35-51, January 2023.

[41] M. Guo, N. Yang, and W. Chen, “Deep-Learning-Based Fault Classification Using Hilbert–Huang Transform and Convolutional Neural Network in Power Distribution Systems,” *IEEE Sensors Journal*, vol. 19, no. 16, pp. 6905-6913, August 2019.

[42] J. Hu, Z. Liu, J. Chen, W. Hu, Z. Zhang, and Z. Chen, “A novel deep learning–based fault diagnosis algorithm for preventing protection malfunction,” *International Journal of Electrical Power & Energy Systems*, 144: 108622, 2023.

[43] J. Fang, K. Chen, C. Liu, and J. He, “An Explainable and Robust Method for Fault Classification and Location on Transmission Lines,” *IEEE Transactions on Industrial Informatics*, pp. 1–10, 2023.

[44] L. Xie, Y. Li, L. F. Luo, Y. Zhang, and Y. Cao, “A traveling wave-based fault location method employing VMD-TEO for distribution network,” *IEEE Transactions on Power Delivery*, vol. 35, no. 4, pp. 1987–1998, Aug. 2020.

[45] K. Jia, T. Bi, Z. Ren, D.W.P. Thomas, and M. Sumner, “High frequency impedance based fault location in distribution system with DGs,” *IEEE Transactions on Smart Grid*, vol. 9, no. 2, pp. 807–816, Mar. 2018.

[46] H. Mirshekali, R. Dashti, A. Keshavarz, A. J. Torabi and H. R. Shaker, “A Novel Fault Location Methodology for Smart Distribution Networks,” *IEEE Transactions on Smart Grid*, vol. 12, no. 2, pp. 1277-1288, March 2021.

[47] K. Chen, J. Hu, Y. Zhang, Z. Yu and J. He, “Fault Location in Power Distribution Systems via Deep Graph Convolutional Networks,” *IEEE Journal on Selected Areas in Communications*, vol. 38, no. 1, pp. 119-131, Jan. 2020.

[48] H. Chen, P. D. S. Assala, Y. Cai, and P. Yang, “Intelligent transient overvoltages location in distribution systems using wavelet packet decomposition and general regression neural networks,” *IEEE Transactions on Industrial Informatics*, vol. 12, no. 5, pp. 1726–1735, Oct. 2016.

[49] M. Pignati, L. Zanni, P. Romano, R. Cherkaoui and M. Paolone, "Fault Detection and Faulted Line Identification in Active Distribution Networks Using Synchrophasors-Based Real-Time State Estimation," *IEEE Transactions on Power Delivery*, vol. 32, no. 1, pp. 381-392, Feb. 2017.

[50] Y. Liu, A. P. Meliopoulos, Z. Tan, L. Sun, and R. Fan, “Dynamic state estimation-based fault locating on transmission lines,” *IET Generation, Transmission & Distribution*, vol. 11, no. 17, pp. 4184-4192, 2017.

[51] D. Lu, Y. Liu, Q. Liao, B. Wang, W. Huang and X. Xi, “Time-Domain Transmission Line Fault Location Method With Full Consideration of Distributed Parameters and Line Asymmetry,” *IEEE Transactions on Power Delivery*, vol. 35, no. 6, pp. 2651-2662, Dec. 2020.

[52] A. Borghetti, “Using mixed integer programming for the volt/var optimization in distribution feeders,” Electric Power Systems Research, vol. 98, pp. 39-50, 2013.

[53] R.-H. Liang and C.-K. Cheng, “Dispatch of main transformer ULTC and capacitors in a distribution system,” *IEEE Transactions on Power Delivery*, vol. 16, no. 4, pp. 625-630, Oct. 2001.

[54] H. Ahmadi, J. R. Martí and H. W. Dommel, “A Framework for Volt-VAR Optimization in Distribution Systems,” *IEEE Transactions on Smart Grid*, vol. 6, no. 3, pp. 1473-1483, May 2015.

[55] T. Senjyu, Y. Miyazato, A. Yona, N. Urasaki and T. Funabashi, “Optimal Distribution Voltage Control and Coordination With Distributed Generation,” *IEEE Transactions on Power Delivery*, vol. 23, no. 2, pp. 1236-1242, April 2008.

[56] H. Yoshida, K. Kawata, Y. Fukuyama, S. Takayama and Y. Nakanishi, “A particle swarm optimization for reactive power and voltage control considering voltage security assessment,” *IEEE Transactions on Power Systems*, vol. 15, no. 4, pp. 1232-1239, Nov. 2000.

[57] H. J. Liu, W. Shi and H. Zhu, “Hybrid Voltage Control in Distribution Networks Under Limited Communication Rates,” *IEEE Transactions on Smart Grid*, vol. 10, no. 3, pp. 2416-2427, May 2019.

[58] Z. Tang, D. J. Hill and T. Liu, “Fast Distributed Reactive Power Control for Voltage Regulation in Distribution Networks,” *IEEE Transactions on Power Systems*, vol. 34, no. 1, pp. 802-805, Jan. 2019.

[59] X. Sun, J. Qiu and J. Zhao, “Optimal Local Volt/Var Control for Photovoltaic Inverters in Active Distribution Networks,” *IEEE Transactions on Power Systems*, vol. 36, no. 6, pp. 5756-5766, Nov. 2021.

[60] S. Li, W. Wu and Y. Lin, “Robust Data-Driven and Fully Distributed Volt/VAR Control for Active Distribution Networks With Multiple Virtual Power Plants,” *IEEE Transactions on Smart Grid*, vol. 13, no. 4, pp. 2627-2638, July 2022.

[61] P. Bagheri and W. Xu, "Model-Free Volt-Var Control Based on Measurement Data Analytics," *IEEE Transactions on Power Systems*, vol. 34, no. 2, pp. 1471-1482, March 2019.
[62] W. Cui, J. Li, and B. Zhang, "Decentralized safe reinforcement learning for inverter-based voltage control," *Electric Power Systems Research*, vol. 211, pp.108609, 2022.
[63] H. Xu, A. D. Domínguez-García, and P. W. Sauer, "Optimal tap setting of voltage regulation transformers using batch reinforcement learning," *IEEE Transactions on Power Systems*, vol. 35, no. 3, pp. 1990–2001, 2020.
[64] X. Chen, G. Qu, Y. Tang, S. Low and N. Li, "Reinforcement Learning for Selective Key Applications in Power Systems: Recent Advances and Future Challenges," *IEEE Transactions on Smart Grid*, vol. 13, no. 4, pp. 2935-2958, July 2022.
[65] Y. Zhang, X. Wang, J. Wang and Y. Zhang, "Deep Reinforcement Learning Based Volt-VAR Optimization in Smart Distribution Systems," *IEEE Transactions on Smart Grid*, vol. 12, no. 1, pp. 361-371, Jan. 2021.
[66] H. Liu, W. Wu and Y. Wang, "Bi-Level Off-Policy Reinforcement Learning for Two-Timescale Volt/VAR Control in Active Distribution Networks," *IEEE Transactions on Power Systems*, vol. 38, no. 1, pp. 385-395, Jan. 2023.
[67] X. Sun and J. Qiu, "Two-Stage Volt/Var Control in Active Distribution Networks With Multi-Agent Deep Reinforcement Learning Method," *IEEE Transactions on Smart Grid*, vol. 12, no. 4, pp. 2903-2912, July 2021.
[68] W. Wang, N. Yu, Y. Gao and J. Shi, "Safe Off-Policy Deep Reinforcement Learning Algorithm for Volt-VAR Control in Power Distribution Systems," *IEEE Transactions on Smart Grid*, vol. 11, no. 4, pp. 3008-3018, July 2020.
[69] Y. Shi, G. Qu, S. Low, A. Anandkumar, and A. Wierman, "Stability constrained reinforcement learning for real-time voltage control," 2022 American Control Conference (ACC), pp. 2715-2721, June 2022.
[70] H. T. Nguyen and D. -H. Choi, "Distributionally Robust Safety Filter for Learning-Based Control in Active Distribution Systems," *IEEE Transactions on Smart Grid*, vol. 14, no. 6, pp. 4972-4975, Nov. 2023.
[71] Y. Zhang, J. Wang, and Z. Li, "Uncertainty Modeling of Distributed Energy Resources: Techniques and Challenges," Current Sustainable/Renewable Energy Reports., 6(2), 42–51, 2019.
[72] K. Jhala, B. Natarajan and A. Pahwa, "Prospect Theory-Based Active Consumer Behavior Under Variable Electricity Pricing," IEEE Transactions on Smart Grid, vol. 10, no. 3, pp. 2809-2819, May 2019.
[73] L. Xie, Y. Mo and B. Sinopoli, "False Data Injection Attacks in Electricity Markets," *2010 First IEEE International Conference on Smart Grid Communications*, pp. 226-231, 2010.
[74] H. S. Karimi, K. Jhala and B. Natarajan, "Impact of Real-Time Pricing Attack on Demand Dynamics in Smart Distribution Systems," *2018 North American Power Symposium (NAPS)*, pp. 1-6, 2018.
[75] K. Jhala, B. Natarajan, A. Pahwa and H. Wu, "Stability of Transactive Energy Market-Based Power Distribution System Under Data Integrity Attack," *IEEE Transactions on Industrial Informatics*, vol. 15, no. 10, pp. 5541-5550, Oct. 2019.
[76] C. Barreto and X. Koutsoukos. "Attacks on Electricity Markets." *2019 57th Annual Allerton Conference on Communication, Control, and Computing*, IEEE, 2019.

[77] H. He, and Y. Jun. "Cyber-physical Attacks and Defences in the Smart Grid: a Survey," *IET Cyber-Physical Systems: Theory and Applications*, vol.1, no.1, pp. 13-27, 2016.

[78] A. Ashok, M. Govindarasu and V. Ajjarapu, "Online Detection of Stealthy False Data Injection Attacks in Power System State Estimation," *IEEE Transactions on Smart Grid*, vol. 9, no. 3, pp. 1636-1646, May 2018 .

[79] A.P. Meliopoulos, G. Cokkinides and G. Stefopoulos, "Quadratic integration method," *Proceedings of the 2005 International Power System Transients Conference*, pp. 19-23, 2005.

[80] A.F. Agarap. "Deep learning using rectified linear units (relu)." arXiv preprint arXiv:1803.08375, 2018.

[81] S. Ivanov, and A. D'yakonov, "Modern deep reinforcement learning algorithms," arXiv preprint arXiv:1906.10025, 2019.

[82] V. Singh, T. Moger, and D. Jena, "Uncertainty handling techniques in power systems: A critical review," *Electric Power Systems Research*, 203, p.107633, Feb. 2022.

[83] H. Zhang, J. Zimmerman, D. Nettleton, and D. J. Nordman, "Random forest prediction intervals," *The American Statistician*, Jun. 2019.

[84] Y. Romano, E. Patterson, and E. Candes, "Conformalized quantile regression," *Advances in neural information processing systems*, 32, 2019.

[85] J. Lu, J. Ding, X. Dai, and T. Chai, "Ensemble stochastic configuration networks for estimating prediction intervals: A simultaneous robust training algorithm and its application," *IEEE Transactions on Neural Networks and Learning Systems*, vol. 31, no. 12, pp. 5426-5440, 2020.

[86] J. Cochran, P. Denholm, B. Speer, and M. Miller, "Grid integration and the carrying capacity of the US grid to incorporate variable renewable energy," (No. NREL/TP-6A20-62607). National Renewable Energy Lab (NREL), Golden, CO, United States, Apr. 2015.

[87] C. Xu, and Y. Xie, Y. "Conformal prediction interval for dynamic time-series," In International Conference on Machine Learning (PMLR), pp. 11559-11569, Jul. 2021.

[88] K. P. Schneider et al., "Analytic Considerations and Design Basis for the IEEE Distribution Test Feeders," *IEEE Transactions on Power Systems*, vol. 33, no. 3, pp. 3181-3188, May 2018.

[89] Solar Power Generation Data. https://www.kaggle.com/datasets/anik-annal/solar-power-generation-data. Accessed: 2024-1-18.

[90] Smart meter energy consumption data in London households. https: //www.kaggle.com/jeanmidev/smart-meters-in-london. Version: 11, Accessed: 2023-11-11.

[91] T. P. Lillicrap, J. J. Hunt, A. Pritzel, N. Heess, T. Erez, Y. Tassa, D. Silver, and D. Wierstra, "Continuous control with deep reinforcement learning," arXiv preprint arXiv:1509.02971, 2015.

[92] Y. Gao and N. Yu, "A Reinforcement Learning-based Volt-VAR Control Dataset and Testing Environment," *IEEE PES Innovative Smart Grid Technologies-Asia (ISGT Asia)*, pp. 61-65, 2022.

[93] H. Fu, H. Tang, J. Hao, Z. Lei, Y. Chen, and C. Fan, "Deep multi-agent reinforcement learning with discrete-continuous hybrid action spaces." arXiv preprint arXiv:1903.04959, 2019.

[94] G. Dulac-Arnold, D. Mankowitz, T. Hester, “Challenges of real-world reinforcement learning,” arXiv preprint arXiv:1904.12901, 2019.

[95] F. U. Nazir, B. C. Pal and R. A. Jabr, “A Two-Stage Chance Constrained Volt/Var Control Scheme for Active Distribution Networks with Nodal Power Uncertainties,” *IEEE Transactions on Power Systems*, vol. 34, no. 1, pp. 314-325, Jan. 2019.

[96] Gridwise Transactive Energy Framework Version 1.0, GridWise Archit. Council, Richland, WA, USA, Jan. 2015.

[97] H. S. Karimi, K. Jhala and B. Natarajan, “Impact of Real-Time Pricing Attack on Demand Dynamics in Smart Distribution Systems,” *2018 North American Power Symposium (NAPS)*, pp. 1-6, 2018.

[98] S. Fan, and J.H. Rob. “The price elasticity of electricity demand in South Australia.” *Energy Policy*, vol. 39, no. 6, pp. 3709-3719, 2011.

[99] L. Baringo and A. J. Conejo, “Offering Strategy Via Robust Optimization,” *IEEE Transactions on Power Systems*, vol. 26, no. 3, pp. 1418-1425, Aug. 2011.

[100] H. Xu, A. D. Domínguez-García and P. W. Sauer, “Optimal Tap Setting of Voltage Regulation Transformers Using Batch Reinforcement Learning,” *IEEE Transactions on Power Systems*, vol. 35, no. 3, pp. 1990-2001, May 2020.

[101] F. Zhuang et al., “A Comprehensive Survey on Transfer Learning,” *Proceedings of the IEEE*, vol. 109, no. 1, pp. 43-76, Jan. 2021.

[102] L. Cheng, and T. Yu, “A new generation of AI: A review and perspective on machine learning technologies applied to smart energy and electric power systems,” *International Journal of Energy Research*, vol. 43, no. 6, pp. 1928-1973, 2019.

[103] W. Ding, M. Abdel-Basset, and R. Mohamed, R., “DeepAK-IoT: An effective deep learning model for cyberattack detection in IoT networks,” *Information Sciences*, 634, pp.157-171, 2023.

[104] A. S. L. V. Tummala and R. K. Inapakurthi, “A Two-stage Kalman Filter for Cyber-attack Detection in Automatic Generation Control System,” *Journal of Modern Power Systems and Clean Energy*, vol. 10, no. 1, pp. 50-59, Jan. 2022.

VITA

Zhengrong Chen was born in Jinhua, China in 1995. He received his Bachelor's degree in Automation, Master's degree in Control Theory and Control Engineering from North China Electric Power University in Beijing, China in 2017 and 2020, respectively. He attended a dual degree program and obtained another Master's degree in Electrical Engineering from University of Wisconsin, Milwaukee in 2019. He joined Georgia Institute of Technology in 2020 to pursue his Ph.D. degree in Electrical and Computer Engineering. His research focuses on developing resilient active distribution networks (ADNs) through protection, control, and optimization, leveraging AI/ML methods. During his Ph.D., Zhengrong has significantly contributed to two DOE projects and one PSERC project, where he developed advanced algorithms and intelligent methods for fault analysis, uncertainty quantification, and voltage control in ADNs. He has published over ten papers in peer-reviewed journals and proceedings and served as a reviewer for top journals/conferences. Zhengrong's research objective is to enhance the reliability, efficiency, and resilience of ADNs by integrating advanced computational techniques and machine learning algorithms.